MECHANISMS OF CLOSTRIDIAL TOXIN BINDING AND TRANSLOCATION

A Dissertation

presented to

the Faculty of the Graduate School

at the University of Missouri-Columbia

In Partial Fulfillment

of the Requirements for the Degree

Doctor of Philosophy

---

by

GREGORY STEPHEN LAMBERT

Dr. Michael Baldwin, Dissertation Supervisor

MAY 2018

The undersigned, appointed by the dean of the Graduate School, have examined the dissertation entitled

MECHANISMS OF CLOSTRIDIAL TOXIN BINDING AND TRANSLOCATION

Presented by Gregory S. Lambert, a candidate for the degree of doctor of philosophy, and hereby certify that, in their opinion, it is worthy of acceptance.

Professor Michael Baldwin

Professor Mark McIntosh

Professor Deborah Anderson

Professor Michael Calcutt

Professor George Stewart

DEDICATION

This work is dedicated to my parents, Stephen and Mary Lambert, who have always been there for me with support, encouragement, and love.

ACKNOWLEDGEMENTS

I would first like to acknowledge Dr. Michael Baldwin for serving as my dissertation advisor. I am truly grateful for the amount of time and effort he has invested in my training, as well as his patience, guidance, and encouragement over the years. I have learned a lot from him, both professionally and personally; it has been a pleasure having him as a mentor.

I would like to acknowledge my doctoral thesis committee, consisting of Drs. Deborah Anderson, Michael Calcutt, Mark McIntosh, and George Stewart, for their time and guidance throughout my graduate education.

I would like to thank: the Molecular Microbiology and Immunology office staff (Jana Clark, Shelly Crawford, Karen Ehlert, Scott Greathouse, and Kathy LaMere) for help with scheduling, technical, and administrative issues; Dr. Manijeh Heidari for her kindness, assistance, and interest in my well-being; and Dr. Michael Henzl for his assistance with the CD spectrophotometer and spectrofluorometer.

I would like to acknowledge the former members of the Baldwin lab, both graduate and undergraduate, for their companionship and aid throughout the years.

Finally, I would like to extend a heartfelt thank you to my family (Stephen, Mary, Lindsay, and Brian Lambert), as well as my fiancée Stephanie and our pets: Zoe, Briony, and Sophie. I am grateful for all of the love, support, and encouragement you have given me.

TABLE OF CONTENTS

LIST OF FIGURES

LIST OF TABLES

ABSTRACT

The bacterial genus *Clostridium* consists of over 150 species of anaerobic, fermentative, spore-forming bacilli. Clostridial species produce up to 20% of all known bacterial exotoxins, which serve as important virulence factors in the 10% of clostridial species that are highly pathogenic.

The seven serotypes of botulinum neurotoxin (BoNTs A-G) and tetanus neurotoxin (TeNT) are the causative agents of the paralytic diseases botulism and tetanus, respectively. Entry of toxins into neurons is mediated through initial interactions with gangliosides, followed by binding to a protein co-receptor. Herein we aimed to understand the mechanism through which individual neurotoxins recognize the carbohydrate motif of gangliosides. Using cell-based and *in vitro* binding assays, in conjunction with structure-driven site-directed mutagenesis, a conserved hydrophobic residue within the BoNTs that contributes to both affinity and specificity towards Sia5-containing gangliosides was identified. We demonstrate that targeted mutations within the Sia5 binding pocket result in the generation of neurotoxins that either bind and enter cells more efficiently (BoNT/A1 and BoNT/B) or display altered ganglioside binding specificity (TeNT). These data support a model in which recognition of Sia5 is largely driven by hydrophobic interactions between the sugar and the Sia5 binding site.

Another key step in intoxication by the clostridial neurotoxins (CNTs) involves translocation domain (HCT)-mediated translocation of the light chain (LC) across the endosomal membrane. Although our understanding of the translocation process has grown in recent years, the exact mechanism by which this occurs is not well defined.

Recent work has indicated that a cytosolic translocation factor (CTF) complex may facilitate translocation of the LC. While two components of this complex have been shown to be important in the context of TeNT (heat shock protein 90, HSP90; and the thioredoxin/thioredoxin-reductase redox system, Trx/TrxR), a potential third component (coatomer subunit gamma; COPG) was recently identified for diphtheria toxin (DT). COPG is a member of the heptameric coat protein I (COPI) complex, which is involved in retrograde vesicular trafficking. Herein, we aimed to identify residues of the tetanus translocation domain (HCT/T) that are responsible for mediating translocation channel formation within the endosomal membrane. Furthermore, we attempted to ascertain whether COPG interacts with HCT/T to facilitate translocation of the TeNT LC.

Clostridium difficile produces two large glucosylating toxins (*C. difficile* toxin A; TcdA/*C. difficile* toxin B; TcdB) and is the causative agent of pseudomembranous colitis and a leading cause of antibiotic-associated diarrhea. TcdA (308 kDa) and TcdB (270 kDa) disrupt the integrity of the intestinal epithelial barrier and provide an environment favorable for *Clostridium difficile* colonization. Recent evidence suggests entry of TcdA into cells is mediated by at least two domains. Here we report the characterization of a second receptor binding domain (RBD2) for TcdA. While both the isolated Combined Repetitive Oligopeptides (CROPs) and RBD2 fragments are rapidly internalized into cells under physiologic conditions, only the CROPs domain appreciably accumulates at the cell surface. Once internalized, CROPs and RBD2 are trafficked to late endosomal compartments. An internal deletion of RBD2 from TcdA holotoxin ablated toxicity in HT29 cells. These data are consistent with the recently proposed dual receptor model of cellular entry.

The toxins produced by the members of the genus *Clostridium* are crucial to the pathogenicity of their respective species. As such, fundamental characteristics of how these toxins function remain of utmost interest to investigators. While marked progress has been made over the years, there are still many details that elude us. Current research aims to fill important knowledge gaps, providing mechanistic information that can be exploited to both combat disease and be used to develop toxin-based therapeutics. The work contained herein contributes to the overall body of knowledge concerning clostridial toxins in a number of areas, focusing on the mechanisms of ganglioside binding by the CNTs, the potential role of cytosolic factors in translocation of TeNT, and the identification of a novel second receptor binding domain in TcdA.

CHAPTER 1: INTRODUCTION

1.1 Bacterial Toxins

Bacterial toxins are important virulence factors. Despite their varied sources and structures, they can be placed into a number of functional groups: 1) Toxins that act on receptors present on the surface of the plasma membrane; 2) Toxins that disrupt plasma membrane integrity by forming pores in the lipid bilayers of cells; 3) Toxins that are directly injected into cells via specialized bacterial machinery; and 4) Toxins that are internalized via receptor-mediated endocytosis, also known as AB toxins. These toxins consist of an enzymatically active A domain, and one or more B domains that are responsible for binding and entering cells. AB toxins have a high value in terms of virulence, as they are often the main cause of symptom manifestation in the diseases with which they are associated (1).

1.2 *Clostridium*

The bacterial genus *Clostridium* consists of over 150 species of anaerobic, fermentative, spore-forming bacilli, the majority of which are common environmental isolates. These species persist in the environment and degrade a large range of substrates via secreted enzymes, making them important ecological contributors. However, clostridial species also produce up to 20% of all known bacterial exotoxins. Consequently, roughly 10% of clostridial species are highly pathogenic. It has been speculated that these toxins may have evolved from the very enzymes that make clostridial species such important ecological contributors (2,3).

Of the ~150 known species, a number are particularly relevant to human disease. *Clostridium perfringens, Clostridium sordellii,* and *Clostridium novyi* produce a number of pore-forming toxins and are causative agents of gas gangrene (4,5). *Clostridium difficile* produces two large glucosylating toxins (TcdA/TcdB) and is the causative agent of pseudomembranous colitis (PMC) and a leading cause of antibiotic-associated diarrhea (AAD) (6-11). *Clostridium botulinum, Clostridium baratii*, and *Clostridium butyricum* produce botulinum neurotoxins (BoNTs), the causative agent of botulism; *Clostridium tetani* produces tetanus neurotoxin (TeNT), the causative agent of tetanus (12,13).

1.3 Clostridial neurotoxins

The seven serotypes of botulinum neurotoxin (BoNTs A-G) and tetanus neurotoxin (TeNT) are collectively known as the clostridial neurotoxins (CNTs), and are the causative agents of botulism and tetanus, respectively (12-18). Recent work suggests that an additional two BoNT serotypes, H and X, may also exist (19). BoNT serotypes can be further separated into subtypes if they contain more than 2.5% amino acid variation (3,20). BoNTs are produced by four phylogenetically distinct groups of *C. botulinum* (I-IV), as well as *C. baratii* and *C. butyricum* (14-17,19,21,22). Each group of *C. botulinum* is physiologically distinct, closely resembling a related, non-neurotoxigenic clostridial organism. Thus, it is the presence of BoNT that dictates their classification (23). Of the aforementioned toxins, BoNTs A, B, E, F, and TeNT are known to naturally intoxicate humans (24).

Average median lethal dose (LD_{50}) values for the CNTs are in the range of 1-3 ng/kg, making them some of the most potent and lethal toxins known (3,13,25,26). First

described in Hippocrates' *Epidemics*, tetanus is characterized by rigidity and spastic paralysis, often as the result of deep wound infection initiated by contamination with environmental spores of *C. tetani* (27). Upon uptake into peripheral motor neurons, TeNT undergoes retrograde axonal transport to the central nervous system (CNS), where it prevents the release of inhibitory neurotransmitters (28,29). In contrast to tetanus toxin, BoNT remains peripherally located and causes flaccid paralysis. First discovered in the early 1800s, adult intoxication by BoNT is most commonly associated with the ingestion of foodstuffs containing preformed toxin (30). However, infant botulism—relatively common in the U.S.—is associated with ingestion of spores of *C. botulinum*. The main underlying causes of mortality by both TeNT and BoNT are due to cardiac and pulmonary complications.

The number of reported tetanus cases in the developed world has decreased drastically since the development of a vaccine in 1924 (31). However, cases still occur regularly in locations without access to the vaccine, as well as sporadically in the developed world (https://www.cdc.gov/tetanus/surveillance.html). Without proper medical treatment, the mortality rate is high. Treatment for intoxication consists of paralytic drugs to control spasms, as well as assistance with breathing and eating (32-34). Unlike tetanus, cases of botulism have remained stable for many years. The most recently available data from the Centers for Disease Control and Prevention (CDC) indicated that 205 confirmed and 10 probable cases occurred in the United States in 2016 (https://www.cdc.gov/botulism/pdf/Botulism-2016-SUMMARY-508.pdf). The existence of the various serotypes of botulinum neurotoxin greatly complicates treatment and vaccination efforts. Since each serotype is antigenically distinct, vaccines and antitoxin

produced against one serotype are unable to neutralize toxin of the other serotypes (35). Additionally, sequential vaccination with multiple serotypes leads to adverse systemic reactions (36-38). Attempts to bypass these negative effects have been mixed. A pentavalent vaccine against BoNTs A-E was developed in the 1970s, but discontinued in 2011 for a number of reasons (39,40). More recent efforts utilizing recombinant subunits or catalytically inactive holotoxin are showing some promise (41-43). Treatment for BoNT intoxication consists of administration of antitoxin. However, only unbound toxin can be neutralized, so supportive respiratory care is also required in heavily intoxicated individuals (35,44,45).

1.4 Clostridial neurotoxin structure and mode of action

The CNTs are AB toxins, initially produced as ~150-kDa single chain proteins that undergo proteolytic processing to produce disulfide-linked di-chain proteins (1,28,46). These proteins consist of two major domains: an N-terminal ~50-kDa zinc-dependent protease domain (light chain, LC, A subunit), and a C-terminal ~100-kDa heavy chain (HC, B subunit) domain. The heavy chain can be further divided into domains based on function: an ~50-kDa N-terminal translocation domain (HCT) and an ~50-kDa C-terminal receptor binding domain (HCR) (13,46-49). Toxin activity is contained in the LC domain, which is specific for SNARE (neuronal soluble N-ethylmaleimide attachment protein receptor) proteins (50-52) (**Figure 1.1**). Crystal structures of BoNTs A, B, E, and TeNT have all been resolved at ~2-3 Å, and highlight a high degree of structural similarity between the CNTs (47,53-55).

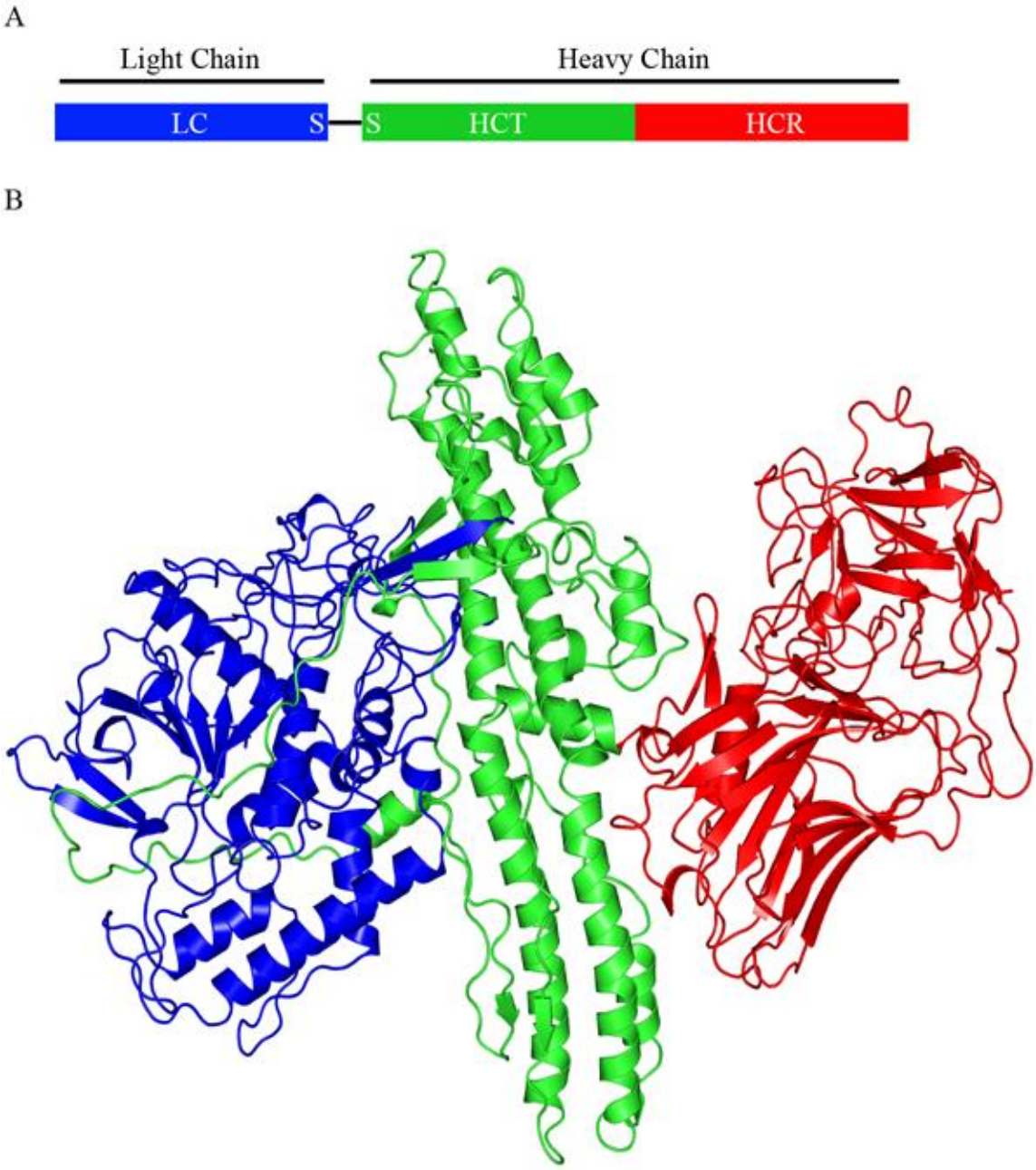

Figure 1.1. Clostridial neurotoxin structure. (A) The CNTs consist of an active light chain (LC; blue) linked via a single disulfide (S-S) to a heavy chain consisting of a translocation domain (HCT; green) and a receptor binding domain (HCR; red). **(B)** Crystal structure of BoNT/A resolved at 3.2 Å, showing the orientation of the LC (blue), HCT (green), and HCR (red) domains (PDB ID: 3BTA).

Intoxication by the CNTs takes place in three sequential steps. First, the HCR domain binds to the presynaptic membrane of α-motor neurons through two-receptor interactions (52,56-58). One of these two receptors is always a glycosphingolipid with ≥1 sialic acid sugar, also known as a ganglioside. Those relevant to CNT binding typically contain a GA1 core (Galactose-4, N-acetylgalactosamine-3, Galactose-2, Glucose-1, Ceramide; Gal4-GalNAc3-Gal2-Glc1-Cer)(59). Interaction with the ganglioside is mediated by a conserved ganglioside binding motif (GBM), with only a few exceptions (60-62). Residues constituting the GBM [E/D…H/K…SXWY…G] reside within a shallow pocket at the distal tip of the HCR domain (63-66). The second of the two receptors can either be a neuronal specific protein or, occasionally, an additional ganglioside (63-65,67-69). Synaptic vesicle protein 2 (SV2) isoforms serve as protein receptors for BoNTs A, D, E, and F; synaptotagmins I and II are the protein receptors for BoNTs B and G. Nidogen and SV2 isoforms mediate entry of TeNT at peripheral and central synapses, respectively (70-77). Additional comments on CNT binding can be found in Chapter 2.

Once bound, toxins are internalized via receptor-mediated endocytosis. Within motor neurons, BoNTs are sorted into acidified endosomal compartments, but TeNT is sorted into a retrograde axonal trafficking pathway. The exact details of this pathway are unknown, but the receptor binding domain of TeNT has been co-localized with Rab5 and Rab7 positive structures (13,78,79). Once trafficking is complete, TeNT is released and allowed to intoxicate inhibitory interneurons of the CNS, whereupon it ends up in acidified endosomal compartments.

The second step of CNT intoxication involves translocation of the LC across the endosomal membrane. Although our understanding of the translocation process has grown in recent years, the exact mechanism(s) by which this occurs is not defined for any member of the CNT family. Once the HCR domain has bound to its cognate receptors and the toxin has been endocytosed, several conditions must be met for productive translocation (12,80-82). Firstly, the HCT domain must be free to insert into the endosomal membrane. This appears to be dependent on intramolecular interactions between HCT, HCR, and LC. Low endosomal pH has been shown to be critical for translocation, as it triggers changes in either the conformation and/or orientation of these three domains. The HC of BoNT/A, as well as constructs lacking either the HCR domain (LC-HCT) or both the LC and HCR domains (HCT), were assayed for their ability to form ion-conducting channels. While the formation of channels by the HC and LC-HCT constructs were only observed at low pH, HCT alone was not pH dependent (81-89). This implies that both the LC and HCR domains act to prevent premature insertion of the HCT domain. In the case of the HCR domain, it is more likely that the orientation of the two domains is altered by low pH. The LC, however, must partially unfold to pass through the HCT channel. It is likely that low pH induces such a conformational change which simultaneously releases inhibition of the HCT domain and prepares the LC for translocation. Once free of inhibition, the HCT domain associates closely with the endosomal membrane, a process believed to be mediated by acidic lipids (82). This close association facilitates the insertion of the HCT domain into the endosomal membrane, forming a channel through which the partially unfolded LC is translocated.

Once the LC is translocated across the endosomal membrane, the thioredoxin/thioredoxin reductase-redox system (Trx/TrxR) is responsible for reducing the disulfide bond between the LC and HC. This releases the LC into the neuronal cytosol, where it is free to act upon its target. The CNT LCs are zinc metalloproteases belonging to the M4 peptidase family, with a conserved zinc-binding motif (HEXXH) (90,91). They cleave one or more of three neuronal SNARE proteins: VAMP2/synaptobrevin 2 (vesicle associated membrane protein 2; cleaved by TeNT, BoNTs B, D, F, and G), SNAP-25 (synaptosomal associated protein of 25 kDa; cleaved by BoNTs A, C, and E), or syntaxin 1 (cleaved by BoNT C) (92-101). BoNT X has altered specificity and cleaves non-canonical VAMP proteins. Cleavage of these proteins prevents the formation of neuronal SNARE complexes, and therefore synaptic vesicle exocytosis (102). The interactions between the CNT LCs and their substrates are well-characterized. Interestingly, substrate cleavage requires a more extended substrate than for most other zinc proteases. In general, all CNT LCs recognize their substrates near the site of cleavage, but some also recognize a distal site that contributes to catalysis (103-106). Some functional differences in the various serotypes can be explained by the size of the cleavage products that they produce (107,108). More specifically, CNTs that cleave smaller segments off of the end of SNARE proteins typically have a longer duration of effect within cells. This information can be exploited for potential therapeutic gain (109,110).

1.5 *Clostridium difficile*

**Clostridium difficile* has recently been reclassified as *Clostridioides difficile*. However, at this point in time, this new name has not been commonly adopted within the

field. As such, the organism will continue to be referred to as *Clostridium difficile* throughout the remainder of this thesis (111).

Clostridium difficile infection (CDI), a prevalent and severe nosocomial infection, is a leading cause of antibiotic-associated diarrhea (AAD) and pseudomembranous colitis (PMC) in the developed world (8-10). Severity of disease can largely be attributed to the presence of two potent exotoxins, TcdA (308 kDa; 2,710 aa) and TcdB (270 kDa; 2,366 aa), which are members of a family of large clostridial glucosylating toxins (LCTs) (6,7,11). These toxins inactivate members of the Ras and Rho families of small GTPases through glycosylation, resulting in disruption of both the actin cytoskeleton and cell-cell junctions, ultimately leading to cell death (112-116).

The causative agent of CDI, *C. difficile*, is an anaerobic, gram positive, spore-forming, motile bacillus first described in 1935 by Hall and O'Toole (117,118). It is asymptomatically present in approximately 5% of healthy adults, and as many as 30-70% of infants. For this reason, its involvement in intestinal disease was initially overlooked (119-123). Clinical use of broad-spectrum antibiotics increased in the 1960s, leading to an increase in cases of AAD and PMC (124). These conditions were initially thought to be caused by *Staphylococcus aureus*; it was not until 1978 that *C. difficile* was determined to be the cause of over 20% of AAD and virtually all PMC (125-129).

CDI is currently the most common nosocomial infection. The CDC estimates that there are ~500,000 infections and 29,000 deaths caused by *C. difficile* annually. A conservative estimate of the cost associated with management of CDI in the United States is upwards of $1.1 billion per year (130,131). Due to its ability to sporulate, *C. difficile* is extremely resistant to most disinfection techniques and is subsequently quite persistent in

healthcare environments (132,133). It is estimated that 25-30% of hospitalized patients serve as asymptomatic carriers of *C. difficile* (134,135). Clinical manifestations of CDI range from self-limiting, mild diarrhea to life-threatening conditions such as PMC and toxic megacolon with risk of bowel perforation (136-139). Transmission occurs via the fecal-oral route, with the pH-resistant spores germinating in the small intestine and opportunistically colonizing the colon if disruption of the normal microbiota has occurred (140-142). The number one risk factor for CDI is treatment with antibiotics which disrupt said microbiota (143-146). Other risk factors include hospitalization, advanced age, pregnancy, immunosuppression, existing gastrointestinal disease, and the use of proton pump inhibitors (147-153). Primary treatment for CDI consists of discontinuing the use of the offending antibiotics, and fluid restoration. Depending on the severity, oral metronidazole, vancomycin, or fidaxomicin may be administered as well (154). In the case of toxic megacolon, surgery with colectomy may be necessary (155,156). Unfortunately, even if these treatments are effective at resolving an initial infection, recurrence/re-infection rates for CDI are ~20%. The most effective treatment for recurring CDI has been found to be the administration of fecal transplants from healthy donors (157,158).

1.6 *Clostridium difficile* toxins

As mentioned above, the LCTs—TcdA and TcdB—are the main virulence factors produced by *C. difficile*. They are encoded by their respective genes, *tcdA* (8,133 bp) and *tcdB* (7,101 bp), on a 19.6-kb pathogenicity locus (PaLoc) that also contains genes for a putative holin (*tcdE*), as well as positive (*tcdR*) and negative (*tcdC*) regulators for their

transcription (159-163). While the majority of clinically-relevant strains are positive for both TcdA and TcdB, strains unable to produce one or both of these toxins have been isolated. Throughout the years, the exact roles these toxins play in CDI have been widely debated (164-171). However, it is now generally accepted that both toxins are capable of causing disease (172). It is important to note that some strains of *C. difficile* also produce a third toxin. This binary ADP-ribosylating toxin (CDT) is unable to cause disease on its own, but may contribute to the pathogenicity of LCT-positive strains (173). Additionally, hypervirulent strains of *C. difficile* have emerged (027/BI/NAP1) that produce increased amounts of TcdA and TcdB (due to a frameshift mutation in the *tcdC* gene), as well as CDT, and are associated with a 16.7% increased mortality rate (174-178).

The domain organization of TcdA and TcdB have been described previously as adhering to an ABCD model (**Figure 1.2**), consisting of four constituent domains. They are: (A) An N-terminal Glucosyltransferase domain (GTD), which transfers a glucose moiety from UDP-glucose onto Threonine 35/37 residues of Rho family GTPases (179-183); (C) A Cysteine Protease domain (CPD), which is responsible for autoproteolytic release of the GTD from the remainder of the toxin (184-188); (D) A translocation domain, which is responsible for delivery of the GTD and CPD domains to the cell cytosol (189-193); and (B) A C-terminal Combined Repetitive Oligopeptides (CROPs) domain, which is believed responsible for toxin binding to host enterocytes through interaction with an unidentified carbohydrate receptor(s) (159,194-202). Partial crystal structures and an electron microscopy map of TcdA have been solved, and allow visualization of the orientation of these domains in the context of the holotoxin (193,196,203).

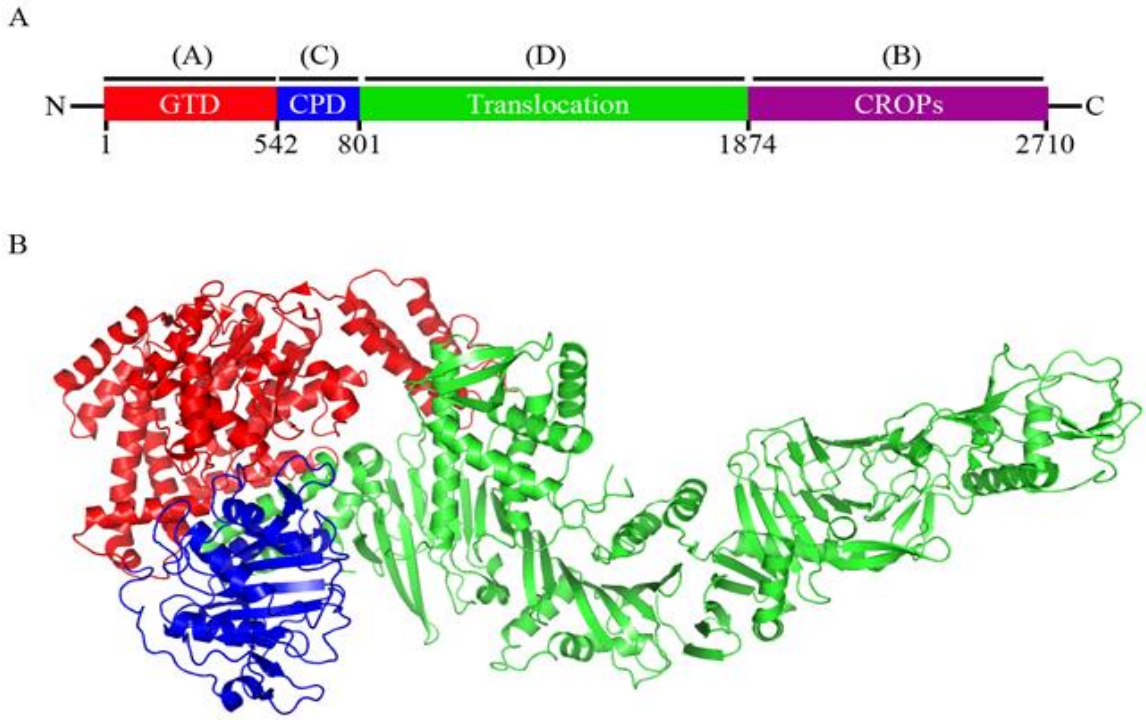

Figure 1.2. ***Clostridium difficile*** **toxin A (TcdA) structure. (A)** The structure of TcdA adheres to an ABCD model. (A; activity) N-terminal Glucosyltransferase domain (GTD), which transfers a glucose moiety from UDP-glucose onto Threonine 35/37 residues of Rho family GTPases; (C; cutting) Cysteine Protease domain (CPD), which is responsible for autoproteolytic release of the GTD from the remainder of the toxin; (D; delivery) Translocation domain, which is responsible for delivery of the GTD and CPD domains to the cell cytosol; (B; binding) C-terminal Combined Repetitive Oligopeptides (CROPs) domain, which is believed responsible for toxin binding to host enterocytes through interaction with an unidentified carbohydrate receptor(s). **(B)** Crystal structure of TcdA residues 1-1832 resolved at 3.2 Å, showing the orientation of the GTD (red), CPD (blue), and translocation (green) domains (PDB ID: 4R04).

As their name would suggest, the CROPs domains from TcdA and TcdB consist of a number of short repeats (SR; ~15 residues) with longer repeats (LR; ~30 residues) spaced out within. TcdA CROPs contains 32 SR and 7 LR; TcdB CROPs has 19 SR and 4 LR (204). In the case of TcdA, the three most C-terminal repeats are important for binding of CROPs to host cells (205,206). Binding of TcdA and TcdB was, up until recently, thought to be solely mediated by their C-terminal CROPs domains. However, studies demonstrating that TcdA and TcdB variants lacking the CROPs retain partial activity suggest the toxins may contain a second, CROPs-independent receptor binding domain (RBD) (187,207,208). Indeed, recent reports identifying Chondroitin sulfate proteoglycan 4, Poliovirus receptor-like 3, and Frizzled proteins as TcdB host cell receptors further support the concept that the LCTs contain a second RBD located between the putative translocation domain and the C-terminal CROPs region (209-211). Additional comments on a second RBD can be found in Chapter 4.

Once bound, TcdA and TcdB are internalized via receptor-mediated endocytosis (212). They then are predicted to undergo low pH-induced structural changes upon endosomal acidification, allowing the translocation domain to span the endosomal membrane and expose the GTD and CPD domains to the cell cytosol (189-192). In the presence of cytosolic inositol hexakisphosphate (InsP6), the CPD domain autoproteolytically cleaves the GTD from the remainder of the toxin. It is then free to glucosylate Rho/Ras family GTPases at the cell membrane (179-188).

1.7 Summary

The toxins produced by the members of the genus *Clostridium* are crucial to the pathogenicity of their respective species. As such, fundamental characteristics of how these toxins function remain of utmost interest to investigators. While marked progress has been made over the years, there are still many details that elude us. Current research aims to fill important knowledge gaps, providing mechanistic information that can be exploited to both combat disease and be used to develop toxin-based therapeutics. The work contained herein contributes to the overall body of knowledge concerning clostridial toxins in a number of areas, focusing on the mechanisms of ganglioside binding by the CNTs, the potential role of cytosolic factors in translocation of TeNT, and the identification of a novel second receptor binding domain in TcdA.

CHAPTER 2: INSIGHTS INTO THE MECHANISMS BY WHICH CLOSTRIDIAL NEUROTOXINS DISCRIMINATE BETWEEN GANGLIOSIDES

As found in: Burns, J. R., Lambert, G. S., and Baldwin, M. R. (2017), Insights into the Mechanisms by Which Clostridial Neurotoxins Discriminate between Gangliosides. Biochemistry, 56 (20): 2571-2583.

2.1 Abstract

Botulinum neurotoxins (BoNTs) and tetanus neurotoxin (TeNT) are the causative agents of the paralytic diseases botulism and tetanus, respectively. Entry of toxins into neurons is mediated through initial interactions with gangliosides, followed by binding to a protein co-receptor. Herein we aimed to understand the mechanism through which individual neurotoxins recognize the carbohydrate motif of gangliosides. Using cell-based and *in vitro* binding assays, in conjunction with structure-driven site-directed mutagenesis, a conserved hydrophobic residue within the BoNTs that contributes to both affinity and specificity towards Sia5-containing gangliosides was identified. We demonstrate that targeted mutations within the Sia5 binding pocket result in the generation of neurotoxins that either bind and enter cells more efficiently (BoNT/A1 and BoNT/B) or display altered ganglioside binding specificity (TeNT). These data support a model in which recognition of Sia5 is largely driven by hydrophobic interactions between the sugar and the Sia5 binding site.

2.2 Introduction

Several species of *Clostridium*, most notably *C. botulinum* and *C. tetani*, are renowned for their ability to produce potent neurotoxins (13,213,214). There are seven major serotypes of botulinum neurotoxin (BoNT, types A–G), and a significant number of amino acid variants identified by nucleotide sequencing (commonly termed subtypes) (215-218). Together with tetanus neurotoxin (TeNT), they form the clostridial neurotoxin (CNT) family of protein exotoxins. Exposure to botulinum or tetanus neurotoxins results in the life-threatening neuroparalytic diseases of botulism and tetanus, respectively. In their active form, CNTs are composed of an ~100-kDa heavy chain (HC), which includes translocation (HCT) and receptor binding (HCR) domains, linked by a single disulfide bond to an ~50-kDa light chain (LC) that constitutes the catalytic domain (47). Intoxication of neurons is a multistep process involving receptor-mediated endocytosis, translocation of LC into the cytosol, and proteolytic cleavage of neuronal SNARE (soluble *N*-ethylmaleimide-sensitive fusion protein attachment protein receptor) proteins. SNARE proteolysis abrogates synaptic vesicle exocytosis, ultimately resulting in the paralysis of the innervated muscle or gland (12,48,219).

Currently, eight subtypes of BoNT/A (termed A1-A8) have been identified, ranging in amino acid similarity from 98% (A1 versus A5) to 84% (A1 versus A3). To date, only a limited number of studies have been performed to compare functional differences between the subtype toxins (220-223). Analysis of BoNT subtypes A1-A5 has demonstrated BoNT/A4 to be ~1000-fold less active than A1; BoNT/A3 has a dramatically shorter duration of action within neurons; and BoNT/A2 enters cells more rapidly than A1. Moreover, multiple studies using *ex vivo* cell cultures, animal models,

and human subjects reveal that BoNT/A2 has greater clinical efficacy and less spread of its action to a neighboring muscle as compared with BoNT/A1 (224-230). However, despite the accumulating evidence that subtypes have unique pharmacologic characteristics, the mechanistic basis for such differences have not yet been defined.

Neuronal binding of CNTs associated with human disease (BoNT types A, B, E, F and TeNT) is mediated by the HCR domain, which simultaneously recognizes host synaptic vesicle proteins and complex gangliosides present on the presynaptic membrane (48). Studies performed by multiple investigators revealed that gangliosides bind to these toxins through a shallow cleft formed by a series of residues referred to as the conserved ganglioside binding motif (GBM; E/D…H/K…SXWY…G) (58,63-65,231,232). Although residues within the GBM are necessary for interaction with the GalNAc3-Gal4 moiety of gangliosides, the GBM alone does not account for the high affinity and specificity of ganglioside binding between individual CNTs (64). TeNT stabilizes interaction with ganglioside through formation of an additional hydrogen bond between Asn1219 and the GalNAc3 sugar (64,65). As a consequence, binding of TeNT to gangliosides containing the core GalNAc3-Gal4 moiety is not influenced by the addition of one or more *N*-acetylneuraminic acid residues. In contrast, BoNTs associated with human disease (BoNT types A, B, E, and F) bind with high affinity only to gangliosides containing an α2, 3-linked *N*-acetylneuraminic acid sugar (denoted as Sia5) attached to Gal4 (64). In the case of BoNT/F, binding of Sia5 is mediated by hydrogen bonds formed to Arg1111 and Arg1256 in addition to hydrophobic interactions with the Sia5 binding site. While Arg1111 and Arg1256 are not conserved, structural data suggest that

BoNTs A and B contain alternative residues which perform an analogous function (**Figure 2.1**) (64,231,232).

In the present study, we focused on understanding the mechanism(s) by which individual clostridial neurotoxins bind to, and discriminate between, individual gangliosides. Biochemical characterization of wild-type and mutated HCR domains suggest that hydrogen bonds formed between the toxin and Sia5 make only moderate contributions to the affinity and specificity of the interaction. Rather, a semi-conserved hydrophobic residue within the BoNTs was identified that plays an important role in Sia5 recognition. Replacement of isoleucine 1239 in HCR/B with the corresponding phenylalanine residue of BoNTs A, E and F increased affinity for gangliosides GT1b and GD1a by an order of magnitude as compared to wild-type. Moreover, HCR/B^{I1239F} was shown to both enter cortical neurons and inhibit the activity of BoNT/B holotoxin more efficiently than wild-type HCR/B. The importance of the semi-conserved hydrophobic residue was further substantiated by the construction of a novel TeNT variant that preferentially bound gangliosides containing the Sia5 sugar. These data support a model in which recognition of Sia5 by BoNTs is driven primarily through hydrophobic interactions between the protein and the sugar moiety.

2.3 Experimental Procedures

2.3.1 Site-directed mutagenesis of BoNT and TeNT HCR domains.

A previously described, modified pET28a expression vector (Millipore Sigma, Billerica, MA, USA)—hereafter referred to as pET28-3×FLAG—containing a 3×FLAG epitope immediately downstream of the hexahistidine epitope tag, was used as the

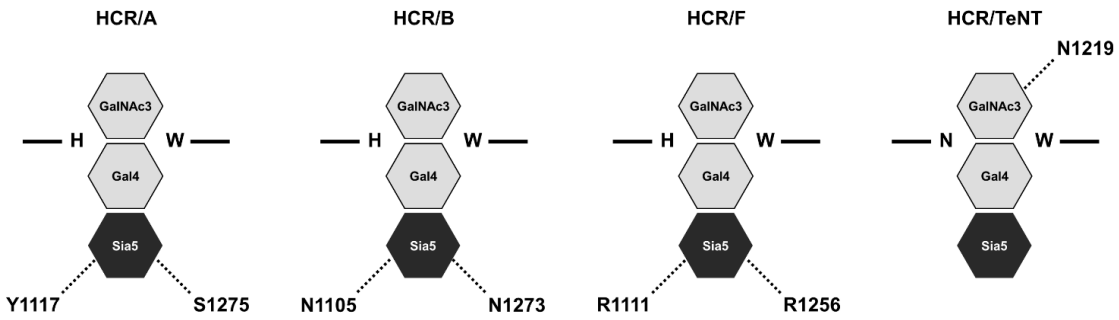

Figure 2.1. Schematic of HCR-mediated ganglioside binding. In each of the panels, monosaccharides are represented by hexagons. GalNAc3 and Gal4 are colored in light grey while Sia5 is highlighted in dark grey. HCR amino acid residues likely involved in ganglioside binding are represented using their single letter codes. Hydrogen bonds are indicated by dotted lines between the amino acid in question and the indicated sugar.

expression vector for all HCR constructs (233). *Escherichia coli* codon-optimized HCR/A1 (aa 870-1295), HCR/A2 (aa 870-1295), HCR/B (aa 859-1290), HCR/E (aa 849-1251), HCR/F (aa 868-1278), and HCR/T (aa 865-1315) DNA were synthesized (Genscript, Piscataway, NJ, USA) and subcloned into pET28-3×FLAG via unique 5' KpnI and 3' XhoI restriction sites. Point mutations were introduced into the BoNT and TeNT HCR sequences by site-directed mutagenesis using the Quikchange® II Site-Directed Mutagenesis Kit (Agilent Technologies, Santa Clara, CA, USA) and confirmed by automated DNA sequencing. In contrast to BoNTs A, B, E, and F, TeNT contains a second binding site that binds gangliosides through terminal sialic acid residues (65-67). Therefore, to compare ganglioside binding mediated solely by the conserved ganglioside binding site (formed by the GBM), all experiments were performed on the HCR/T^{R1226L} background (67).

2.3.2 Generation of a chimeric TeNT-BoNT/A protein using Splicing by Overlap Extension-PCR.

A chimeric HCR/T protein containing a short sequence of amino acids derived from BoNT/A (1270-1279) was generated by Splicing by Overlap Extension-PCR (234). For each PCR fragment, primers were constructed such that a 5' overhang of 30 nucleotides encoding BoNT amino acids was complementary to the 5' end of the second PCR fragment. In the first round of PCR, two fragments of approximately 1300 and 300 base pairs were amplified and subsequently gel purified. A second round of PCR was then carried out by mixing equimolar amounts of the two purified products with only primers from the two far ends. The overlapping complementary sequences introduced in

round 1 served as primers and the two sequences containing the BoNT insertion were joined. DNA was digested using KpnI and PstI restriction enzymes, ligated into pET28-3×FLAG and verified by automated DNA sequencing of the entire HCR coding region.

2.3.3 Expression and purification of HCR proteins.

For purification of HCR, *E. coli* BL-21(DE3) harboring pET28-3×FLAG HCR was inoculated into 2 liters of Luria-Bertani (LB) broth supplemented with 50 µg/ml kanamycin for 3 hours at 37ºC and 250 r.p.m. (an OD_{600} of ~0.6). Isopropyl β-D-1-thiogalactopyranoside (IPTG) was added to a final concentration of 1 mM and incubation continued overnight following temperature reduction to 16ºC. Bacterial cells were harvested by centrifugation at 6000 ×*g* for 20 min at 4ºC, lysed by French press, and clarified by centrifugation at 15000 ×*g* for 30 min at 4ºC. Lysates were filtered through a 0.22-µm cellulose acetate syringe type filter prior to sequential column chromatography: Ni^{2+}-nitrilotriacetic acid (NTA) agarose (Qiagen, Germantown, MD, USA) affinity chromatography followed by size exclusion chromatography using a S200-HR gel filtration column (GE Healthcare Bio-Sciences, Pittsburgh, PA, USA). Column fractions containing purified 3×FLAG-HCR were pooled, concentrated using an Amicon type centrifugal filtration device, and dialyzed against 30 mM HEPES-NaOH, 150 mM NaCl, pH 7.6. Purified 3×FLAG-HCRs were stored undiluted at -80ºC until use. A representative SDS-PAGE gel showing the relative purity of the HCR domains used in these studies is shown in **Figure 2.2**.

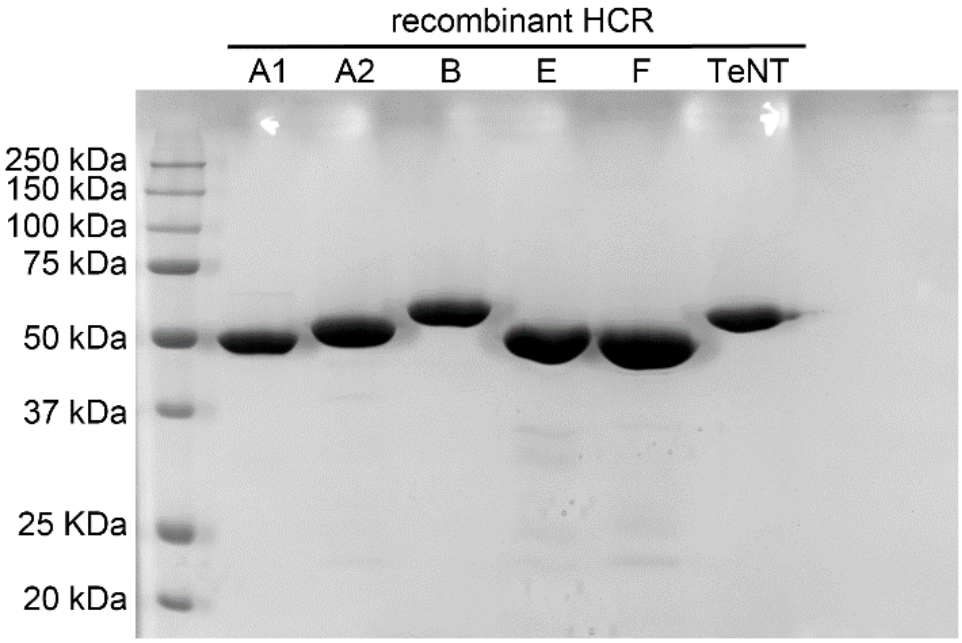

Figure 2.2. Representative gel showing purified HCR proteins. Representative wild-type and variant HCRs (7.5 μg) were resolved by SDS-PAGE and visualized by staining with Coomassie Blue. Unless otherwise stated all proteins employed in this study were stably expressed and estimated to be at least 90% pure as determined by SDS-PAGE followed by visualization with Coomassie Blue.

2.3.4 Circular Dichroism.

An AVIV model 202 far-UV spectrometer was used to collect spectra (198–250 nm) of wild-type and mutated HCR domains (0.5 mg/ml) in 10 mM potassium phosphate buffer, pH 7.2. Spectra were collected at 25°C, using a 1-mm path length quartz cuvette. Baselines were recorded using potassium phosphate buffer and subtracted from the sample spectrum. Measurements were only made down to wavelengths where the instrument dynode voltage indicated the detector was still in its linear range. Background corrected spectra for wild-type and mutated HCR domains are shown in **Figure 2.3**.

2.3.5 Ganglioside binding assay.

A solid-phase ganglioside binding assay was carried out as described previously (221). Briefly, 5 µg of purified bovine brain gangliosides (Matreya, LLC, State College, PA, USA) were coated onto a non-protein binding 96-well plate (Corning Costar #3591; Corning, NY, USA). Nonspecific binding sites were blocked by incubation with 2% (w/v) bovine serum albumin (BSA) in carbonate buffer solution, pH 9.6. Various concentrations of HCRs were added to the plates and incubated at 4ºC for 90 min. Post incubation, 96-well plates were washed three times, after which an antibody solution containing mouse anti-FLAG-M2 monoclonal antibody (1:8000, Sigma-Aldrich, St. Louis, MO, USA) and goat anti-mouse-IgG horseradish peroxidase (HRP) conjugate (1:10000, Thermo Fisher Scientific, Waltham, MA, USA) was applied and incubated for 20 min at 4ºC. Following incubation, the plate was washed three times and bound HCR detected using Ultra TMB (Thermo Fisher Scientific) as the HRP substrate. The reaction was terminated by the addition of an equal volume of 0.1 M H_2S0_4. The absorbance at

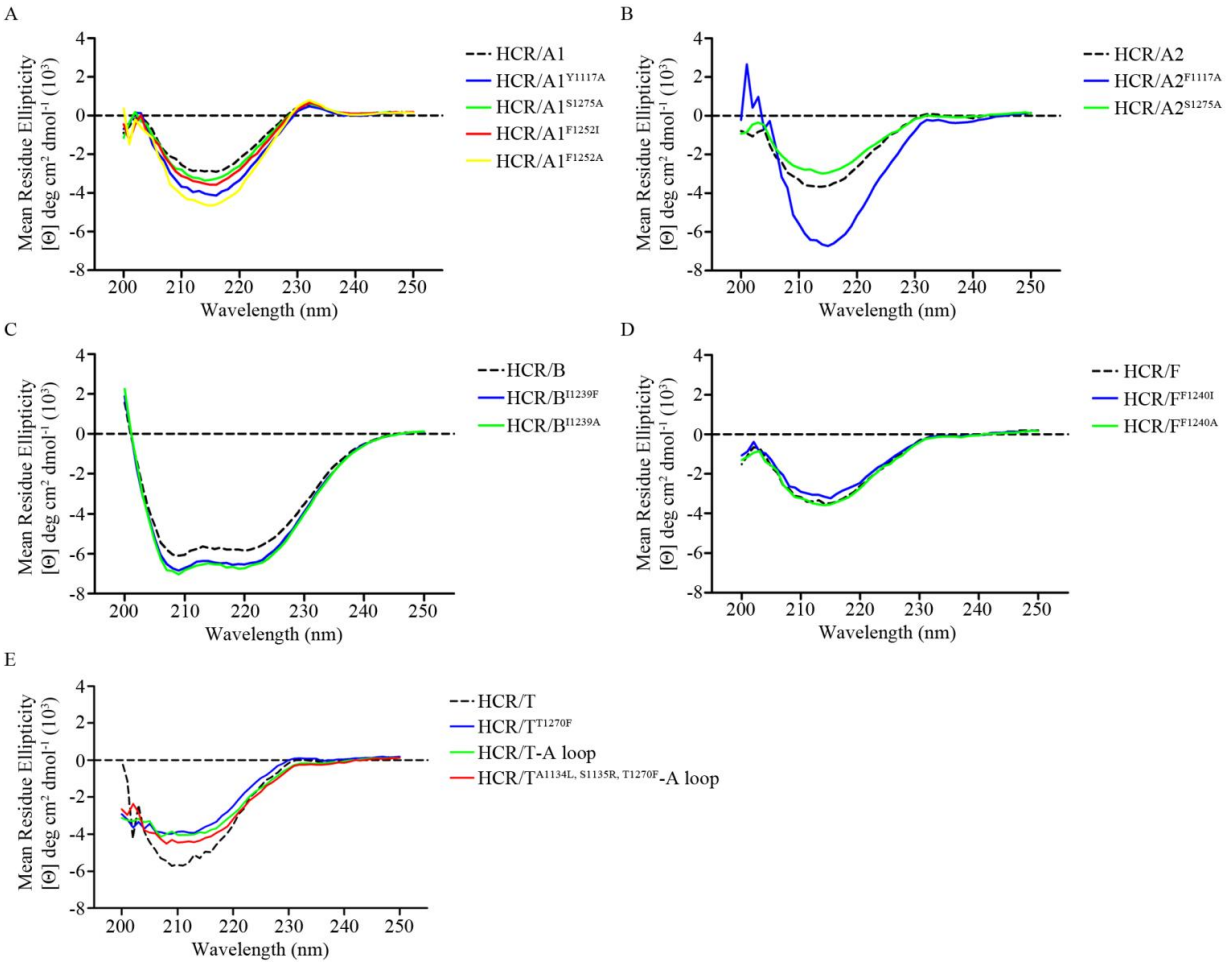

Figure 2.3. CD spectra of wild-type and mutated HCR domains. The far-UV CD spectra (198-240 nm) of HCR derivatives (0.5 mg/ml in water) were recorded using an AVIV model 202 spectrometer. **(A)** HCR/A1 and mutated derivatives, **(B)** HCR/A2 and mutated derivatives, **(C)** HCR/B and mutated derivatives, **(D)** HCR/F and mutated derivatives, and **(E)** HCR/T and mutated derivatives.

450 nm was determined using a plate reader (BioTek, Winooski, VT, USA). The apparent equilibrium dissociation constant (K_d) was estimated by fitting the data to a one-site binding model where $Y = B_{max} \times X / (K_d + X)$ using GraphPad Prism version 6. The goodness of fit was estimated by calculating R^2, with values < 0.9 indicating the model was not appropriate. K_d values for individual experiments are reported as the arithmetic mean and standard error of at least three independent trials performed in triplicate (summarized in **Table 2.1**).

2.3.6 Culture of primary rat cortical neurons.

Rat embryonic day 18 (E18) cortices (Brainbits, LLC, Springfield, IL, USA) were mechanically dissociated and plated in Neurobasal medium supplemented with B-27 (Thermo Fisher Scientific) on poly-D-lysine coated glass cover slips. Half of the culture medium was changed with fresh Neurobasal medium every 4 days starting on day 5.

2.3.7 Binding and entry of HCR domains into cortical neurons: indirect immunofluorescence.

Neurons (10-14 days *in vitro*) were washed twice with pre-warmed (37°C) Hank's Balanced Salt Solution (HBSS) and incubated with indicated concentrations of HCRs in buffer for 5 min at 37°C. Buffers were either high potassium (high K^+) to stimulate membrane depolarization (15 mM HEPES-NaOH, 95 mM NaCl, 56 mM KCl, 2.2 mM $CaCl_2$, 0.5 mM $MgCl_2$, pH 7.4) or low potassium (low K^+) to mimic resting conditions (15 mM HEPES-NaOH, 145 mM NaCl, 5.6 mM KCl, 2.2 mM $CaCl_2$, 0.5 mM $MgCl_2$, pH 7.4). Cells were washed three times in HBSS and fixed in phosphate buffered saline

Table 2.1. Relative affinities of HCR derivatives for the indicated gangliosides.

	Apparent K_d (nM)*							
	GT1b		GD1a		GD1b		GM1a	
HCR/A1	483 ± 29	(12)	522 ± 26	(18)	8232 ± 487	(9)	>10,000	(9)
HCR/A1^{Y1117A}	38 ± 7	(6)	48 ± 5	(6)	>10,000	(6)	>10,000	(6)
HCR/A1^{Y1117F}	263 ± 17	(6)	n.d.		n.d.		n.d.	
HCR/A1^{S1275A}	208 ± 16	(6)	n.d.		n.d.		n.d.	
HCR/A1^{F1252I}	n.d.		>10,000	(3)	n.d.		>10,000	(3)
HCR/A1^{F1252A}	n.d.		>10,000	(3)	n.d.		>10,000	(3)
HCR/A1^{F1252T}	n.d.		>10,000	(3)	n.d.		>10,000	(3)
HCR/A2	355 ± 25	(9)	565 ± 47	(9)	>10,000	(3)	>10,000	(3)
HCR/A2^{F1117A}	20 ± 2	(6)	68 ± 5	(6)	>10,000	(3)	>10,000	(3)
HCR/A2^{F1117Y}	258 ± 28	(6)	n.d.		n.d.		n.d.	
HCR/A2^{S1275A}	335 ± 29	(6)	n.d.		n.d.		n.d.	
HCR/B	470 ± 28	(9)	1111 ± 85	(12)	>10,000	(3)	>10,000	(3)
HCR/B^{I1239F}	34 ± 3	(3)	75 ± 7	(6)	9833 ± 546	(3)	>10,000	(3)
HCR/B^{I1239A}	n.d.		>10,000	(3)	n.d.		>10,000	(3)
HCR/B^{I1239T}	n.d.		>10,000	(3)	n.d.		>10,000	(3)
HCR/E	242 ± 23	(2)	219 ± 12	(6)	>10,000	(2)	>10,000	(3)
HCR/F	57 ± 3	(2)	63 ± 3	(9)	>10,000	(2)	>10,000	(3)
HCR/F^{F1240I}	n.d.		349 ± 40	(3)	n.d.		>10,000	(3)
HCR/F^{F1240A}	n.d.		>10,000	(3)	n.d.		>10,000	(3)
HCR/F^{F1240T}	n.d.		>10,000	(3)	n.d.		>10,000	(3)
HCR/F^{H1241K}	n.d.		6 ± 0.3	(6)	n.d.		579 ± 52	(6)
HCR/F$^{H1241K, F1240A}$	n.d.		>10,000	(3)	n.d.		2042 ± 177	(6)
HCR/T†	234 ± 48	(3)	57 ± 3	(22)	322 ± 21	(3)	24 ± 2	(22)
HCR/T^{T1270F}	n.d.		6775 ± 771	(3)	n.d.		4083 ± 579	(3)
HCR/T^{T1270A}	n.d.		61 ± 5	(2)	n.d.		28 ± 2	(2)
HCR/T $^{A1134L, S1135R, T1270F}$	n.d.		13 ± 1	(6)	n.d.		78 ± 7	(6)
HCR/T $^{A1134L, S1135R, T1270F}$-A Loop	n.d.		52 ± 5	(4)	n.d.		>10,000	(4)

* all values represent the arithmetic mean and standard error of n (number of experiments shown in brackets) independent experiments performed in triplicate.
n.d. not determined.
† HCR/T (contains R1226L mutation to inactivate the second (non-conserved) ganglioside binding site.

All binding data using HCR/T was performed by Dr. Joshua R. Burns and is reported in his thesis entitled "Mechanisms of Clostridial Neurotoxin Binding and Entry," May 6th, 2016.

(PBS) containing 4% (w/v) paraformaldehyde, 4% (w/v) sucrose for 30 min at room temperature. Cells were subsequently quenched with 0.1 M glycine in PBS, permeabilized with 0.25% v/v Triton X-100 in PBS, and blocked using Image-IT reagent (Thermo Fisher Scientific). Bound HCR was detected by immunofluorescence using mouse anti-FLAG-M2 (1:1000, Sigma-Aldrich) and goat anti-mouse-IgG Alexa 488 (1:200, Thermo Fisher Scientific). Endogenous synaptophysin was detected using rabbit anti-synaptophysin (clone YE269 1:100, Abcam, Eugene, OR, USA) and anti-rabbit-IgG Alexa 568 (1:200, Thermo Fisher Scientific). Cells were processed using standard immunofluorescence procedures, mounted in ProLong® Gold Antifade reagent (Thermo Fisher Scientific), and images acquired using a Leica SPE-2 microscope in confocal scanning mode. Fluorescence intensity within individual fields was measured using Leica Application Suite X (LAS X).

2.3.8 Binding and entry of HCR domains into cortical neurons: Western blotting.

Neurons (10-14 days *in vitro*) were washed twice with pre-warmed HBSS and incubated with indicated concentrations of HCRs in Neurobasal medium for 30 min at 37°C. Next, cells were washed twice with HBSS and further incubated for 90 min at 37°C in Neurobasal medium alone. Finally, cells were washed twice with ice-cold HBSS, lysed with radioimmunoprecipitation assay buffer (RIPA buffer) on ice for 30 min, and lysates clarified by centrifugation at 15000 ×*g* for 30 min at 4ºC. Cell lysates were combined with ¼ volume of 4× SDS-PAGE sample buffer, resolved on 13.5% (w/v) SDS-polyacrylamide gels, transferred to PVDF membranes, and subjected to Western blotting. Blots were sequentially probed with mouse anti-FLAG-M2 (1:10000, Sigma-

Aldrich) and goat anti-mouse-IgG-HRP (1:80000, Thermo Fisher Scientific) and HCRs detected by enhanced chemiluminescence (SuperSignal West Dura, Thermo Fisher Scientific) using a CCD camera system (HD2 Imager, Protein Simple, San Jose, CA, USA). Blots were stripped with Restore PLUS Western Blot Stripping Buffer (Thermo Fisher Scientific) and further probed with a mouse anti-beta actin antibody conjugated to HRP (clone C4, 1:5000, Santa Cruz Biotechnology, Inc. Dallas, TX, USA) and detected as above.

2.3.9 Cellular intoxication assay.

Botulinum neurotoxins types A and B were purchased from List Biological Laboratories (Campbell, CA, USA). Neurons (10-14 days *in vitro*) were washed twice with pre-warmed HBSS and then incubated in high K^+ buffer for 5 min at 37°C, in the presence of 5 nM BoNTs with or without the indicated concentrations of HCR competitor proteins. Cells were then washed thrice with HBSS and incubated for an additional 24 h at 37°C in Neurobasal medium. Following treatment, cells were processed for Western blotting as described above. Membranes were probed for SNAP-25 (clone D9A12, 1:1000, Cell Signaling Technology, Danvers, MA, USA) or VAMP2 (clone 69.1, 1:5000, Synaptic Systems, Goettingen, Germany) as appropriate.

2.4 Results

2.4.1 HCR/A1 and HCR/A2 bind ganglioside in a similar manner.

Evidence suggests that differences in the rates of cellular binding and/or entry may account for the increased toxicity of BoNT/A2 relative to BoNT/A1 *in vivo* (224-

230). One possible mechanism by which the entry of BoNT/A2 could differ is through unique interactions with ganglioside co-receptors (235). A homology model of HCR/A2 was generated using the freely available I-TASSER program (http://zhanglab.ccmb.med.umich.edu/services/) (236), with the co-crystal structure of HCR/A1 bound to GT1b [PDB: 2VU9; (231)] as the model template (**Figure 2.4**). Given the high degree of sequence identity shared between the two toxins (~89% for the HCR domain), the overall shape of the HCR/A2 ganglioside binding pocket is preserved, with conservation among residues forming the GBM and those predicted to make hydrogen bonds to either the Sia5 (Ser1275) or Sia6 (Arg1276) sugars. However, HCR/A1 Tyr1117—which is predicted to stabilize binding to Sia5 through hydrophobic packing and the formation of two hydrogen bonds—is replaced by phenylalanine (Phe1117) in HCR/A2 (**Figure 2.4A**, green color). Consequently, it was hypothesized that HCR/A2 would display moderately reduced affinity for ganglioside as compared to HCR/A1. In addition, several additional amino acid substitutions in close proximity to the ganglioside binding site were observed, though none of these residues appear likely to interact directly with the carbohydrate moiety (**Figure 2.4A**, cyan color).

Prior to investigating the ganglioside binding properties of BoNT/A2, we confirmed that a recombinant HCR/A2 bound and entered cortical neurons similar to the parental toxin. In agreement with previous observations (220,235), binding of HCR/A2 to cortical neurons was enhanced under depolarizing conditions (high K^+ buffer) and co-localized with the synaptic vesicle resident protein synaptophysin (**Figure 2.5**), thus supporting the suitability of recombinant HCR/A2 as a surrogate for the native holotoxin.

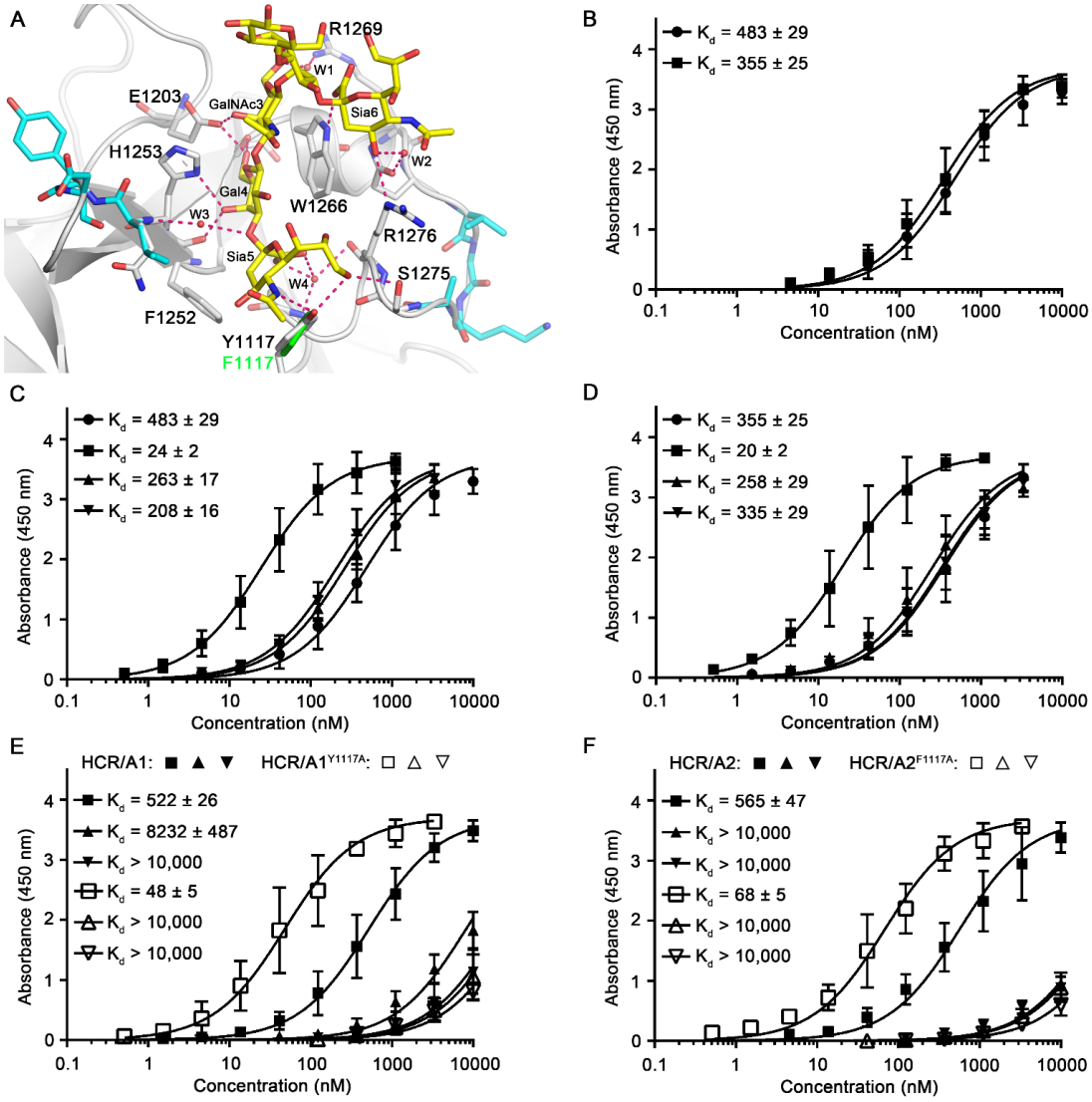

Figure 2.4. HCR/A1 and HCR/A2 bind gangliosides in a similar manner. (A) Ribbon representation of the HCR/A1 (grey Cα) in complex with a GT1b analog (stick representation, yellow carbon) illustrating the positioning of the oligosaccharide within the ganglioside binding cleft and the intermolecular hydrogen bond interactions (dashed lines). The four bridging water molecules are shown as spheres in red color. All residues making contact with the oligosaccharide are conserved between HCR/A1 and HCR/A2 with the exception of Tyr1117 which is replaced by phenylalanine in HCR/A2 (green). Additional residues in close proximity to the GT1b oligosaccharide that differ between HCR/A1 and HCR/A2 are shown in cyan. **(B)** Various concentrations of HCR/A1 (●) or HCR/A2 (■) were examined for the ability to bind ganglioside GT1b. **(C)** Binding of wild-type HCR/A1 (●) and mutated HCR/A1 ($A1^{Y1117A}$ ■; $A1^{Y1117F}$ ▲; $A1^{S1275A}$ ▼) to ganglioside GD1a. **(D)** Binding of wild-type HCR/A2 (●) and mutated HCR/A2 ($A2^{F1117A}$ ■; $A2^{F1117Y}$ ▲; $A2^{S1275A}$ ▼) to ganglioside GD1a. The ganglioside binding specificity of wild-type (black symbols) and mutated (white symbols) HCR/A1 **(E)** or HCR/A2 **(F)** proteins was compared using gangliosides GD1a (■/□), GD1b (▲/△) and GM1a (▼/▽). All values represent the arithmetic mean and standard error of a minimum of three independent determinations performed in triplicate. K_d values for all HCR derivatives are summarized in **Table 2.1**.

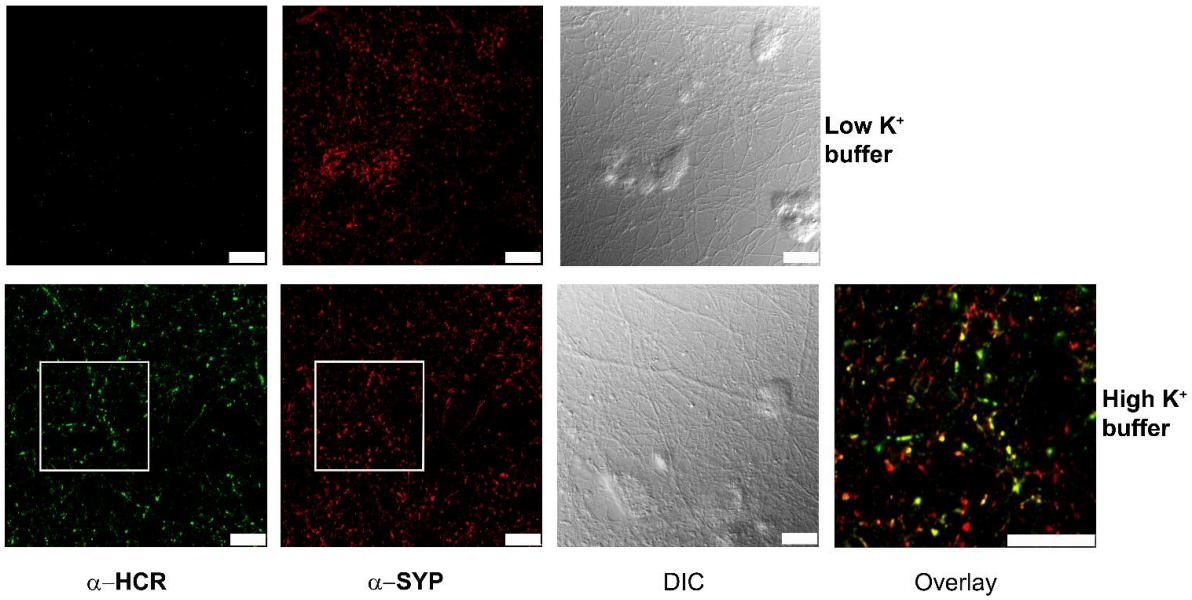

Figure 2.5. HCR/A2 enters neurons by way of recycling secretory vesicles. Rat cortical neurons were incubated with 50 nM HCR/A2 for 5 min at 37°C in either low K^+ buffer (*upper panels*) or high K^+ buffer (*lower panels*) to stimulate synaptic vesicle recycling. Cells were processed for immunocytochemistry and HCR/A2 was detected using a mouse anti-FLAG monoclonal antibody (green). Cells were co-stained with Synaptophysin (SYP) antibodies to identify neuronal synapses (red). An enlarged optical section of the region highlighted by the white box showing co-localization between the two proteins. Scale bar = 10 μm in all fields.

Personal communication from Dr. Michael R. Baldwin.

Analysis of the interaction of HCR/A1 and HCR/A2 with a panel of gangliosides demonstrated that both toxins bound to gangliosides GT1b and GD1a with similar affinities (**Figure 2.4B** and **Table 2.1**), while binding to gangliosides lacking a terminal Sia5 sugar (GD1b and GM1a) was greatly reduced (**Figure 2.4D** and **2.4F**; **Table 2.1**). Consistent with these data, replacement of HCR/A1 Tyr1117 with the corresponding phenylalanine residue of HCR/A2 or vice-versa did not significantly alter the affinity for GT1b (**Figure 2.4C** and **2.4E**). Furthermore, alanine replacement of Ser1275 in either HCR/A1 or /A2 did not noticeably affect ganglioside binding, suggesting that hydrogen bonds formed by either Tyr1117 or Ser1275 do not play critical roles in the recognition of Sia5 (**Figure 2.4C** and **2.4E**; **Table 2.1**). Indeed, alanine replacement of the tyrosyl or phenyl rings of HCR/A1 and HCR/A2 respectively, increased binding affinity to gangliosides GT1b and GD1a by an order of magnitude, without altering ganglioside binding specificity (**Figure 2.4D** and **2.4F**; **Table 2.1**). The observation that alanine replacement of Tyr1117 increases affinity towards GT1b and GD1a has been previously reported (237), and can now also be extended to alanine replacement of Phe1117 in HCR/A2.

2.4.2 HCR/A1^{Y1117A} and HCR/A2^{F1117A} variants enter cells more rapidly than wild-type proteins.

The prior invention disclosure also demonstrated that replacement of Tyr1117 with Ala, Cys, or Val all resulted in a 3-fold increase in overall neurotoxicity (237). Therefore, the functional consequences of Phe1117 replacement in A2 were investigated. Consistent with previous reports, the entry of HCR/A2 relative to HCR/A1 was elevated at low concentrations of toxin (**Figure 2.6A**) (235), though total uptake of both proteins

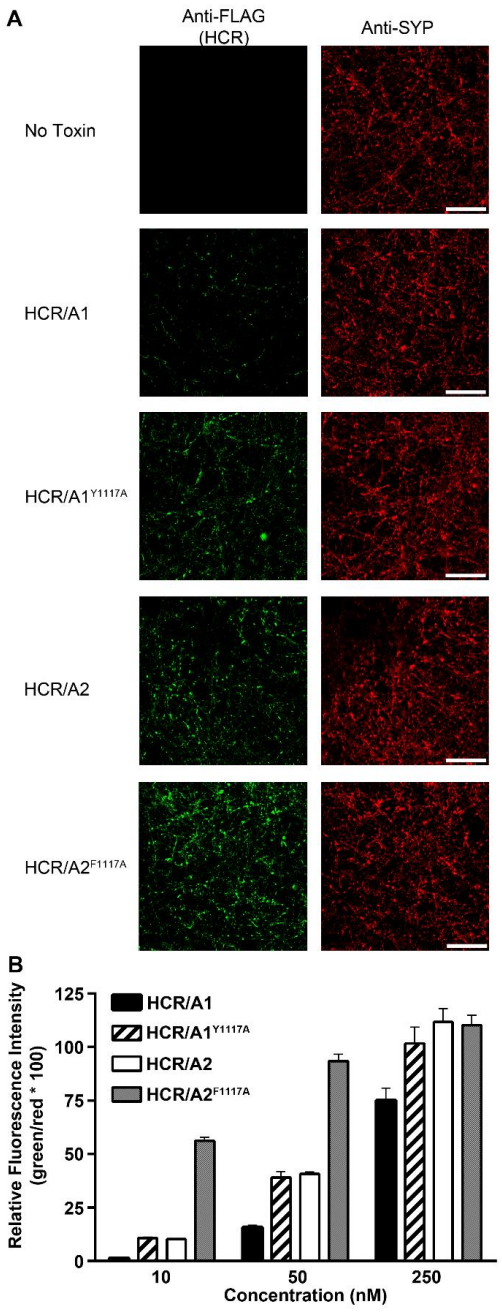

Figure 2.6. HCR/A1^{Y1117A} and HCR/A2^{F1117A} variants enter cells more rapidly than wild type proteins. (A) Primary rat cortical neurons were incubated with the indicated HCR domains [50 nM] for 5 min at 37°C in high K^+ buffer to stimulate vesicle recycling. Cells were washed, fixed, permeabilized, and subjected to immunostaining analysis. Binding of HCR derivatives was detected using an anti-FLAG antibody. Synaptophysin was labeled as a marker for presynaptic terminals. The scale bar represents 10 µm in all panels. **(B)** Quantification of relative binding by individual HCR domains. All values represent the arithmetic mean and standard error of fluorescence intensity from 15 random fields and is representative of 3 biological repeats.

Personal communication from Dr. Michael R. Baldwin.

was similar at ~10 μM concentration (data not shown). In agreement with the *in vitro* binding data, both HCR/A1^{Y1117A} and HCR/A2^{F1117A} bound and entered neurons ~2-4-fold more efficiently than the parental HCR proteins as determined by immunofluorescence assay (**Figure 2.6A-B**), and was further substantiated by Western blotting of cell lysates from intoxicated neurons (**Figure 2.7A**). Next, the ability of HCR derivatives to inhibit the intracellular activity of native BoNT/A1 holotoxin in cortical neurons was tested. As reported previously, cleavage of SNAP25 by BoNT/A1 was inhibited in a dose dependent fashion by HCR/A1, and to a greater efficiency by co-incubation with either HCR/A1^{Y1117A} or HCR/A2 (**Figure 2.7B**) (70,235,238). HCR/A2^{F1117A} was the most effective inhibitor, being ~10-fold more efficient than HCR/A1 (**Figure 2.7B**). Recently, Barbieri and co-workers proposed that a higher degree of receptor occupancy, rather than rates of internalization, may account for the increased cellular toxicity of BoNT/A2 relative to BoNT/A1 (235). It was hypothesized that regions surrounding the ganglioside binding pocket may contribute to affinity, without altering the specificity of HCR/A for gangliosides. Yet, an HCR/A1 variant (QFN1254-1256LYD; IERS1271-1274VGKA) containing the corresponding residues from HCR/A2 bound GT1b *in vitro* with similar affinity to the wild-type HCR/A1 (**Figure 2.8**). While this suggests that non-conserved residues surrounding the ganglioside binding pocket do not directly influence ganglioside binding, we cannot exclude the possibility that such changes between A1 and A2 alter the affinity of the toxins for the membrane bilayer.

2.4.3 A conserved hydrophobic residue plays a key role in recognition of Sia5.

Previous independent studies have argued that BoNT types A, B, E, and F preferentially bind to gangliosides containing Sia5 while TeNT is unique in binding to

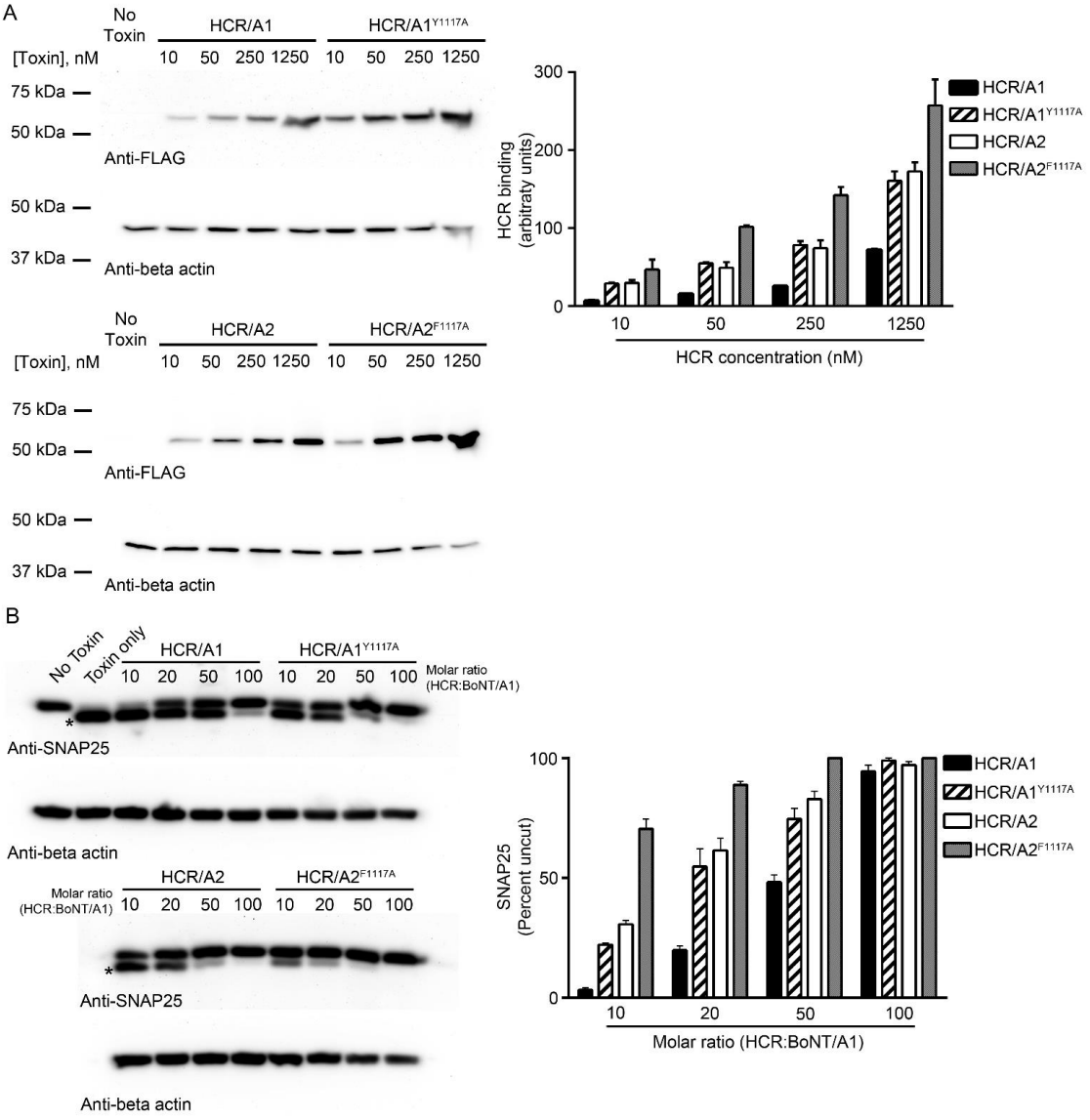

Figure 2.7. HCR derivatives inhibit the activity of BoNT/A1 in primary cortical neurons. (A) *Left panel*, primary rat cortical neurons were exposed to HCRs (indicated concentrations) for 30 min in Neurobasal medium. Cells were washed and further incubated in HCR-free media for 90 min to allow for HCR internalization. Cell lysates (25 µg total protein) were subjected to immunoblot analysis. Cells that were not exposed to toxins served as the control (No Toxin). Beta-actin was detected as an internal control for loading of cell lysates. *Right panel*, HCR binding was quantified by densitometry using AlphaView software and normalized to total beta-actin expression. Densitometry values (arbitrary units) represent the arithmetic mean and standard error of 5 independent experiments. **(B)** *Left panel*, cells were exposed to BoNT/A (5 nM, 5 min) under depolarizing conditions (High K^+ buffer). Cells were then washed and incubated for an additional 24 h in medium alone. Cell lysates (30 µg total protein) were subjected to immunoblot analysis. Cells that were not exposed to BoNT/A1 served as the control (No Toxin), while beta-actin serves as a loading control. Cleavage of SNAP-25 by BoNT/A yielded a smaller fragment that is indicated by an asterisk. *Right panel*, Cleavage of SNAP-25 was quantified by densitometry using AlphaView software. Values represent the arithmetic mean and standard error of 5 independent experiments.

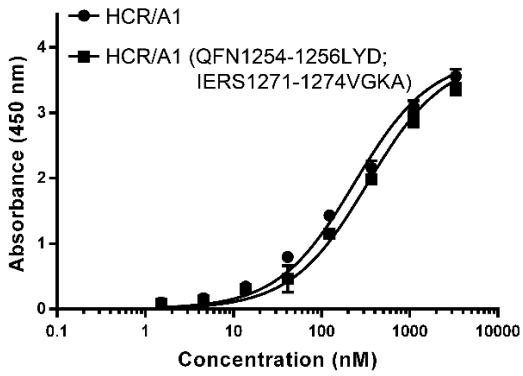

Figure 2.8. HCR/A1 and chimeric HCR/A1-A2 binding kinetics. Various concentrations of either wild-type HCR/A1 or HCR/A1 containing the indicated residues from HCR/A2 were examined for their ability to bind ganglioside GT1b. All values represent the arithmetic mean and standard deviation of at least four independent experiments performed in triplicate.

gangliosides in a Sia5-independent manner (64,239,240). In agreement with these observations, comparative analysis revealed that HCR domains of BoNT serotypes A, B, E, F and TeNT all bound to ganglioside GD1a (Sia5), albeit with moderate differences in binding affinity, while only TeNT efficiently bound to ganglioside GM1a (no Sia5, **Figures 2.9A-B**). This leads to the question of why BoNTs and TeNT differ in their requirement for the Sia5 sugar. Superposition of the HCR/A1-GT1b, HCR/A1-GD1a, HCR/B-GD1a, HCR/F-GD1a, and HCR/T-GT1b analog complexes show that the overall interaction with ganglioside is similar among the toxins (PDB numbers 2VU9, 5TPC, 4KBB, 3RSJ, and 1FV2 respectively). In each case, the GalNAc3-Gal4 moiety is bound at the base of the binding pocket, forming extensive interactions with residues forming the GBM. In contrast, there are large differences at the top of the ganglioside binding cleft, wherein BoNTs contain a series of semi-conserved residues that form a more closed Sia5 binding site. In particular, the BoNTs all contain a hydrophobic residue (phenylalanine in BoNTs A, E, and F; isoleucine in BoNTs B, C, and D) located at the interface of the GBM and the Sia5 pocket that is replaced by threonine in TeNT (**Figure 2.10**).

Substitution of the hydrophobic residue of HCR/A (Phe1252) or HCR/F (Phe1240) with the corresponding isoleucine residue of HCR/B reduced ganglioside binding by 1-2 orders of magnitude, while replacement with either alanine (**Figure 2.11A-B**) or threonine (**Table 2.1**) abolished ganglioside binding. It was not possible to test the role of Phe1214 in HCR/E as mutation of this residue to either alanine, threonine or isoleucine caused the protein to aggregate in solution (data not shown). Next, the effect of mutating HCR/F Phe1240 to alanine was tested in a previously described HCR/F

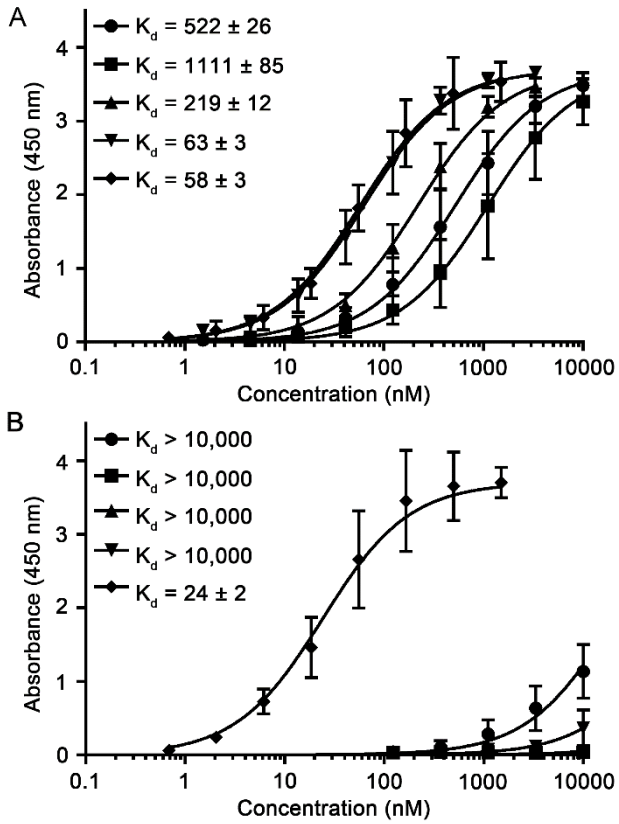

Figure 2.9. Wild-type HCR binding kinetics. Various concentrations of HCR/A1 (●), HCR/B (■), HCR/E (▲), HCR/F (▼) and HCR/T (◆) were examined for their ability to bind ganglioside GD1a **(A)** or GM1a **(B)**. All values represent the arithmetic mean and standard deviation of at least four independent experiments performed in triplicate. K_d values for all HCR derivatives are summarized in **Table 2.1**.

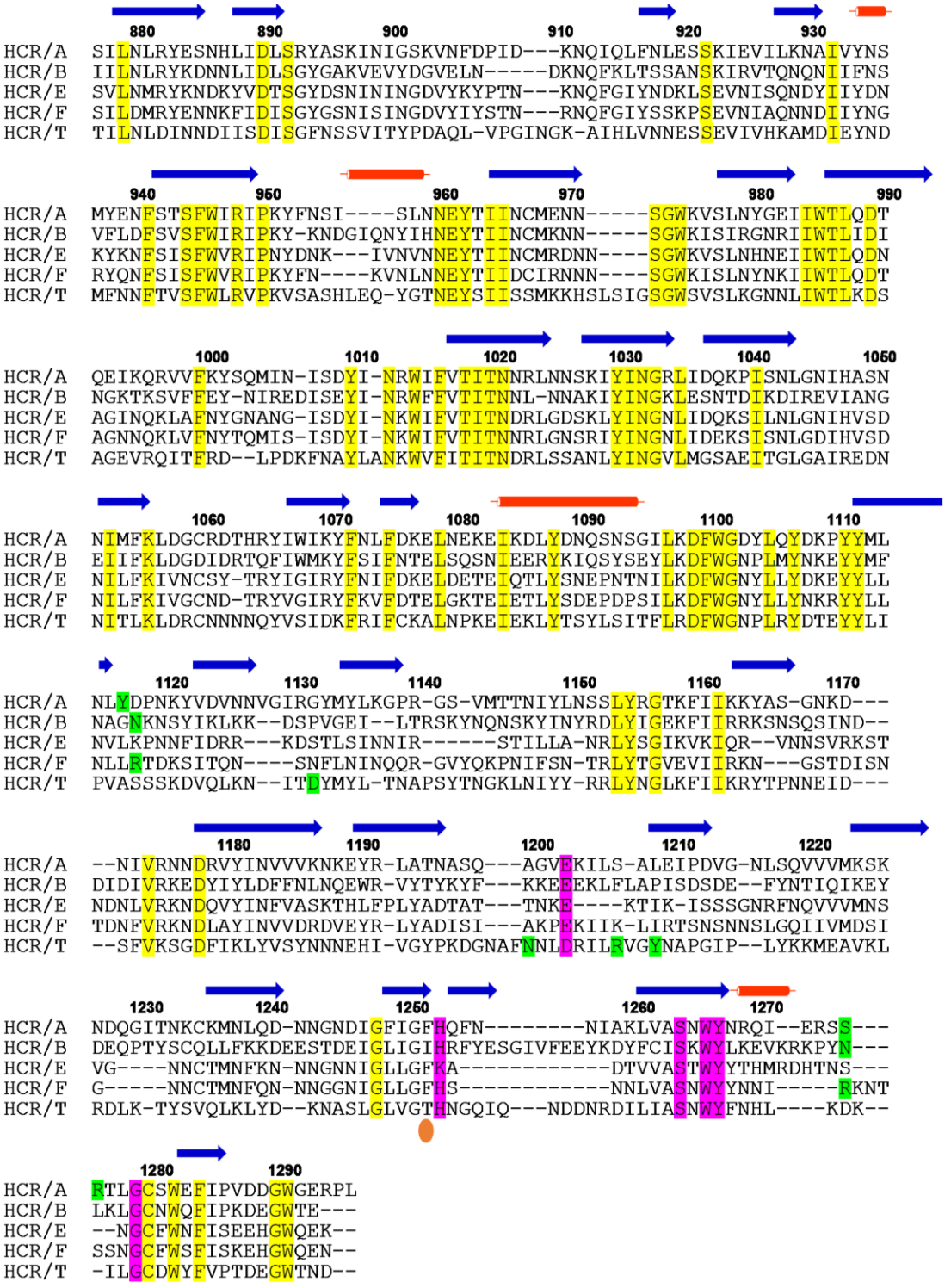

Figure 2.10. Structure based sequence alignment of BoNT (serotypes A, B, E and F) and TeNT HCR domains. HCR residues forming the conserved ganglioside binding motif (GBM) are highlighted in pink, while residues involved in binding specificity are colored in green. The semi-conserved hydrophobic residue unique to the BoNTs is indicated with an orange oval. Conserved residues are colored in yellow.

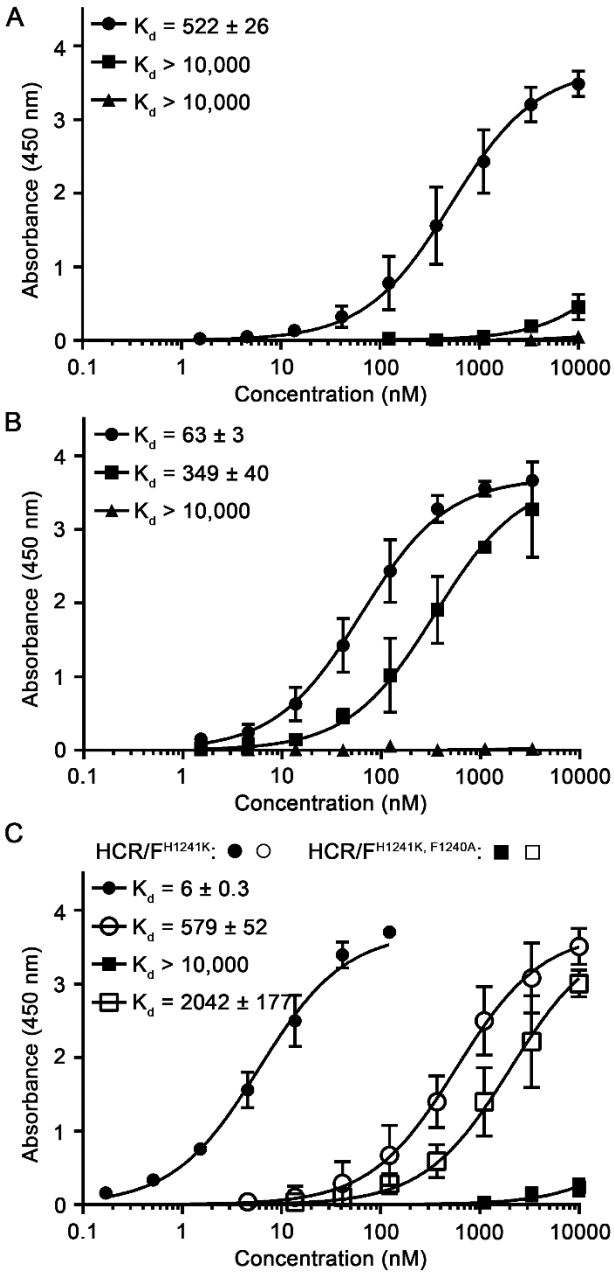

Figure 2.11. A conserved hydrophobic residue facilitates binding at the Sia5 position. Various concentrations of HCR domains were analyzed for their ability to bind GD1a (dark symbols) or GM1a (white symbols) as indicated: **(A)** HCR/A1 (●) or HCR/A1 Phe1252 variants (HCR/A1^{F1252I} ■, HCR/A1^{F1252A} ▲); **(B)** HCR/F (●) or HCR/F Phe1240 variants (HCR/F^{F1240I} ■, HCR/F^{F1240A} ▲); and **(C)** HCR/F^{H1241K} (●/○) or HCR/F$^{H1241K, F1240A}$ (■/□) variant. All values represent the arithmetic mean and standard error of a minimum of three independent determinations performed in triplicate. K_d values for all HCR derivatives are summarized in **Table 2.1**.

variant (H1241K) capable of binding to gangliosides in a Sia5-independent manner (64). Consistent with these observations, HCR/F^{H1241K} bound with high affinity to GD1a and, to a lesser extent, GM1a. In contrast, while HCR/$F^{H1241K, F1240A}$ bound GM1a with similar affinity to HCR/F^{H1241K}, binding to GD1a was not observed (**Figure 2.11C**).

2.4.4 Replacement of isoleucine1239 with phenylalanine increases binding and entry of HCR/B.

While substitution of Ile1239 with alanine or threonine abolished binding to ganglioside GD1a, introduction of the corresponding phenylalanine residue of HCR/A1 and HCR/F increased binding by an order of magnitude (**Figure 2.12A** and **Table 2.1**). Comparative analysis of HCR/B and HCR/B^{I1239F} binding to additional gangliosides demonstrated both wild-type and mutated HCR/B displayed similar specificity, preferentially recognizing gangliosides containing a terminal Gal4-Sia5 linkage (**Figure 2.12A-B**). As an aside, it is noted that the relative affinities of HCR/A1 and HCR/B for GT1b reported herein are similar (483 nM vs. 470 nM, respectively). This observation differs from the previous work of Binz and colleagues who reported that HCR/B bound GT1b with significantly higher affinity than HCR/A1 (58). The source of this discrepancy cannot be explained at this time.

Next, the biological activity of HCR/B^{I1239F} was investigated by monitoring both uptake into neurons and the ability of HCR derivatives to compete with native BoNT/B holotoxin. The binding and entry of HCR/B and HCR/B^{I1239F} into primary cortical neurons was enhanced under depolarizing conditions (high K^+ buffer, **Figure 2.13A**) and is consistent with prior studies which demonstrated that entry of BoNT/B is mediated by

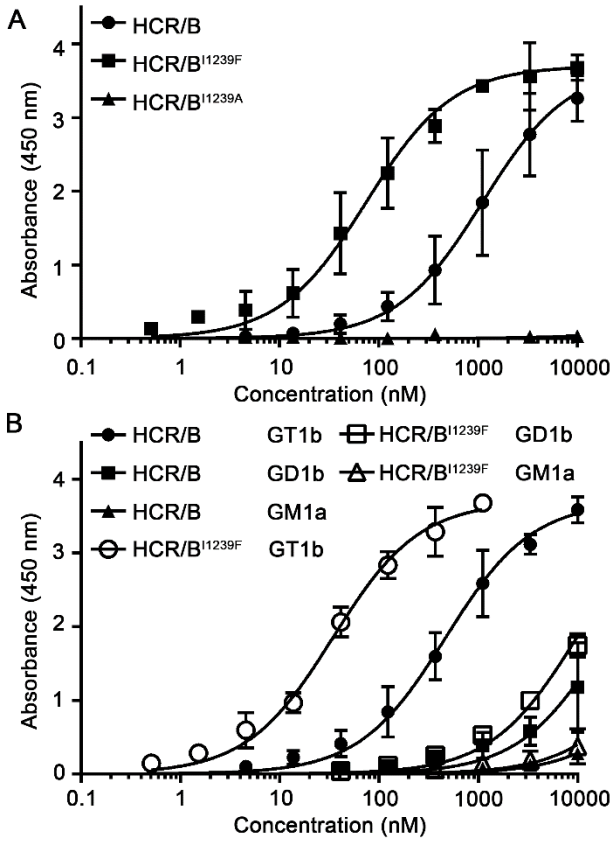

Figure 2.12. HCR/B^{I1239F} binds gangliosides with greater affinity than wild-type HCR/B. (A) HCR/B (●) or HCR/B Ile1239 variants (HCR/BI^{1239F} ■, HCR/B^{I1239A} ▲) were analyzed for their ability to bind GD1a. **(B)** The ganglioside binding specificity of HCR/B (black symbols) or HCR/B^{I1239F} (white symbols) was compared using gangliosides GT1b (●/○), GD1b (■/□) and GM1a (▲/△). All values represent the arithmetic mean and standard error of a minimum of three independent determinations performed in triplicate. K_d values for all HCR derivatives are summarized in **Table 2.1**.

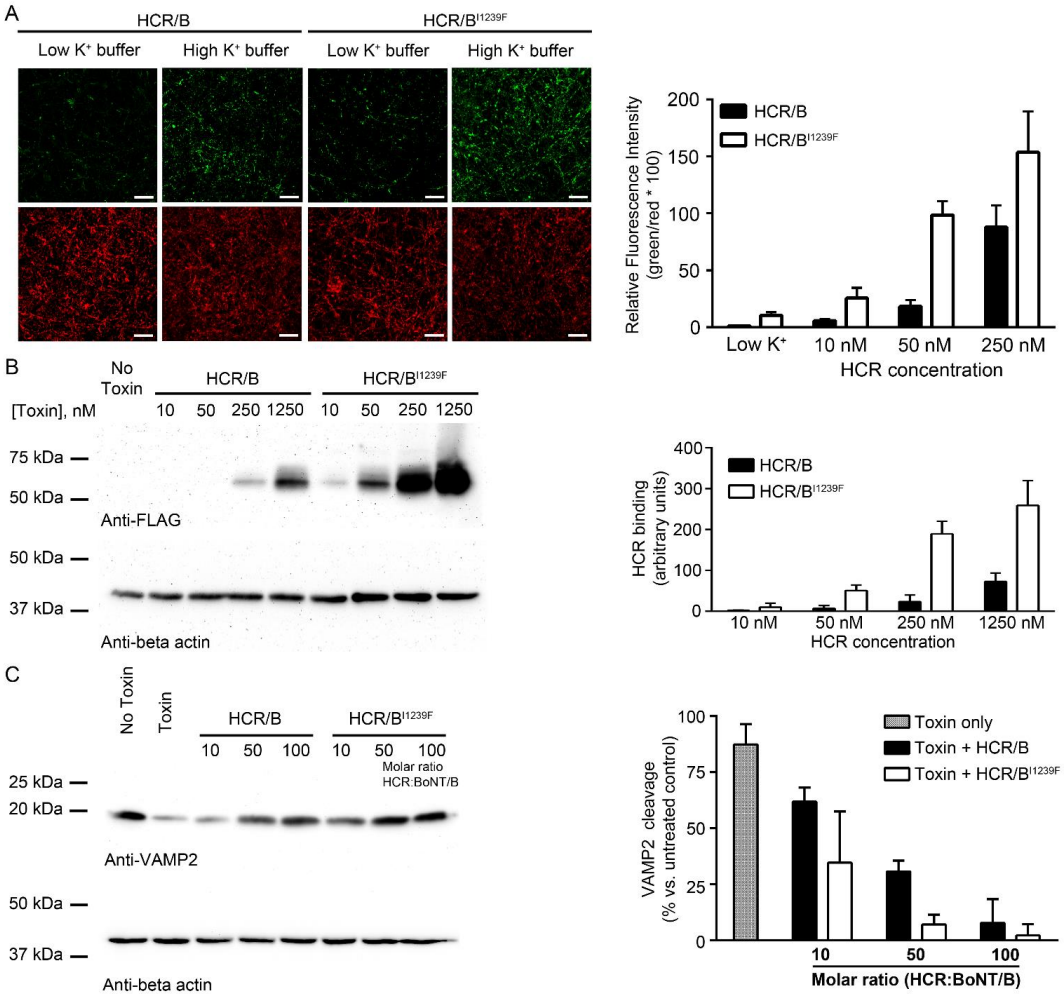

Figure 2.13. HCR/B^{I1239F} binds and enters cells more efficiently than wild-type HCR/B. (A) *Left panel*, primary rat cortical neurons were exposed to HCR/B or HCR/B^{I1239F} (50 nM, 5 min) in either low K^+ buffer (to mimic the resting state) or high K^+ buffer to stimulate vesicle recycling. Cells were washed, fixed, permeabilized, and subjected to immunostaining analysis. Binding of HCR derivatives was detected using an anti-FLAG antibody. Synaptophysin was labeled as a marker for presynaptic terminals. The scale bar represents 10 µm in all panels. *Right panel*, quantification of relative binding by HCR domains at the indicated concentrations. HCR concentration in low K^+ buffer was 50 nM. All values represent the arithmetic mean and standard error of fluorescence intensity from 15 random fields and is representative of 2 biological repeats. **(B)** *Left panel*, primary rat cortical neurons were exposed to HCRs (indicated concentrations) for 30 min in Neurobasal medium. Cells were washed and further incubated in HCR-free media for 90 min to allow for HCR internalization. Cell lysates (25 µg total protein) were subjected to immunoblot analysis. Cells that were not exposed to HCR served as the control (No Toxin). Beta-actin was detected as an internal control for loading of cell lysates. *Right panel*, HCR binding was quantified by densitometry using AlphaView software and normalized to total beta-actin expression. Densitometry values (arbitrary units) represent the arithmetic mean and standard error of 5 independent experiments. (**C**) *Left panel*, cells were exposed to BoNT/B (5 nM, 5 min) under depolarizing conditions (High K^+ buffer). Cells were then washed and incubated for an additional 24 h in medium alone. Cell lysates (30 µg total protein) were subjected to immunoblot analysis. Cells that were not exposed to BoNT/B served as the control (No Toxin), while beta-actin serves as a loading control. Cleavage of VAMP2 by BoNT/B results in a loss of detectable signal on Western blotting. *Right panel*, Cleavage of VAMP2 was quantified by densitometry using AlphaView software and expressed relative to no toxin control. Values represent the arithmetic mean and standard error of 5 independent experiments.

synaptotagmins I and II (77,241). In accord with the ganglioside binding data, binding and entry of HCR/B^{I1239F} was enhanced ~10-fold relative to wild-type HCR/B as judged by immunofluorescence assay and Western blotting (**Figure 2.13A-B**). A competition assay showed that HCR/B^{I1239F} competed with native BoNT/B for neuronal binding more effectively that wild-type HCR/B (**Figure 2.13C**), signifying that introduction of the Ile1239Phe mutation into BoNT/B would increase toxin potency. Collectively, the data presented in **Figures 2.11-2.13** suggest the semi-conserved hydrophobic residue within the BoNTs plays an important role in the recognition of Sia5.

2.4.5 Engineering of a TeNT variant dependent on Sia5 for ganglioside binding.

The observation that TeNT binds to gangliosides GD1a and GM1a with near identical affinity argues that Sia5 does not contribute to interaction in a significant way. Therefore, we reasoned that by altering the Sia5 binding pocket of TeNT to more closely resemble that of the BoNTs, it should be possible to induce interactions with Sia5. However, initial replacement of Thr1270 with phenylalanine completely ablated binding to both GD1a and GM1a (**Figure 2.14A**). As a result, additional substitutions were introduced into TeNT designed to increase interactions with Sia5. Firstly, Ser1135 was replaced with arginine, which in the HCR/F-GD1a complex forms a hydrogen bond to Sia5 in addition to forming hydrophobic interactions between the aliphatic region of the side chain and the sugar ring. At the same time, Ala1134 was replaced with the corresponding leucine from HCR/F to help support the positioning of the Arg1135 side chain as well as to increase the overall hydrophobicity of the region. As shown in **Figure 2.14B**, the introduced substitutions (HCR/T$^{A1134L, S1135R, T1270F}$) restored binding to GM1a

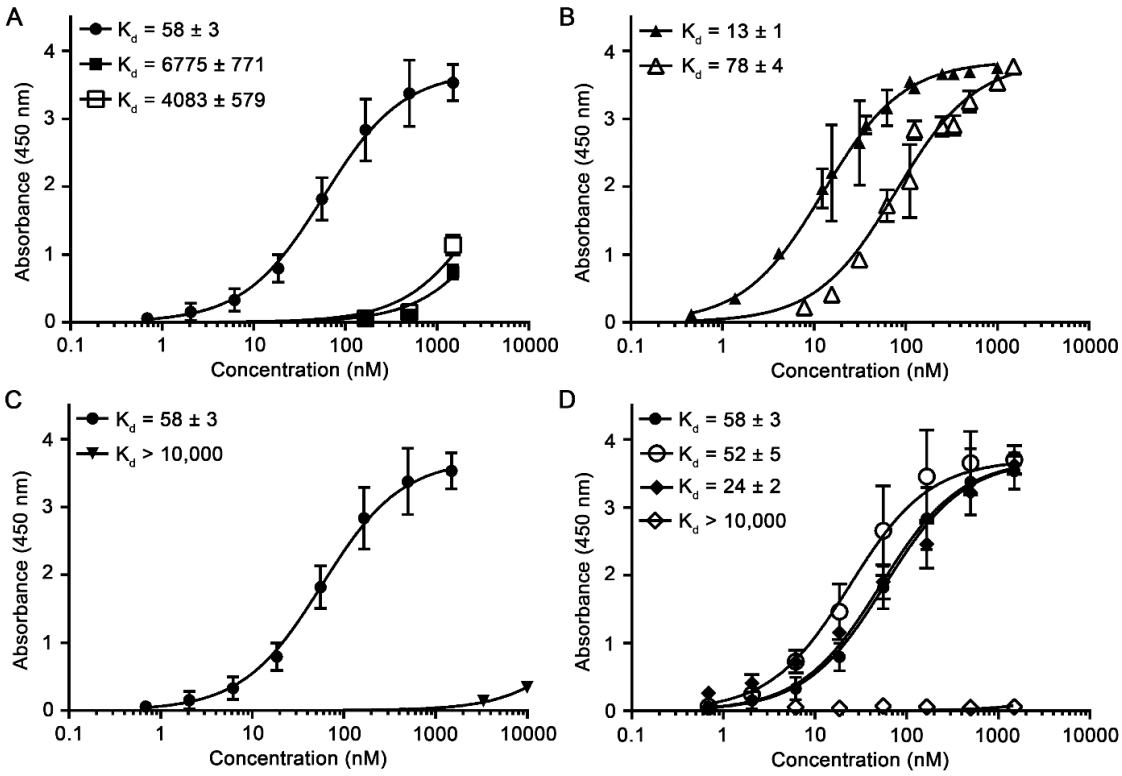

Figure 2.14. A TeNT variant that binds specifically to gangliosides containing a Sia5 moiety. Various concentrations of HCR derivatives were analyzed for their ability to bind gangliosides GD1a (black symbols) or GM1a (white symbols) as indicated: **(A)** HCR/T (●) or HCR/T^{T1270F} (■/□); **(B)** HCR/$T^{A1134L, S1135R, T1270F}$ (▲/△); **(C)** HCR/T (●) or HCR/T-$_{A\ Loop}$ (▼); and **(D)** HCR/T (●/○) or HCR/$T^{A1134L, S1135R, T1270F}$-$_{A\ Loop}$ (◆/◇). All values represent the arithmetic mean and standard error of a minimum of three independent determinations performed in triplicate. K_d values for all HCR derivatives are summarized in **Table 2.1**.

and caused a modest increase in affinity for GD1a as compared to wild-type TeNT. BoNT/F makes an additional interaction with Sia5 through a non-conserved arginine residue (Arg1256). While direct replacement of the corresponding position was considered, differences in the orientation of the loop linking α-helix 4 with β-strand 30 (residues 1294-1302) of HCR/T relative to HCR/F suggested this was not feasible. Therefore, it was decided to replace the entire loop region of HCR/T with the equivalent sequence of HCR/F. However, HCR/T$^{A1134L,\ S1135R,\ T1270F}$-$F_{Loop}$ and HCR/T$^{A1134L,\ S1135R,\ T1270F}$ did not differ in affinity for gangliosides GD1a or GM1a (data not shown). Based on this observation, additional exchanges were performed using the corresponding loop regions of BoNTs A (residues 1270-1279), B (residues 1267-1279), and E (residues 1228-1237). Among these chimeric proteins, HCR/T$^{A1134L,\ S1135R,\ T1270F}$-$A_{Loop}$ variant was stable upon purification and therefore suitable for further investigation. Unexpectedly, while HCR/T$^{A1134L,\ S1135R,\ T1270F}$-$A_{Loop}$ bound to GD1a with similar affinity as HCR/T, binding to GM1a was not observed (**Figure 2.14C**). The reason for the specific loss of GM1a binding is not clear. However, insertion of the A loop alone is sufficient to disrupt binding to ganglioside (**Figure 2.14D**), suggesting that the overall structure of the Sia5 binding site plays a key role in regulating binding to gangliosides.

2.5 Discussion

Clostridial neurotoxins (CNTs) bind and enter nerve terminals via interactions with synaptic vesicle resident proteins and an array of complex gangliosides present on the presynaptic membrane (48,62,70-73,77,242-247). In this classical double receptor model (248), the carbohydrate components of gangliosides are suggested to act as the

initial attachment sites for the toxin due to their high local concentration on the presynaptic membrane and high lateral mobility. The carbohydrate moiety itself binds in a shallow groove formed by the ganglioside binding motif (GBM; E/D…H/K…SXWY…G), located at the distal tip of the HCR domain (63,64,231,232). While this motif is essential for ganglioside recognition, it does not fully account for differences in both the affinity and specificity of individual CNTs towards a subset of gangliosides (64,231,232). In this study, we aimed to understand the basis by which CNTs discriminate between the carbohydrate moieties of individual gangliosides. Our data support a model in which recognition of Sia5 by BoNTs is driven primarily through hydrophobic interactions between the protein and the sugar moiety.

A recent study by Stenmark, Widmalm, and co-workers identified the terminal carbohydrate branch of GD1a ([α-Neu5Ac-(2→3)]-β-Gal-(1→3)-β-GalNAc-) as the active moiety that binds with a high degree of propensity to BoNT/A1 (249). Molecular docking simulations using carbohydrate fragments of GD1a revealed that a *galacto*-configured sugar (Gal or GalNAc) preferentially binds at a subsite formed by the conserved His1253 and Trp1266 residues of the GBM (denoted as subsite B, **Figure 2.15A**). Ligands carrying a terminal Sia-α(2→3)-Gal moiety also occupy site B, with the Sia sugar largely occupying the adjacent A subsite largely defined by Tyr1117 and Phe1252 (denoted site A in **Figure 2.15A**) (249). These findings are consistent with earlier studies of ganglioside binding by BoNT/A1 (240,250,251), in addition to the data provided here for HCR/A1 and HCR/A2 (summarized in **Table 2.1**). Similarly, HCR/B, HCR/E, and HCR/F, but not HCR/T, also show specificity towards gangliosides

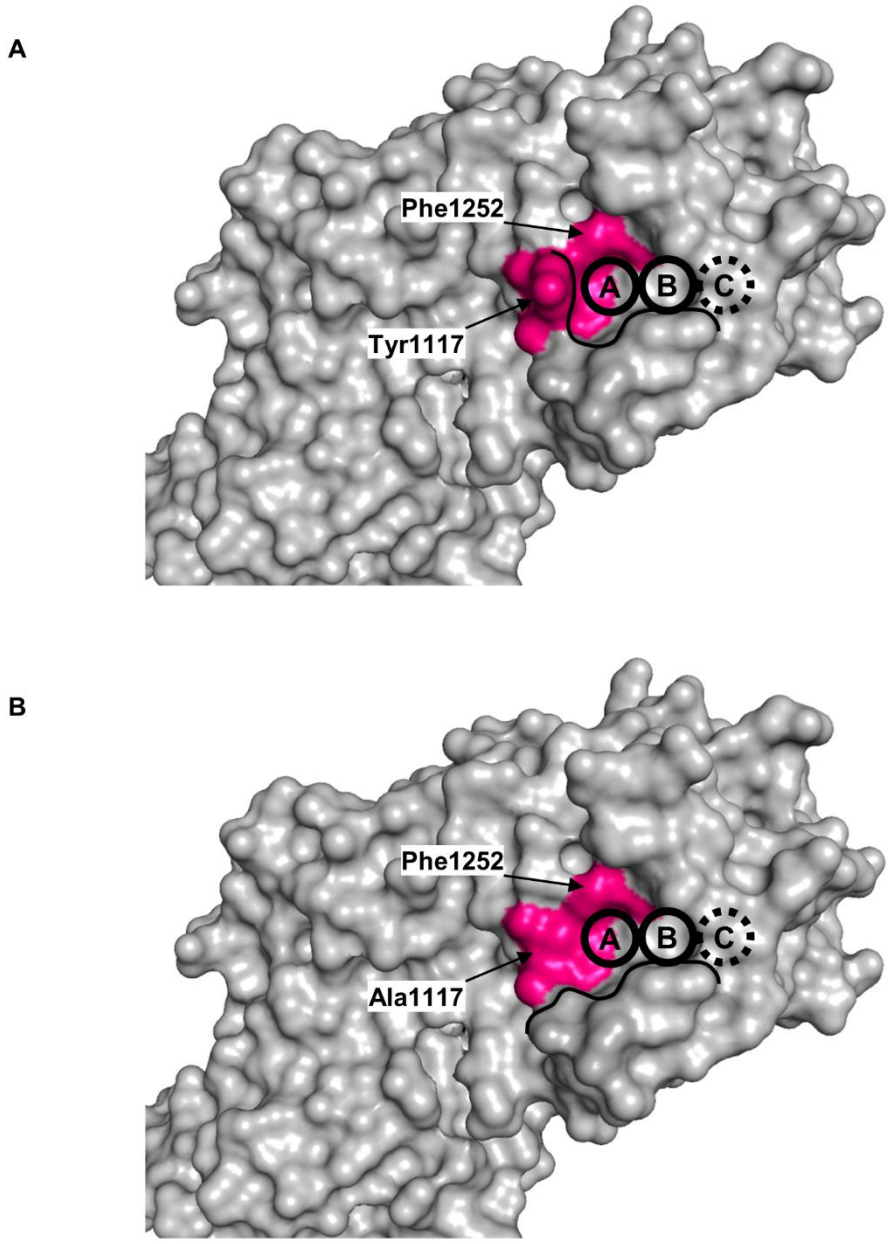

Figure 2.15. Ganglioside binding pocket of HCR/A1. Surface representation (grey color) of HCR/A1 **(A)** and HCR/A1^{Y1117A} **(B)**. The ganglioside binding pocket with defined subsites (A-C) is highlighted using dark circles. The positions of Tyr1117/Ala1117 and the semi-conserved hydrophobic residue (Phe1252 for HCR/A1) that largely define the A subsite are colored pink.
"Adapted with permission from Hamark, C.; Berntsson, R. P.; Masuyer, G.; Henriksson, L. M.; Gustafsson, R.; Stenmark, P.; Widmalm, G., Glycans Confer Specificity to the Recognition of Ganglioside Receptors by Botulinum Neurotoxin A. *Journal of the American Chemical Society* **2017,** *139* (1), 218-230. Copyright (2017) American Chemical Society."

containing a terminal Sia5-Gal4 moiety (i.e., GT1b and GD1a, **Figures 2.9 and 2.12**, **Table 2.1**). Thus, these data further support the model of Stenmark, Widmalm, and co-workers, wherein the carbohydrate moiety of gangliosides is responsible for determining specificity of binding.

Given the high degree of sequence and structural conservation in the ganglioside binding pockets of TeNT and the BoNTs, how does one account for the observed differences in specificity of binding? Insight into this question has emerged in recent years with the determination of the solution structures of several HCR domains in complex with analogs of ganglioside carbohydrate moieties (63,64,231,232). It was previously reported that substitution of two arginine residues in HCR/F (Arg1111 and Arg1256)—which form hydrogen bonds to Sia5—reduced affinity towards GD1a by ~70-fold (64). While these arginine residues are not conserved, structural data suggested other BoNT serotypes possessed additional residues located outside of the GBM that performed analogous functions. In particular, structural data suggested HCR/A1 Tyr1117 and Ser1275 form hydrogen bonds (two and one, respectively) to Sia5 which, in conjunction with additional hydrophobic interactions, were proposed to stabilize binding to GT1b (231). However, mutational analysis of HCR/A1 and HCR/A2 suggested that both Tyr1117 and Ser1275 make only minimal contributions to ganglioside binding (**Figure 2.4** and **Table 2.1**). This is further supported by the recent crystal complex data showing different hydrogen bonding networks for Sia5 between the HCR/A●GT1b, HCR/A1●GD1a, and HCR/A1●sialyl-T antigen complexes (231,249). Though it cannot be excluded that packing of Sia5 against the tyrosyl ring of HCR/A1 Y1117 is important for binding, this argument is weakened by the observation that alanine replacement

improved affinity for GT1b and GD1a *in vitro*, accelerated uptake into neurons, and increased neuronal toxicity, as judged by competition assay (**Figures 2.4**, **2.6**, and **2.7**). These data are in agreement with a previously described BoNT/A1^{Y1117A} variant and can now be extended to BoNT/A2 (237). While the mechanistic basis for this change is unclear, it should be noted that in both the HCR/A●GT1b and HCR/A1●GD1a complexes, Tyr1117 rotates around the C-beta C-gamma bond to accommodate Sia5 upon binding (231,249); this may suggest that the interaction of the tyrosyl side chain with the Sia5 group is energetically unfavorable and therefore reduces overall binding affinity. Indeed, modeling of the HCR/A1^{Y1117A} variant suggests the removal of the ring structure expands the ganglioside binding pocket, potentially providing lower constraints on the conformations Sia5 can adopt within the A subsite (**Figure 2.15B**).

The observation that alanine replacement of HCR/F Arg1111 and Arg1256 reduced affinity towards GD1a without ablating binding (64), suggested that hydrophobic interactions between the protein and Sia5 could be important to stabilize ganglioside binding. Structural alignment of CNT HCR domains identified a semi-conserved hydrophobic residue within the BoNTs (Phe in BoNTs A, E, and F; Ile in BoNTs B, C, and D) that shapes the A subsite of the ganglioside binding pocket. Replacement of the phenylalanine residues of HCR/A1 and HCR/F (Phe1252 and Phe1240 respectively) with the corresponding isoleucine residue of HCR/B caused a 1-2 log decrease in binding to GD1a, while substitution with alanine abolished binding (**Figures 2.11A-B**). While alanine replacement of Ile1239 in HCR/B caused a similar ablation of binding, HCR/B^{I1239F} bound GT1b and GD1a ~10-fold more efficiently than wild-type HCR/B (**Figure 2.12** and **Table 2.1**). Similar to HCR/A1^{Y1117A}, the increased affinity of

HCR/B^{I1239F} for gangliosides *in vitro* also resulted in accelerated entry into neurons and greater toxicity as judged by the ability to compete with BoNT/B holotoxin for binding and entry (**Figure 2.13**). CD spectroscopy of wild-type and mutated HCR variants revealed only minor differences in the respective spectra, arguing that changes in ganglioside binding were not the result of major changes in protein secondary structure (**Figure 2.3**). These data argue that BoNT/B^{I1239F} will possess greater toxicity *in vivo*, potentially expanding its clinical efficacy in the treatment of neurologic conditions. Furthermore, these observations highlight the need to fully characterize the biological activities of subtype variants, as individual amino acid changes can have unexpected effects on toxin activity.

Finally, a variant of TeNT was engineered that was dependent on Sia5 for ganglioside binding. While HCR/T^{T1270F} displayed a large decrease in affinity for ganglioside, further substitutions designed to increase the overall hydrophobicity of the A subsite (Ala1134Leu and Ser1135Arg) restored binding to near wild-type levels (**Figures 2.14A-B**). Thus, while the conserved hydrophobic residue present in the BoNTs appears to play a key role in the recognition of Sia5, it does not appear to be the sole determinant of ganglioside binding specificity. In agreement with this statement was the observation that replacement of the short loop linking α-helix 4 with β-helix 30 (residues 1294-1302) of HCR/T with the corresponding region from HCR/A1 was sufficient to disrupt the ability to bind ganglioside GM1a without affecting binding to GD1a (**Figure 2.14D**).

In summary, these studies provide new insights into the mechanism of ganglioside recognition by individual clostridial neurotoxins and suggest that the specificity of ganglioside binding is determined in large part through the interaction of the Sia5 sugar

with the hydrophobic A subsite of the ganglioside binding pocket. Understanding the mechanisms of ganglioside recognition opens up the possibility of generating novel toxin variants with improved and/or expanded clinical potential.

CHAPTER 3: A POTENTIAL ROLE FOR CYTOSOLIC FACTORS IN TETANUS NEUROTOXIN TRANSLOCATION

3.1 Introduction

Protein translocation into or across lipid membranes is not only a central problem in cellular biology, but also represents an essential step in the intoxication process of numerous bacterial AB toxins (252). In some cases (e.g. cholera toxin, pertussis toxin) protein translocation is achieved by exploitation of aspects of the ER-associated protein degradation pathway (1,253), but in other cases (e.g. diphtheria toxin, anthrax toxin, clostridial neurotoxins), the translocation machinery is built into the B moiety itself, as established by the ability to translocate the A component across a planar lipid bilayer without the use of host cell components (80,254,255). How then, do such toxins achieve translocation? It is speculated that upon exposure to conditions prevalent within the endosomal lumen, the toxin undergoes large conformational changes which drive the integration of the B moiety into the membrane, resulting in the formation of an ion-conducting pore (256,257). While the pore lumen is often proposed to act as a channel through which the A moiety passes, this has only been conclusively demonstrated for anthrax toxin (257). In fact, accumulating evidence suggests that unlike anthrax toxin—which forms a multimeric pore structure within the membrane (258)—the clostridial neurotoxins and diphtheria toxin translocate the A component using alternative strategies (259,260). Thus, determining the atomic resolution structures of AB toxins inserted into the membrane bilayer will provide new insights into the divergent strategies employed by these molecules to facilitate A subunit translocation.

The seven serotypes of botulinum neurotoxin (BoNTs A-G) and tetanus neurotoxin (TeNT) are collectively known as the clostridial neurotoxins (CNTs), and are the causative agents of botulism and tetanus, respectively (12-18). The CNTs are prototypical AB toxins, consisting of two major domains: an N-terminal ~50-kDa zinc-dependent protease domain (light chain, LC, A subunit), and a C-terminal ~100-kDa heavy chain (HC, B subunit) domain. The heavy chain can be further divided into an ~50-kDa N-terminal translocation domain (HCT) and an ~50-kDa C-terminal receptor binding domain (HCR) (13,46-49). Initially produced as ~150-kDa single chain proteins, they undergo proteolytic processing into disulfide-linked di-chain proteins (1,28,46).

In order for the LC to cleave its cellular target(s), neuronal SNARE proteins, it must first be translocated across the endosomal membrane and released from the remainder of the toxin. Although not well characterized for any member of the CNT family, translocation of the LC is believed to be mediated by the HCT domain. The prevailing model is that acidic lipids facilitate the close interaction between this domain and the endosomal membrane, driving insertion of the HCT domain and forming a pore through which the LC can be translocated (82). However, before this interaction can occur, a number of low pH-induced conformational changes must occur (12,80-82). There is evidence that the orientation of the CNT domains at neutral pH acts to prevent premature insertion of the HCT domain into membranes. More specifically, both the LC and HCR domains appear to independently prevent the formation of pores by the HCT domain at neutral pH. This may be important, as the HCT domain alone has been shown to be capable of forming pores, regardless of pH (81-89). In addition to releasing this inhibition, low pH is also thought to be responsible for inducing partial unfolding of the

LC, which is necessary for its translocation. Therefore, it appears as if the CNTs are uniquely designed to undergo structural changes necessary for concerted translocation at low pH.

Once exposed to the host cell cytosol, the disulfide bond linking the LC to the HCT domain must be reduced and the protein must re-fold into its native conformation. Previous studies utilizing small molecule inhibitors have identified cytosolic factors that are likely involved in these steps (261,262). Notably, the thioredoxin/thioredoxin-reductase redox (Trx/TrxR) system has been shown to be responsible for reduction of the disulfide. While not directly shown to be responsible for LC re-folding, CNT activity requires the presence of heat shock protein 90 (HSP90) (261,262). Given that this protein is a chaperone, it would logically follow that it assists with this function.

Might other cytosolic factors contribute to CNT intoxication? Interestingly, both of these cytosolic factors are components of a cytosolic translocation factor (CTF) complex necessary for translocation of diphtheria toxin (DT) (263). Such a coincidence may suggest that this CTF complex is a shared component necessary for AB toxin function. If this is the case, then additional components of this CTF complex may associate with CNT HCT domains. It would also be informative to determine what residues within the CNT HCT are important for recruitment of this complex.

An additional component of the DT CTF complex, COPG, was recently identified. COPG is a member of the heptameric COPI complex, which is involved in retrograde vesicular trafficking (264). Investigation of putative transmembrane regions in the DT translocation domain (DTT) yielded a 10-aa leucine-containing motif that was thought to be responsible for recruitment of the CTF complex. Interestingly, this motif appeared to

be semi-conserved between DT and other AB toxins, such as anthrax toxin and the CNTs (265). Upon further investigation, it was determined that interaction with COPG was actually mediated by basic lysine residues in the vicinity of this proposed motif (264). TeNT contains two regions similar to these lysine-containing regions in DT. For the purposes of this study, the first region will be referred to as Motif 1 (M1; aa K720, K723, K725, K736, R737) and the second, Motif 2 (M2; aa K845, K846, K850, K853).

In the present study, we hypothesized that upon endosomal insertion, cytosol-exposed residues within the TeNT translocation domain recruit a cytosolic translocation factor complex—similar to that employed by DT—to facilitate the translocation of LC.

3.2 Experimental Procedures

3.2.1 Expression, purification, and dye-labeling of recombinant TeNT HCT proteins.

A modified pET28a expression vector (Millipore Sigma, Billerica, MA, USA)—hereafter referred to as pET28-3×FLAG (containing a 3×FLAG epitope immediately downstream of the hexahistidine epitope tag) —was used as the expression vector for TeNT HCT and DTT proteins (233).

E. coli codon-optimized TeNT HCT (aa 555-868) DNA was synthesized via polymerase chain reaction using the TeNT holotoxin gene as a template. Primers included the Strep-tag II® epitope immediately downstream of the HCT gene. This PCR product was then cloned into pET28-3×FLAG via appropriate restriction endonuclease sites (SacI/XhoI). Site specific cysteine residues were introduced into the TeNT HCT sequence by site-directed mutagenesis using the Quikchange® Lightning Site-Directed

Mutagenesis Kit (Agilent Technologies, Santa Clara, CA, USA) and confirmed by automated DNA sequencing.

For purification of HCT proteins containing cysteine mutations, *E. coli* BL-21 AI (Thermo Fisher Scientific) harboring TeNT HCT constructs was inoculated into 50 ml of Turbo Prime-olate (Athena Environmental Sciences, Inc. Baltimore, MD, USA) supplemented with kanamycin and antifoam reagent (Antifoam 204, Millipore Sigma) for 6 hours at 37ºC and 300 r.p.m. (an OD_{600} of ~0.6). Isopropyl β-D-1-thiogalactopyranoside (IPTG) and arabinose were added to final concentrations of 1 mM and 0.2% w/v, respectively. Incubation was continued overnight following temperature reduction to 16ºC. Bacterial cells were harvested by centrifugation at 5000 ×*g* for 25 min at 4ºC, lysed by French press, and clarified by centrifugation at 14000 ×*g* for 15 min at 4ºC. Lysates were filtered through a 0.22-μm cellulose acetate syringe type filter prior to column chromatography. Ni^{2+}-nitrilotriacetic acid (NTA) agarose (Qiagen, Germantown, MD, USA) affinity chromatography was performed before labeling with a 25-fold molar excess of IANBD amide (Setareh Biotech, Eugene, OR, USA) at 4°C overnight. Following quenching with 1 mM glutathione, proteins were further purified via Strep-Tactin® chromatography and stored at 4°C until use (**Figure 3.1**).

For the diphtheria toxin translocation domain (DTT, aa 202-378), DNA was synthesized via polymerase chain reaction using an *E. coli* optimized diphtheria toxin gene as a template. Primers included the Strep-tag II® epitope immediately downstream of the HCT gene. This PCR product was then cloned into pET28-3×FLAG via appropriate restriction endonuclease sites (SacI/XhoI).

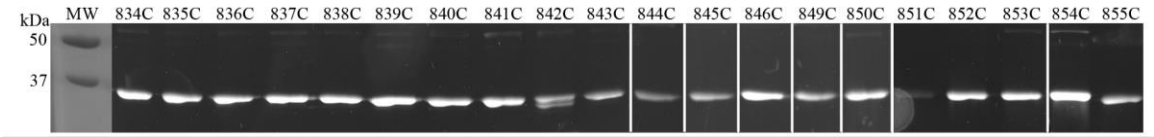

Figure 3.1. Representative gel of IANBD-labeled HCT/T proteins containing cysteine mutations. Representative IANBD-labeled variant HCT/Ts (2 μg) were resolved by SDS-PAGE and visualized by ultraviolet excitation. Unless otherwise stated, all proteins employed in this study were stably expressed and estimated to be at least 90% pure as determined by SDS-PAGE followed by visualization with Coomassie Blue.

E. coli BL-21 AI harboring wild-type HCT/T or DTT was inoculated into LB supplemented with kanamycin and antifoam reagent for 6 hours at 37ºC and 300 r.p.m. (an OD_{600} of ~0.6). Isopropyl β-D-1-thiogalactopyranoside (IPTG) and arabinose were added to final concentrations of 1 mM and 0.2% w/v, respectively. Incubation was continued overnight following temperature reduction to 16ºC. Bacterial cells were harvested by centrifugation at 5000 ×*g* for 25 min at 4ºC, lysed by French press, and clarified by centrifugation at 14000 ×*g* for 45 min at 4ºC. Lysates were filtered through a 0.22-µm cellulose acetate syringe type filter prior to column chromatography. Proteins were purified via sequential Ni^{2+}-nitrilotriacetic acid (NTA) agarose (Qiagen) and Strep-Tactin® affinity chromatography, and then stored at 4°C until use (**Figure 3.2**).

3.2.2 Expression and purification of recombinant TeNT holotoxin proteins.

DNA encoding TeNT was amplified by polymerase chain reaction using appropriate primers and cloned into the pHis1522 expression vector (MoBiTech, Göttingen, Germany) using appropriate restriction endonuclease sites (BsrGI/EagI), resulting in a fusion protein containing N-terminal His_6 and C-terminal Strep-tag II® epitopes. Site specific lysine residues were mutated in the native TeNT sequence by site-directed mutagenesis using the Quikchange® Lightning Site-Directed Mutagenesis Kit (Agilent Technologies) and confirmed by automated DNA sequencing. The following mutations were made to produce $TeNT^{M1}$ (aa K720S, K723V, K725N, K735A, R736A), $TeNT^{M2}$ (aa K845A, K846A, K850A, K853A), and $TeNT^{M1M2}$ (aa K720S, K723V, K725N, K735A, R736A, K845A, K846A, K850A, K853A). Proteins were expressed using the *Bacillus megaterium* expression system as described previously (266,267), and

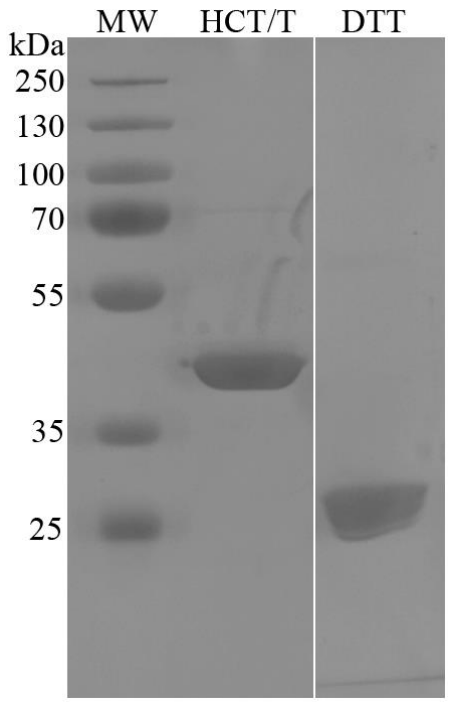

Figure 3.2. Representative gel showing purified HCT/T and DTT proteins. Representative HCT/T and DTT proteins (5 μg) were resolved by SDS-PAGE and visualized by staining with Coomassie Blue. Unless otherwise stated, all proteins employed in this study were stably expressed and estimated to be at least 90% pure as determined by SDS-PAGE followed by visualization with Coomassie Blue.

were purified by sequential chromatography using Ni^{2+}-NTA agarose and StrepTactin® sepharose. Peak fractions were concentrated using an Amicon filtration device (Ultracel-30 type filter), dialyzed into PBS, and stored at -80°C until use (**Figure 3.3**).

3.2.3 Culture of primary rat cortical neurons.

Rat embryonic day 18 (E18) cortices (Brainbits, LLC, Springfield, IL, USA) were mechanically dissociated and plated in Neurobasal medium supplemented with B-27 (Thermo Fisher Scientific) on poly-D-lysine coated plates. Half of the culture medium was changed with fresh Neurobasal medium every 4 days starting on day 5.

3.2.4 Liposome preparation.

Liposomes were freshly prepared by the freeze-thaw and extrusion method as described previously (268). A 1:4 molar ratio of POPA:POPC lipid (30 mg total lipid) dissolved in chloroform was dried under a gentle stream of nitrogen, and placed under vacuum overnight to remove residual solvent. The dried lipid cake was hydrated in potassium buffer (10 mM HEPES-KOH, 150 mM KCl, 1 mM EDTA, pH 7.4) to a final concentration of 30 mg/ml by brief sonication at 42°C. The rehydrated lipid was then subjected to three cycles of rapid freeze-thaw, followed by extrusion through a 200-nm pore membrane (Nucleopore) using a mini-extruder apparatus (Avanti Polar Lipids, Alabaster, AL, USA). Immediately prior to use, liposomes were exchanged into neutral potassium free buffer (10 mM HEPES-KOH, 150 mM NaCl, 1 mM EDTA, pH 7.4) by passage over a pre-equilibrated column of G-25 Sephadex.

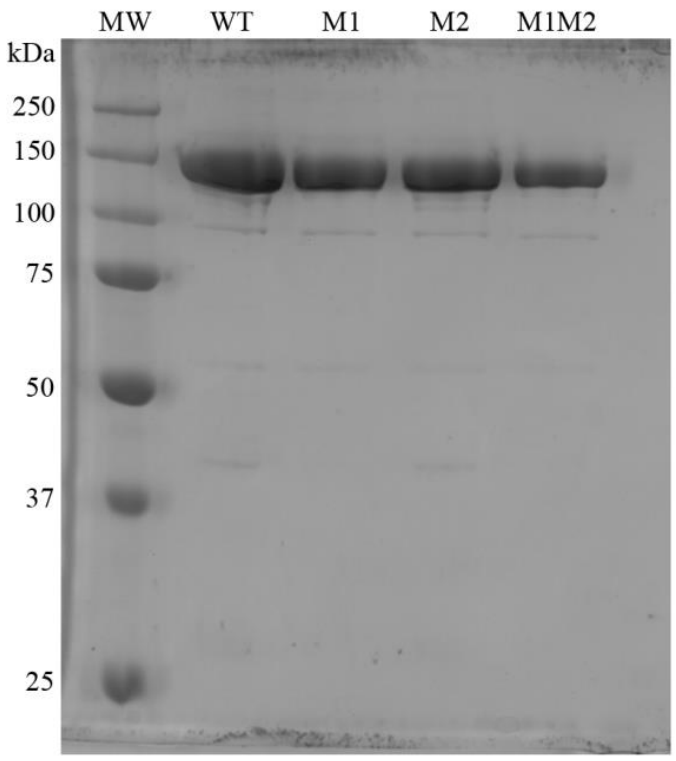

Figure 3.3. Representative gel showing purified TeNT proteins. Representative wild-type and variant TeNT proteins (5 μg) were resolved by SDS-PAGE and visualized by staining with Coomassie Blue. Unless otherwise stated, all proteins employed in this study were stably expressed and estimated to be at least 90% pure as determined by SDS-PAGE followed by visualization with Coomassie Blue.

3.2.5 Fluorescence measurements and analysis.

Steady-state fluorescence emission was measured using an SLM Aminco 8100 steady-state fluorescence spectrometer equipped with double-grating excitation and emission monochromators. The spectrometer was further upgraded with the ISS Phoenix package and operated with ISS Vinci software (ISS Inc., Champaign, IL, USA). All measurements were taken in a 10 mm × 10 mm cuvette oriented perpendicular to the excitation beam and maintained at 25 °C using a Peltier device in 1 nm steps. For NBD measurements, the emission spectra from 500 to 600 nm were collected and the excitation wavelength was 480 nm, using slits of 4 nm on both monochromators.

For each construct, HCT proteins were diluted to 100 nM in pH 6 buffer and the spectra recorded. POPC:POPA liposomes produced as described above were added to the cuvette for 1 minute, then readings were taken again. Fold change in fluorescence was calculated by dividing signal in the presence of liposomes by that in the absence of liposomes. Changes in spectral peaks ($\Delta\lambda$) were calculated by subtracting the peak values in the presence of liposomes by those in the absence of liposomes. Buffer, liposome, and unlabeled controls were run and subtracted from experimental values as appropriate (not shown).

3.2.6 Potassium ion release assay.

Liposomes (~5 μM) were diluted into 5 ml of pH 4 buffer with constant stirring and were allowed to equilibrate. TeNT HCT or TeNT HCT cysteine mutant proteins were then added to the solution at a concentration of 100 nM and potassium ion release monitored using an ion-selective electrode (Orion, ThermoFisher Scientific) until the

change in voltage reached a steady state (~180 seconds for all proteins tested). After 5 min of incubation, 50 µl of a 0.1% v/v Triton X-100 solution was added to estimate the total potassium concentration within the system. Specific K^+ release was determined by subtraction of basal release values obtained from liposomes incubated in buffer alone. Additional control assays were performed to ensure the observed release was due to pH-dependent insertion of HCT proteins (data not shown).

3.2.7 Cellular intoxication assay.

Neurons (14-21 days *in vitro*) were incubated for 24 hours in the presence of TeNT proteins. Cells were then washed twice with cold PBS and lysed using radioimmunoprecipitation assay (RIPA) buffer at 4°C for 20 min. Total cell lysates were combined with SDS-PAGE sample buffer, resolved on 13.5% (w/v) SDS-polyacrylamide gels, transferred to Immobilon PVDF membranes, and subjected to Western blotting using antibodies against VAMP2 (clone 69.1, 1:5000, Synaptic Systems, Goettingen, Germany) and goat anti-mouse-IgG-HRP (1:100000; Thermo Fisher Scientific). The membranes were washed, incubated with SuperSignal Dura (Thermo Fisher Scientific), and visualized using a CCD imaging system. Blots were stripped with Restore PLUS Western Blot Stripping Buffer (Thermo Fisher Scientific) and further probed with a mouse anti-beta actin antibody conjugated to HRP (clone C4, 1:5000, Santa Cruz Biotechnology, Inc. Dallas, TX, USA) and detected as above.

3.2.8 Immunoprecipitation of cellular factors.

TeNT HCT and DTT proteins (1 nmol each protein) were co-incubated with rat brain cytosolic lysate at 4°C overnight, in the presence of 30 µl anti-FLAG M2 affinity beads. Beads were then washed thrice with cold PBS, and incubated with FLAG peptide [150 ng/µl] at 4°C for 30 mins. Supernatant was combined with SDS-PAGE sample buffer, resolved on 4-12% (w/v) gradient SDS-polyacrylamide gels, and transferred to Immobilon PVDF membranes. Membranes were then subjected to Western blotting using antibodies against COPG (1:1000, Santa Cruz Biotechnology), HSP90 (1:1000, Cell Signaling Technology), or His_6 (1:5000, Genscript), followed by goat anti-mouse-IgG and anti-rabbit-IgG HRP conjugates (1:80000; Thermo Fisher Scientific). The membranes were washed, incubated with SuperSignal Dura (Thermo Fisher Scientific), and visualized using a CCD imaging system.

3.2.9 Statistical analysis.

All data were analyzed using GraphPad Prism, version 6.0 (La Jolla, CA).

3.3 Results

3.3.1 Identification of HCT/T residues potentially involved in channel formation.

Upon endocytosis, CNTs are envisioned to be bound to dual receptors within the acidic lumen of endosomal compartments. Though CNTs contain no conserved histidine residues (outside of those coordinating the catalytic zinc atom), there are several conserved Asp and Glu residues within the HCT domain that are predicted to have high pKa values (range, pH 5.2-6.9) by the PROPKA 3.0 software (www.propka.org). This

property suggests these residues will undergo protonation at endosomal pH values, causing the electrostatic surface of the corresponding face of the HCT domain to become positively charged. Notably, all the conserved carboxylates of high pKa are located on the same face of TeNT as the interchain disulfide bond and the hydrophobic HCT segment (residues 669-691) identified by Montal and colleagues as a putative transmembrane helix (hereafter referred to as the translocation competent face) (269). These data suggest that at endosomal pH, the translocation competent face (now carrying a net positive charge) can interact with the negatively charged phospholipids such that the HCT domain can sit down onto the membrane bilayer so that the long translocation domain helices will be parallel to the lipid bilayer.

This model is further supported by hydropathy analysis of TeNT using White-Wimley whole residue hydrophobicity scales (270,271) which predict the translocation competent face contains distinct regions with high interfacial and insertional propensities that change as the pH of the medium changes from pH 7.0 (plasma membrane) to pH 5.0 (late endosome). White-Wimley analysis further predicts the formation of at least two (or possibly three) helix-turn-helix motifs capable of membrane penetration. In **Figure 3.4**, the left images are views of the translocation competent face, while the right images show the other face that projects away from the membrane surface. Notably, the predicted interfacial (rose/teal) and insertional regions (dark teal/brick red) span the entire HCT domain and become more prominent at low pH. To better understand the interaction of TeNT with the membrane bilayer, and to determine whether the putative TeNT translocation motif is exposed to the cytosol *in vivo*, recombinant HCT/T proteins containing cysteine mutations were generated, labeled with IANBD-amide, and assayed

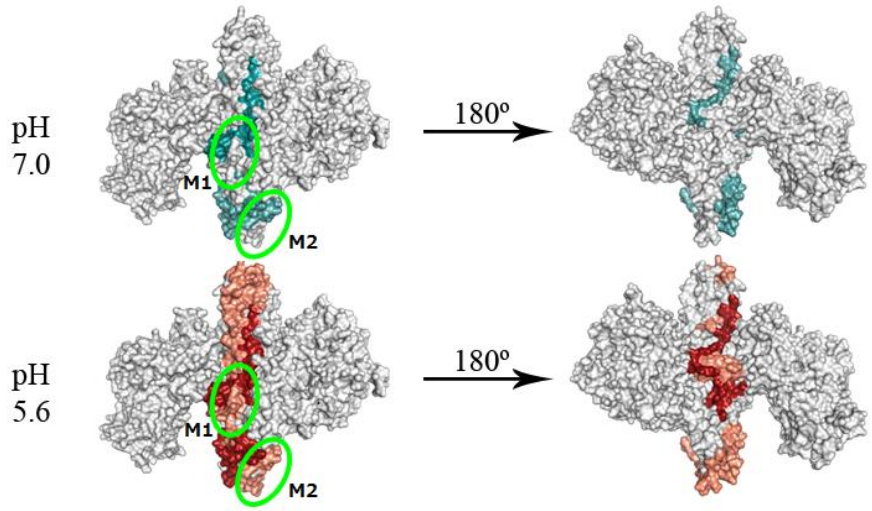

Figure 3.4. Hydropathy analysis of HCT/T using MPEx. The **M**embrane **P**rotein **Ex**plorer tool (http://blanco.biomol.uci.edu/mpex/) was used to assess hydropathy of HCT/T at pH 7.0 (top) and pH 5.6 (bottom). Left images are views of the translocation competent face, while the right images show the other face that projects away from the membrane surface. Predicted interfacial (rose/teal) and insertional regions (dark teal/brick red) span the entire HCT/T domain and become more prominent at low pH. Regions corresponding to Motif 1 (M1) and Motif 2 (M2) are circled in green.

Personal communication from Dr. Michael R. Baldwin.

for steady-state fluorescence emission in the presence or absence of liposomes (**Figure 3.1** and **Table 3.1**). Fold change in fluorescence and magnitude of blue shift was calculated for all constructs. Interestingly, there appears to be a solvent-exposed region (aa 845-852) flanked on either side by largely inserted regions. Even more interesting is that this region almost perfectly overlaps with Motif 2. This is consistent with the idea that the lysine-rich Motif 2 is exposed to the cytosol. To ensure that these proteins did not suffer defects in pore formation, they were assessed for their ability to form pores in liposomes. All NBD-labeled HCT/T cysteine mutants were similar to wild type HCT/T in their ability to induce release of potassium ions from liposomes (**Figure 3.5**).

3.3.2 Functional analysis of TeNT and TeNT translocation variants.

Interaction between the lysine-rich regions of DT and COPG has been shown to be important for translocation. In order to determine if this interaction is also important in the context of TeNT intoxication, lysine-containing regions were mutated to produce $TeNT^{M1}$, $TeNT^{M2}$, and $TeNT^{M1M2}$ (**Figure 3.3**). These proteins were used alongside wild-type TeNT to intoxicate rat cortical neurons, and VAMP2 cleavage was detected by Western blotting (**Figure 3.6**). $TeNT^{M1}$ and $TeNT^{M1M2}$ displayed approximately 1 log and 3 log decreases in activity, respectively. $TeNT^{M2}$ did not appear any less active than wild-type TeNT, and may potentially be more active than wild-type TeNT.

3.3.3 Identification of cellular factors that interact with HCT/T.

The requirement for HSP90 and the Trx/TrxR system as members of the CTF appears to be shared between DT and the CNTs (261-263). Therefore, we hypothesized

Table 3.1. Change in fluorescence and peak wavelengths of IANBD-labeled HCT/T proteins

Construct	Δ Fluorescence (Fold)*	Δλ
A834C	5	-10
N835C	5	-9
S836C	4	-10
K837C	6	-15
F838C	4	-13
I839C	2	-5
G840C	4	-10
I841C	4	-11
T842C	3	-8
E843C	4	-9
L844C	4	-13
K845C	1	-2
K846C	2	-3
S849C	1	-2
K850C	2	-1
I851C	1	-5
N852C	2	-2
K853C	3	-5
V854C	5	-9
F855C	1	-2

*All values represent fold difference in fluorescence rounded to the nearest whole number. Values ≥ 3 (green cells) represent residues that are likely in a highly hydrophobic environment while values < 3 (red cells) represent solvent exposed residues.
Values represent the mean of three independent experiments.

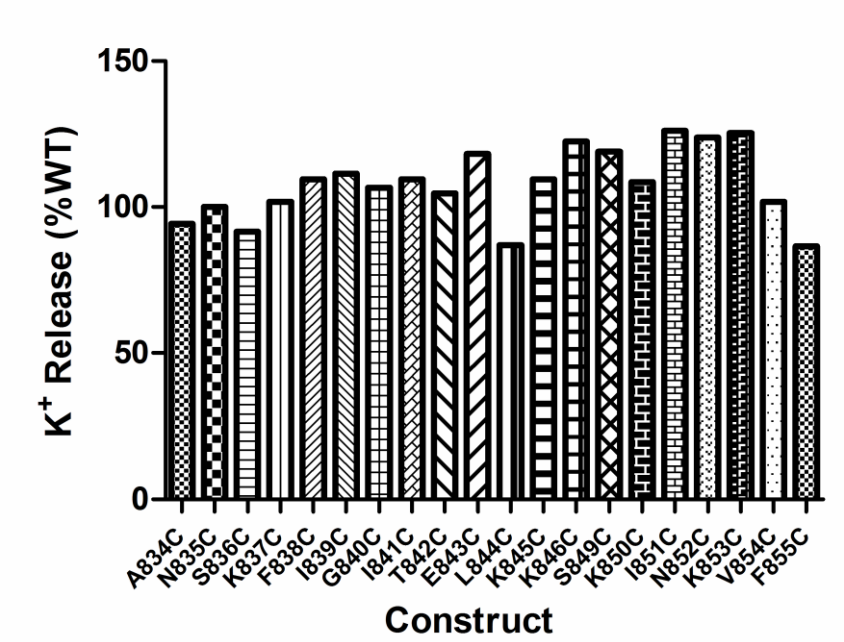

Figure 3.5. Potassium ion (K^+) release from liposomes by IANBD-labeled HCT/T proteins. Liposomes (~5 µM) were diluted into 5 ml of pH 4 buffer with constant stirring and were allowed to equilibrate. TeNT HCT or TeNT HCT cysteine mutant proteins were then added to the solution at a concentration of 100 nM and potassium release monitored using an ion-selective electrode until the change in voltage reached a steady state (~180 seconds for all proteins tested). After 5 minutes of incubation, 50 µl of a 0.1% v/v Triton X-100 solution was added to estimate the total potassium concentration within the system. Specific K^+ release was determined by subtraction of basal release values obtained from liposomes incubated in buffer alone. Additional control assays were performed to ensure the observed release was due to pH-dependent insertion of HCT proteins (data not shown). Total release is shown as percent of wild-type HCT/T. Values expressed as the mean of three independent experiments. All constructs induce ≥ 86% release compared to wild type.

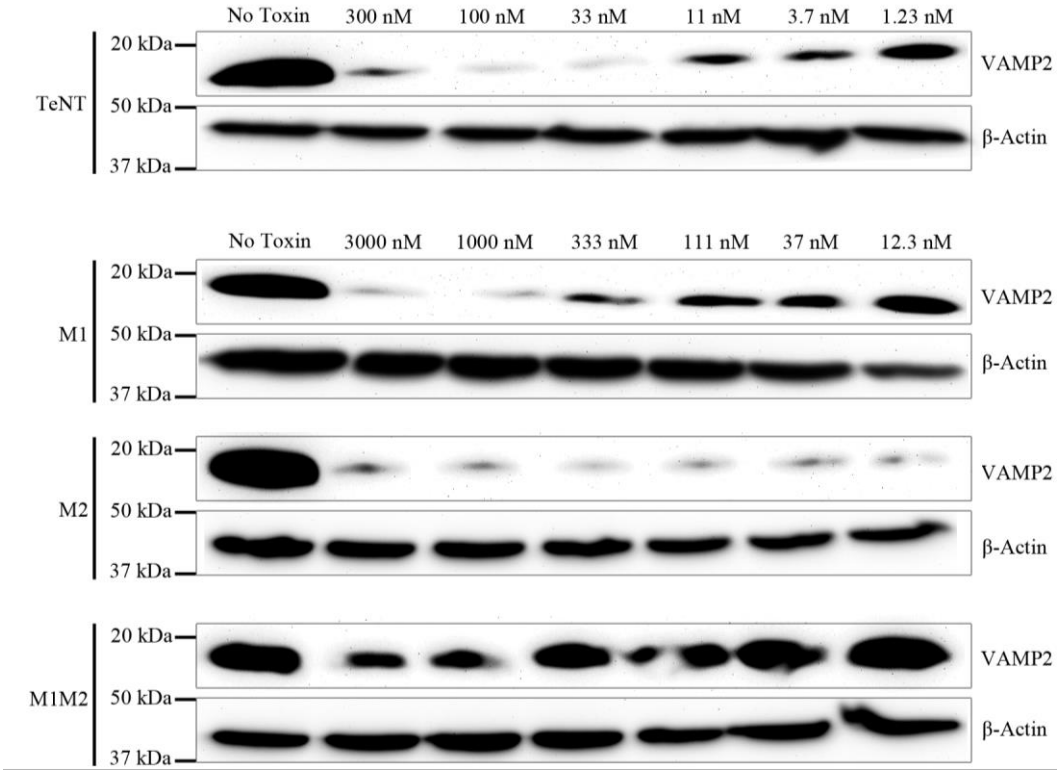

Figure 3.6. Cleavage of VAMP2 by TeNT and TeNT variants. (**A)** Neurons (14-21 days *in vitro*) were incubated for 24 hours in the presence of TeNT proteins at the indicated concentrations. Cells were then washed twice with cold PBS and lysed using radioimmune precipitation assay (RIPA) buffer at 4°C for 20 min. Total cell lysates were combined with SDS-PAGE sample buffer, resolved on 13.5% (w/v) SDS-polyacrylamide gels, transferred to Immobilon PVDF membranes, and subjected to Western blotting using antibodies against VAMP2 (clone 69.1, 1:5000, Synaptic Systems, Goettingen, Germany) and goat anti-mouse-IgG-HRP (1:100000; Thermo Fisher Scientific). The membranes were washed, incubated with SuperSignal Dura (Thermo Fisher Scientific), and visualized using a CCD imaging system. Blots were stripped with Restore PLUS Western Blot Stripping Buffer (Thermo Fisher Scientific) and further probed with a mouse anti-beta actin antibody conjugated to HRP (clone C4, 1:5000, Santa Cruz Biotechnology, Inc. Dallas, TX, USA) and detected as above. Cells that were not exposed to TeNT proteins served as the control (No Toxin), while beta-actin serves as a loading control. Cleavage of VAMP2 by TeNT results in a loss of detectable signal by Western blotting. Image representative of a single experiment.

that COPG may also be a shared component of this complex. In order to determine if COPG associates with HCT/T, FLAG-tagged HCT/T and DT were generated (**Figure 3.2**). Anti-FLAG-M2 immunoprecipitation of rat brain cytosolic lysate by HCT/T was performed with DT serving as a positive control for association with COPG, and beads alone serving as a negative control (**Figure 3.7**). Western blot analysis indicated that, like DT, HCT/T associated with COPG (**Figure 3.7A**). While a requirement for HSP90 by the CNTs has been shown via small molecule inhibitors (261), our observation that HSP90 and HCT/T associate is a novel finding and is consistent with its proposed role as a chaperone that assists with refolding of the LC (**Figure 3.7B**). Anti-His_6 Western blotting was used as a control for protein recovery.

3.4 Discussion

A key step in intoxication by the CNTs involves HCT-mediated translocation of the LC across the endosomal membrane. Although our understanding of the translocation process has grown in recent years, the exact mechanism by which this occurs is not well defined. In this study, we attempted to determine what residues of HCT/T were responsible for inserting into the endosomal membrane, as well as determine if residues of HCT/T interact with COPG to facilitate translocation.

First, we attempted to discern what residues of HCT/T might be inserting into the endosomal membrane using liposomes as an environmental mimic. Using the **M**embrane **P**rotein **Ex**plorer tool (MPEx, http://blanco.biomol.uci.edu/mpex/) in conjunction with a previously-described region in DT as references, we created cysteine mutations at locations in HCT/T corresponding to a putative transmembrane region (aa 834-846, 849-

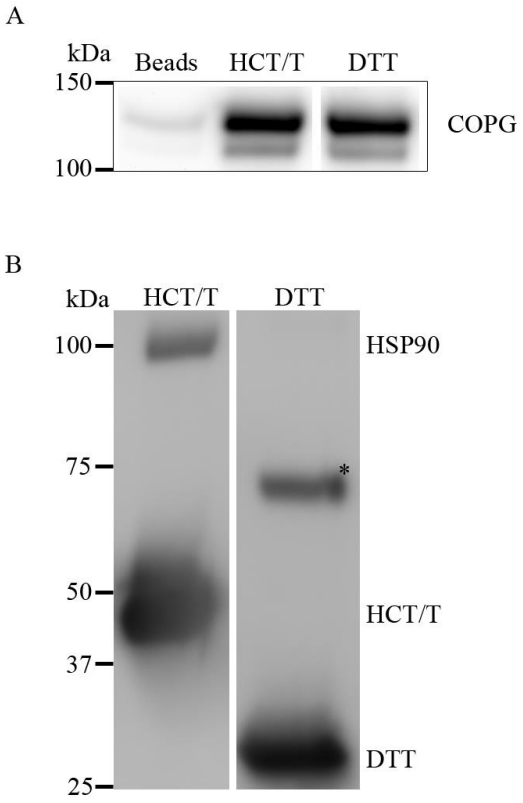

Figure 3.7. Immunoprecipitation of cellular factors by HCT/T. TeNT HCT and DTT proteins (1 nMol each protein) were co-incubated with rat brain cytosolic lysate at 4°C overnight, in the presence of 30 µl anti-FLAG-M2 affinity beads. Beads were then washed thrice with cold PBS, and incubated with FLAG peptide [150 ng/µl] at 4°C for 30 mins. Supernatant was combined with SDS-PAGE sample buffer, resolved on 4-12% (w/v) gradient SDS-polyacrylamide gels, and transferred to Immobilon PVDF membranes. Membranes were then subjected to Western blotting using antibodies against COPG (1:1000, Santa Cruz Biotechnology, **A**), HSP90 (1:1000, Cell Signaling Technology, **B**), or His_6 (1:5000, Genscript, **B**), followed by goat anti-mouse-IgG and anti-rabbit-IgG HRP conjugates (1:80000; Thermo Fisher Scientific). The membranes were washed, incubated with SuperSignal Dura (Thermo Fisher Scientific), and visualized using a CCD imaging system. Asterisk (*) indicates a cross reactive band that co-purifies with DTT independent of the presence of rat brain lysate.

855). We then labeled these cysteine residues using fluorescent NBD dye and recorded steady-state fluorescence emission in the presence or absence of liposomes. NBD is strongly fluorescent in nonpolar environments (272,273). Based on previous studies utilizing this technique, a $\geq$ 3-fold increase in fluorescence emission is indicative of occlusion within such an environment. Additionally, we recorded the change in spectrum peaks ($\Delta\lambda$), as pronounced blue shifts are also known to result from movement of the dye into nonpolar environments. Based on the results in **Table 3.1**, we cannot definitively conclude that this region of HCT/T transverses the endosomal membrane, or even necessarily the liposomal membrane. However, the observed pattern of two presumably inserted regions flanking an exposed region would certainly be consistent with a cytosol-exposed region.

We next attempted to determine if mutation of the lysine residues of $TeNT^{M1}$, $TeNT^{M2}$, or both together ($TeNT^{M1M2}$) were deleterious to toxin activity, presumably via abrogation of interaction with COPG. Interestingly, $TeNT^{M1}$ and $TeNT^{M1M2}$ displayed 1 log and 3 log decreases in activity, respectively. $TeNT^{M2}$, however, paradoxically appeared to be as, or more, active than wild-type TeNT. However, it should be noted that only a single replicate experiment has been performed and thus this observation should not be over-interpreted at this time. One conceivable explanation for this observation is that the presence of multiple COPG binding sites is actually sub-optimal, and that binding to a single motif alone is preferred. This postulate is supported by the observation that certain CNTs appear to possess two lysine-rich regions, while others possess a single site. Further studies are required to determine whether mutations within the lysine-rich motifs can be correlated with the ability to interact with cytosolic factors such as COPG/HSP90.

Along the same lines, further characterization of binding, pore formation, and LC activity are needed for each of the TeNT constructs to determine the specificity of the introduced mutations.

Given that other components of the CTF are shared between DT and the CNTs, we next asked the question of whether or not COPG is a member of the CTF complex for HCT/T. Immunoprecipitation of rat brain cytosolic lysate using HCT/T and anti-FLAG-M2 beads yielded both COPG and HSP90. In addition to identifying an additional shared component of the CTF complex in COPG, we directly showed the novel association between HSP90 and HCT/T. This is consistent with its proposed role as a chaperone that assists with refolding of the LC. Additional immunoprecipitation assays will need to be run using HCT/T constructs containing the M1, M2, and M1M2 mutations in order to conclude which exact residues are important in facilitating these interactions.

In conclusion, COPG appears to be a member of the CTF complex for TeNT translocation, and one or more basic lysine residues within putative transmembrane regions may facilitate interaction between HCT/T and COPG. Further study is required to definitively elucidate the complexities of this interaction.

CHAPTER 4: EVIDENCE FOR DUAL RECEPTOR-BINDING SITES IN *CLOSTRIDIUM DIFFICILE* TOXIN A

As found in: Lambert, G. S. and Baldwin, M. R. (2016), Evidence for dual receptor-binding sites in *Clostridium difficile* toxin A. FEBS Lett, 590: 4550–4563.

4.1 Abstract

TcdA (308 kDa) and TcdB (270 kDa) disrupt the integrity of the intestinal epithelial barrier and provide an environment favorable for *Clostridium difficile* colonization. Recent evidence suggests entry of TcdA into cells is mediated by at least two domains. Here we report the characterization of a second receptor binding domain (RBD2) for TcdA. While both the isolated combined repetitive oligopeptides (CROPs) and RBD2 fragments are rapidly internalized into cells under physiologic conditions, only the CROPs domain appreciably accumulates at the cell surface. Once internalized, CROPs and RBD2 are trafficked to late endosomal compartments. An internal deletion of RBD2 from TcdA holotoxin ablated toxicity in HT29 cells. These data are consistent with the recently proposed dual receptor model of cellular entry.

4.2 Introduction

Clostridium difficile infection (CDI) is a prevalent and severe nosocomial infection as well as a leading cause of antibiotic-associated diarrhea and pseudomembranous colitis in the developed world (8-10). Severity of disease can largely be attributed to the presence of two potent exotoxins, TcdA (308 kDa) and TcdB (270

kDa), which are members of a family of large clostridial glycosylating toxins (LCTs) (6,7,11). Other members of this family include lethal and hemorrhagic toxins from *Clostridium sordellii*, alpha-toxin from *Clostridium novyi*, and TpeL from *Clostridium perfringens*. These toxins inactivate members of the Ras superfamily of small GTPases through glycosylation, resulting in disruption of the actin cytoskeleton, cell-cell junctions, and cell death (112-116).

The structures of TcdA and TcdB have been described previously as adhering to an ABCD model, consisting of the following domains: (A) N-terminal Glucosyltransferase Domain (GTD), which transfers a glucose moiety from UDP-glucose onto Threonine 35/37 residues of Rho family GTPases (179-183); (C) Cysteine Protease Domain (CPD), which is responsible for autoproteolytic release of the GTD from the remainder of the toxin (184-188); (D) delivery domain, which is responsible for translocation of the GTD and CPD domains to the cell cytosol (189-193); and (B) C-terminal Combined Repetitive Oligopeptides (CROPs) domain, which is believed responsible for toxin binding to host enterocytes through interaction with an unidentified carbohydrate receptor(s) (159,194-202).

Binding of these two toxins was, up until recently, thought to be solely mediated by their C-terminal CROPs domains. However, studies demonstrating that TcdA and TcdB variants lacking the CROPs retain partial activity suggest the toxins may contain a second, CROPs-independent receptor binding domain (RBD) (187,207,208). This is supported by the observation that TpeL, an LCT produced by *C. perfringens* type C strains, lacks a CROPs domain but still exhibits cytotoxic activity (274,275). Subsequently, Aktories and co-workers demonstrated that TpeL utilizes LDL receptor-

related protein 1 (LRP1) as a host cell receptor, and that a C-terminal TpeL fragment (residues 1335-1779) bound to cells with similar affinity to the holotoxin (276). Furthermore, a corresponding fragment from TcdB (residues 1349-1811) was demonstrated to bind HeLa and Vero cells with similar affinity to CROPs-deficient TcdB (residues 1-1811) (276). Finally, recent reports identifying Chondroitin sulfate proteoglycan 4, Poliovirus receptor-like 3 and Frizzled proteins as TcdB host cell receptors support the concept that the LCTs contain a second RBD located between the putative translocation domain and the C-terminal CROPs region (209-211). Although TcdA and TcdB share a high degree of sequence homology (11,115), they appear to utilize unique receptors for cellular entry and play distinct roles in the development of disease (277). As such, it is of importance to characterize both of these major virulence factors.

The mechanisms by which the large clostridial glycosylating toxins bind and enter cells have yet to be fully resolved. In the present study we demonstrate saturable binding of CROPs to HT29 cells, followed by transport through early endosomal compartments to the lysosome where the protein is degraded. In comparison, accumulation of a second, CROPs-independent receptor binding domain (RBD2) within TcdA at the plasma membrane was not observed. Rather, under physiologic conditions RBD2 is internalized into EEA1-positive compartments where it appears to accumulate, with a small population transiting to the lysosome. While the CROPs domain is dispensable for toxicity *in vitro*, our data suggest RBD2 may play an important role in intoxication beyond simply binding to the cell surface. In conclusion, our data are consistent with the recently proposed dual receptor model of binding in which abundant carbohydrate

sequences expressed on the surface of enterocytes form high-avidity ligands for CROPs, facilitating binding of RBD2 to a lower abundance receptor that directs the toxin to endosomal compartments allowing for productive intoxication.

4.3 Experimental Procedures

4.3.1 Expression and purification of recombinant TcdA proteins.

Codon-optimized DNA encoding Toxin A (TcdA) from *Clostridium difficile* strain 630 (NCBI Reference Sequence: YP_001087137.1) was chemically synthesized by Genscript (Piscataway, New Jersey, U.S.A.). Individual domains of TcdA ($TcdA^{1\text{-}1361}$, CROPs [residues 1874-2710], RBD2 [residues 1361-1874], and RBD2-CROPs [$TcdA^{1361\text{-}CT}$, residues 1361-2710]) were amplified by polymerase chain reaction using appropriate primers and cloned into a modified pET28a expression vector (Millipore Sigma) using appropriate restriction endonuclease sites (KpnI/EagI) resulting in fusion proteins containing N-terminal His_6 and 3×FLAG tags. Proteins were expressed in *E. coli* BL-21 cells and purified using sequential Ni^{2+}-NTA, size-exclusion, and anion-exchange chromatography. Peak fractions were concentrated by dialysis against 40% w/v polyethylene glycol (PEG) in phosphate buffered saline (PBS), subsequently dialyzed against PBS alone, and stored at -80°C until use.

DNA encoding catalytically active forms of TcdA (TcdA, $TcdA^{1\text{-}1874}$, $TcdA^{\Delta RBD2}$, and $TcdA^{RBD2B}$) was amplified by polymerase chain reaction using appropriate primers and cloned into the pHis1522 expression vector (MoBiTech, Göttingen, Germany) using appropriate restriction endonuclease sites (BsrGI/EagI), resulting in fusion proteins containing C-terminal His_6 tags. Proteins were expressed using the *Bacillus megaterium*

expression system as described previously (266,267), and were purified by sequential Ni^{2+}-NTA and size-exclusion chromatography. Peak fractions were concentrated using an Amicon filtration device (Ultracel-30 type filter), dialyzed into PBS, and stored at -80°C until use.

Protein purity was estimated by SDS-polyacrylamide gel electrophoresis followed by densitometry as shown in **Figure 4.1**. Purified proteins were also resolved by chromatography on a calibrated Superdex 200 column (10 mM Tris-HCl, pH 7.4, 150 mM NaCl). Fitting the elution profile of the recombinant proteins to a calibration curve derived from a set of known analytes (Thyroglobulin 670000 Da; γ-globulin 158000 Da; Ovalbumin 44000 Da; Myoglobin 17000 Da; Vitamin B12 1350 Da) suggests all proteins are monomeric under conditions used throughout the study (data not shown).

4.3.2 Cell culture.

HT29 cells were purchased from the American Type Culture Collection (ATCC product number: HTB38™; Manassas, VA, USA) and cultivated under standard conditions in Roswell Park Memorial Institute (RPMI) 1640 medium supplemented with 10% v/v fetal bovine serum (FBS), 100 µM penicillin, and 100 µg/ml streptomycin.

4.3.3 Immunofluorescence analysis of TcdA binding/internalization.

HT29 cells were plated at a density of 1×10^5 cells per well onto poly-D-lysine treated glass coverslips in 24-well cell culture plates and allowed to grow for 48 hours prior to use. Cells were treated with TcdA proteins at a concentration of 5 µM in complete medium for 1 hour at 37°C. Following treatment, cells were washed three times

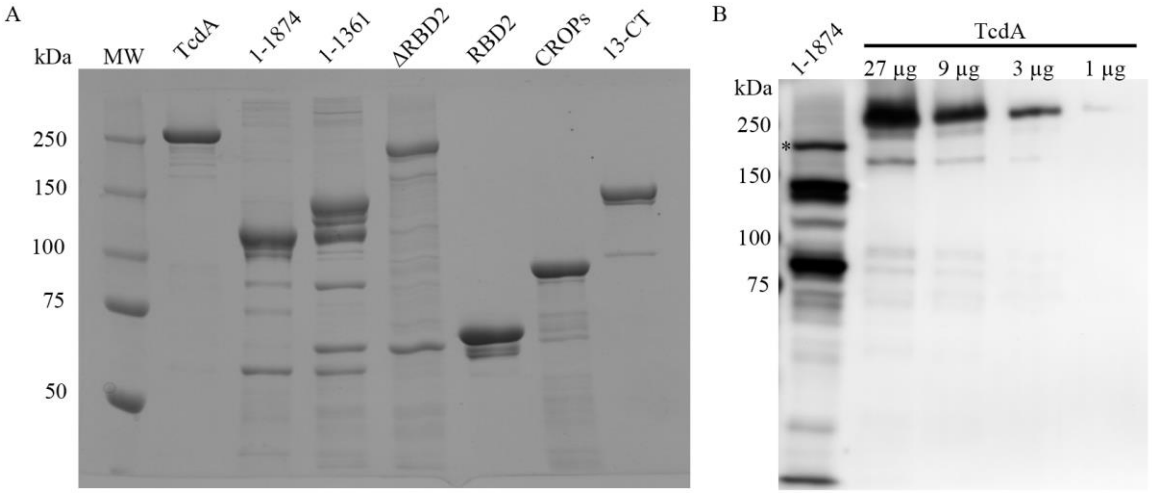

Figure 4.1. Western blot estimation of TcdA 1-1874 concentration. (A) Equivalent amounts (5 µg) of the indicated TcdA proteins were resolved on an 8% (w/v) SDS-polyacrylamide gel and stained with Coomassie Brilliant Blue R-250. Proteins were estimated to have greater than 80% purity by densitometric analysis of gels, with the exception of $TcdA^{1\text{-}1361}$ and $TcdA^{RBD2B}$ (~50% pure; **Figure 4.10**), and $TcdA^{1\text{-}1874}$ (~5% pure). **(B)** The purity and concentration of $TcdA^{1\text{-}1874}$ was estimated by Western blot using antibodies against His_6 (mouse, 1:2500; Genscript) and goat anti-mouse-HRP (1:80000; Thermo Fisher Scientific), followed by comparison with known amounts of TcdA probed with the same antibodies. Full length $TcdA^{1\text{-}1874}$ is indicated with an asterisk.

with Hanks' balanced salt solution (HBSS) and fixed in 4% w/v paraformaldehyde/4% w/v sucrose in PBS at 4°C. Cells were then subjected to immunostaining using a combination of the following antibodies, depending on experiment: FLAG (mouse M2 antibody, 1:10000, Sigma-Aldrich), EEA1 (rabbit, 1:75, Cell Signaling Technology), GM130 (rabbit, 1:3200, Cell Signaling Technology), LAMP-1 (rabbit, 1:200, Cell Signaling Technology). This was followed by staining with appropriate secondary antibodies labeled with Alexa Fluor dyes (1:300, Thermo Fisher Scientific). Cell nuclei were stained with TO-PRO®-3 Iodide (1:500, Thermo Fisher Scientific). Coverslips were mounted onto glass slides using ProLong® Gold antifade reagent, and images were collected using a Leica SPE 2 system in confocal mode. Analysis and quantification of images was carried out using Leica Application Suite (LAS) software and assembled in Adobe Photoshop CS3 extended.

Where indicated, HT29 cells were pre-treated with inhibitors (50 µg/ml cycloheximide; 250 nM bafilomycin A1; 1 µg/ml nocodazole; 100 µM leupeptin) or solvent for 30 minutes prior to treatment with TcdA proteins. These concentrations were maintained throughout the experiments.

For analysis of protein entry via presence or absence of cell permeabilization, incubation times of 5 and 15 minutes were added and the permeabilization step replaced with incubation with PBS for necessary samples.

4.3.4 4°C plate binding assay.

HT29 cells were plated at a density of 1×10^6 cells per well into a 6-well cell culture plate, and were allowed to grow for 48 hours prior to use. Cells were then treated

with TcdA proteins for 30 min at 4°C, washed three times with HBSS, and were lysed with RIPA buffer at 4°C for 30 min. Lysates were combined with SDS-PAGE sample buffer, resolved on 13.5% (w/v) SDS-polyacrylamide gels, and transferred to Immobilon PVDF membranes. Membranes were then subjected to Western blotting using antibodies against FLAG (mouse M2 antibody, 1:10000, Sigma-Aldrich) and goat anti-mouse-HRP (1:80000, Thermo Fisher Scientific). The membranes were washed, incubated with SuperSignal Dura (Thermo Fisher Scientific), and visualized using a CCD imaging system.

4.3.5 Flow cytometric binding analysis.

HT29 cells were suspended by Accutase® (Innovative Cell Technologies, Inc., San Diego, CA, USA) treatment and 2×10^6 cells per sample were aliquoted into a 96-well cell culture plate. Cells were gently pelleted at 250 ×*g* and washed once with ice-cold PBS. Cells were then treated with increasing concentrations of TcdA proteins for 30 min at 4°C, washed three times with ice-cold PBS followed by 250 ×*g* centrifugation, and fixed in 4% w/v paraformaldehyde/4% w/v sucrose in PBS at 4°C. Cells were then subjected to immunostaining using antibodies against FLAG (mouse M2 antibody, 1:10000, Thermo Fisher Scientific) and goat anti-mouse R-PE (1:100, Thermo Fisher Scientific). Stained cells were subjected to flow cytometry (CyanADP flow cytometer, Beckman Coulter, Pasadena, CA), and fifty thousand events were collected per sample. Data were analyzed using Summit v4.3 (Beckman Coulter).

4.3.6 HT29 intoxications and competition assay.

HT29 cells were plated onto glass coverslips at a density of 1×10^6 cells per well in a 24-well cell culture plate, and were allowed to grow to confluence. Cells were then treated for 24 hours with indicated doses of TcdA (range: 0-1 nM) or $TcdA^{1\text{-}1874}$ (range: 0-100 nM), 100 nM $TcdA^{1\text{-}1361}$, 100 nM $TcdA^{\Delta RBD2}$, or 100 nM $TcdA^{RBD2B}$. Following treatment, cells were washed three times with HBSS, and cells were fixed with 4% w/v paraformaldehyde/4% w/v sucrose in PBS at 4°C. Coverslips were mounted onto glass slides using ProLong® Gold Antifade reagent, and differential interference contrast (DIC) microscopy images were collected using a Leica SPE 2 system. Images were analyzed using Leica Application Suite (LAS) software. For competition assays, 0.1 nM TcdA or 1 nM $TcdA^{1\text{-}1874}$ were premixed with competitor proteins (RBD2 and CROPs) prior to addition to cells and then processed as described above. Cytopathic effect was determined by scoring images on a scale (0-3) developed previously by our laboratory: (0: no rounding; 1: 1-33% rounding; 2: 34-66% rounding; 3: >66% rounding) (278).

4.3.7 Rac glucosylation assay.

HT29 cells were plated at a density of 2×10^6 cells per well in a 12-well cell culture plate and allowed to grow to confluence. Cells were then treated with 100 nM TcdA, $TcdA^{1\text{-}1361}$, $TcdA^{\Delta RBD2}$, or $TcdA^{1\text{-}1874}$ for 48 hours. Following treatment, cells were washed three times in HBSS, trypsinized, and gently pelleted at 250 ×*g*. Cells were then lysed with RIPA buffer at 4°C for 30 min, and clarified by centrifugation at 20,000 ×*g*. Lysates were combined with SDS-PAGE sample buffer, resolved on 13.5% w/v SDS-polyacrylamide gels, transferred to Immobilon PVDF membranes, and subjected to

Western blotting using antibodies against non-glucosylated Rac1 (1:500, 4°C overnight; clone mAB102, BD Biosciences) and goat anti-mouse-HRP (1:80000, Thermo Fisher Scientific). The membranes were washed, incubated with SuperSignal Dura (Thermo Fisher Scientific), and visualized using a CCD imaging system. Membranes were subsequently stripped with Restore PLUS Western Blot Stripping Buffer (ThermoFisher Scientific), washed with PBS and reprobed using an anti-beta actin HRP conjugate antibody (1:5000, Santa Cruz Biotechnology) to ensure equivalent loading of samples.

4.3.8 Circular dichroism.

An AVIV model 202 far-UV spectrometer was used to collect spectra (195–250 nm) of TcdA RBD2 (0.5 mg/ml) at pH 7.4. Spectra were collected at 4°C and 37°C, using 1-mm path length quartz cuvettes. Data analysis was carried out using CDPro software (279).

4.3.9 Statistical analysis.

Densitometric analysis was performed using Protein Simple AlphaView version 3.0 software (Santa Clara, CA). All data were analyzed using GraphPad Prism, version 6.0 (La Jolla, CA).

4.4 Results

4.4.1 Functional analysis of recombinant TcdA and protein variants.

While TcdA constructs lacking the CROPs domain have been shown to retain partial activity (207,208), the presence of a second receptor binding site in TcdA has not

been definitively shown. Given the marked sequence similarity between the LCTs, it was hypothesized that such a domain (amino acids 1361-1874, henceforth referred to as RBD2) would overlap with the corresponding regions of TcdB (residues 1349-1811) and TpeL (residues 1335–1779) respectively. Initially, recombinant TcdA (RBD2 and CROPs), $TcdA^{1-1874}$ (RBD2 only), and $TcdA^{1-1361}$ (lacking both RBD2 and CROPS) were constructed (**Figures 4.1** and **4.2A**) and assessed with regards to their ability to intoxicate HT29 cells (**Figure 4.2B-C**). While TcdA and $TcdA^{1-1874}$ induced maximal cell rounding at low nanomolar concentrations, $TcdA^{1-1361}$ was unable to cause rounding even at a dose of 100 nM. The activity of $TcdA^{1-1874}$ on HT29 cells was approximately 5-10 fold lower than TcdA at equivalent concentrations and agrees with previous studies demonstrating the CROPs domain is dispensable for toxicity (207,208). In order to assess the biological relevance of the isolated CROPs domain and putative RBD2, competition experiments were performed utilizing these proteins. The simultaneous incubation of HT29 cells with TcdA in a 1000-fold molar excess of either CROPs or RBD2 did not reduce the cytopathic effect of the holotoxin (**Figure 4.2D**). In comparison, RBD2 was able to reduce the cytopathic effect of $TcdA^{1-1874}$ at all ratios tested, presumably through competition for cell surface receptors. As expected, no competition between $TcdA^{1-1874}$ and CROPs was observed; this is consistent with previous suggestions that $TcdA^{1-1874}$ and CROPs utilize unique host cell receptors (207,208).

4.4.2 Binding of TcdA variants to HT29 cells.

In order to directly test the capability of CROPs and RBD2 to bind HT29 cells, three complementary binding assays were performed. Binding to HT29 cells was initially

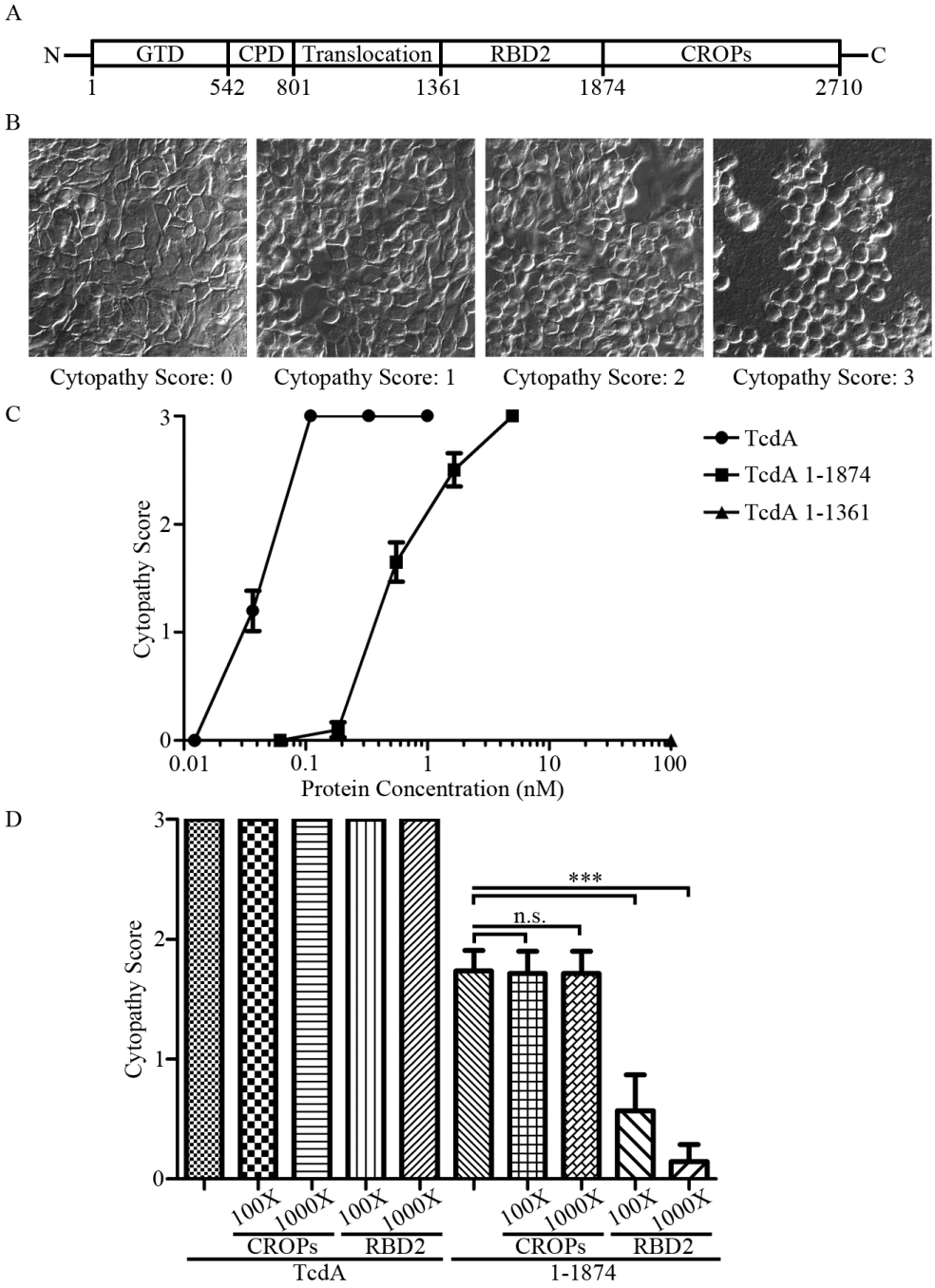

Figure 4.2. Biological activity of TcdA constructs. **(A)** Schematic representation of TcdA holotoxin with relevant amino acids indicated. **(B)** Representative images of four distinct cytopathy scores (0-3) used to quantify cytopathic effect, as described in the Experimental Procedures section. **(C)** HT29 cells were incubated for 24 hours with indicated concentrations of TcdA (●), $TcdA^{1-1874}$ (■), or $TcdA^{1-1361}$ (▲). DIC images were collected and fields scored as described in the Experimental Procedures section. Values expressed as mean ± SEM (2 individual experiments, n=10 fields per treatment). EC50 values are estimated at 75 pM and 0.5 nM for TcdA and $TcdA^{1-1874}$ respectively. **(D)** Intoxications of HT29 cells by TcdA and $TcdA^{1-1874}$ were carried out as above, with the addition of TcdA RBD2 and CROPs at 1:100 and 1:1000 molar ratios. Cytopathic effect was determined as in **(B)**. Values expressed as mean ± SEM (2 individual experiments, n≥3 fields per treatment) (***, $p<0.001$; n.s., not significant, one-way ANOVA with Dunnett post-test).

investigated at 4°C via Western blotting and quantified by densitometry (**Figure 4.3A**). Compared to the receptor-deficient toxin variant ($TcdA^{1-1361}$), only constructs containing the CROPs domain (i.e. CROPs and $TcdA^{1361-CT}$) showed an increase in binding. In order to more quantitatively address this question, binding was also investigated via flow cytometry, revealing a similar pattern of binding to the previous assay (**Figure 4.3B**). Thirdly, binding was assessed visually via immunofluorescence assay at both 4°C and 37°C (**Figure 4.3C**). In agreement with the plate binding and flow cytometry data, peripheral binding of CROPs, but not RBD2, to HT29 cells was observed at 4°C. Increasing the incubation time up to 6 hours did not result in detectable binding of RBD2, suggesting it was not simply the result of a low affinity interaction (**Figure 4.4**). A similar pattern of binding was also observed with CROPs and RBD2 in NIH 3T3 and A431 cells (data not shown). In contrast, incubation of HT29 cells with either CROPs or RBD2 at 37°C resulted in punctate staining consistent with internalization into intracellular vesicular compartments. While the sequence of the expressed TcdA RBD2 (residues 1361-1874) was based on homologous fragments from TcdB and TpeL toxins, the recently solved structure of a TcdA fragment (residues 1-1832) revealed that RBD2 starts from within an elongated scaffold of β-sheets (~1150-1800) (203). Thus, to ascertain whether the lack of binding by RBD2 at 4°C was due to a temperature-induced misfolding of the protein, circular dichroism (CD) spectroscopy was performed (**Figure 4.3D**). The CD spectra of RBD2 at 4°C and 37°C were essentially identical, containing ~49% beta sheet (estimated using the CDPro software package; Colorado State University, Fort Collins, CO, USA). This is in reasonable agreement with the crystal

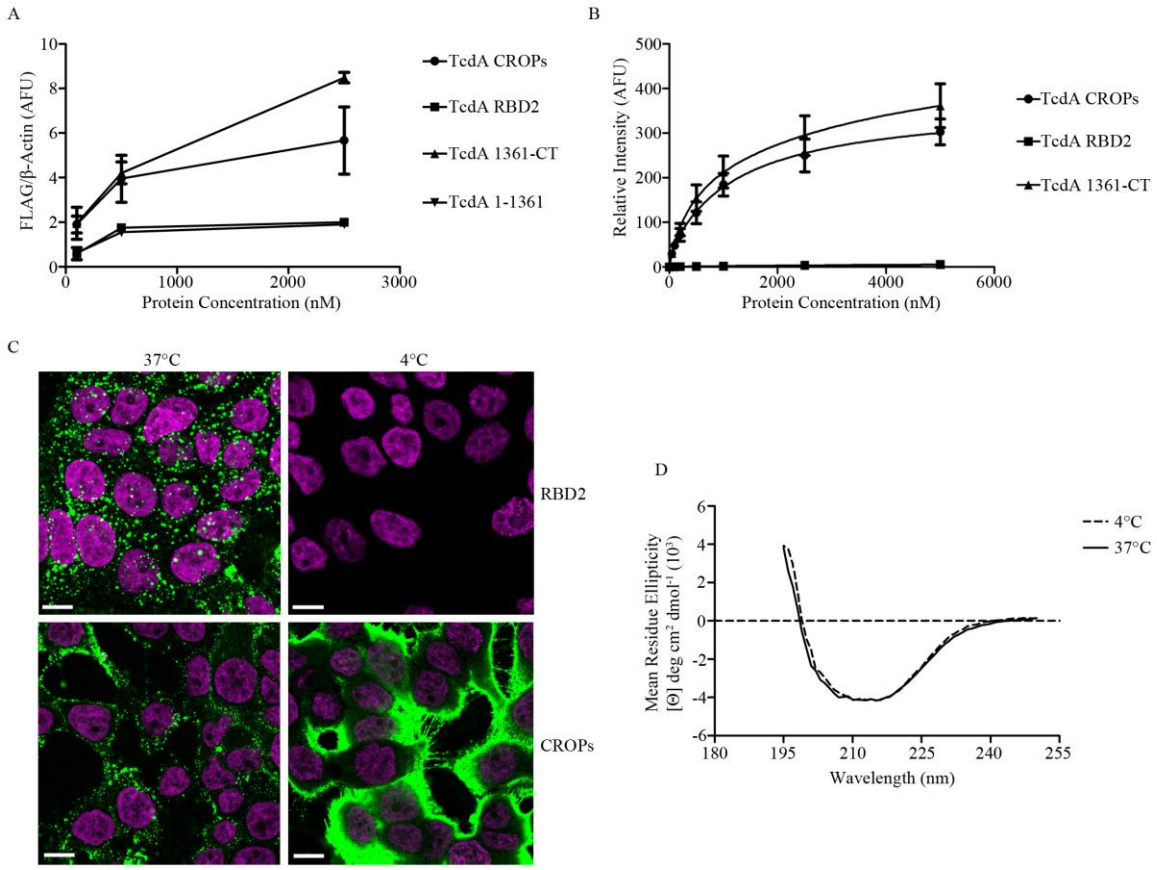

Figure 4.3. Binding of TcdA proteins to HT29 cells. **(A)** Binding of TcdA proteins to HT29 cells at 4°C was assessed via a plate binding assay as described in the Experimental Procedures section. Binding was quantified by densitometry and values expressed as mean intensity ± SEM (≥2 individual experiments). **(B)** TcdA protein binding at 4°C was quantified via flow cytometry as described in the Experimental Procedures section. Values expressed as mean intensity ± SEM (3 individual experiments; 50,000 events per sample). **(C)** Binding and/or entry of TcdA proteins was visualized via immunofluorescence at 4°C and 37°C. FLAG-tagged TcdA proteins are shown in green, TO-PRO®-3 iodide nuclear stain shown in magenta (40× magnification, scale bar equal to 10 μm.) **(D)** Far-UV CD spectra of TcdA RBD2 at pH 7.4 and either 4°C (dotted line) or 37°C (solid line).

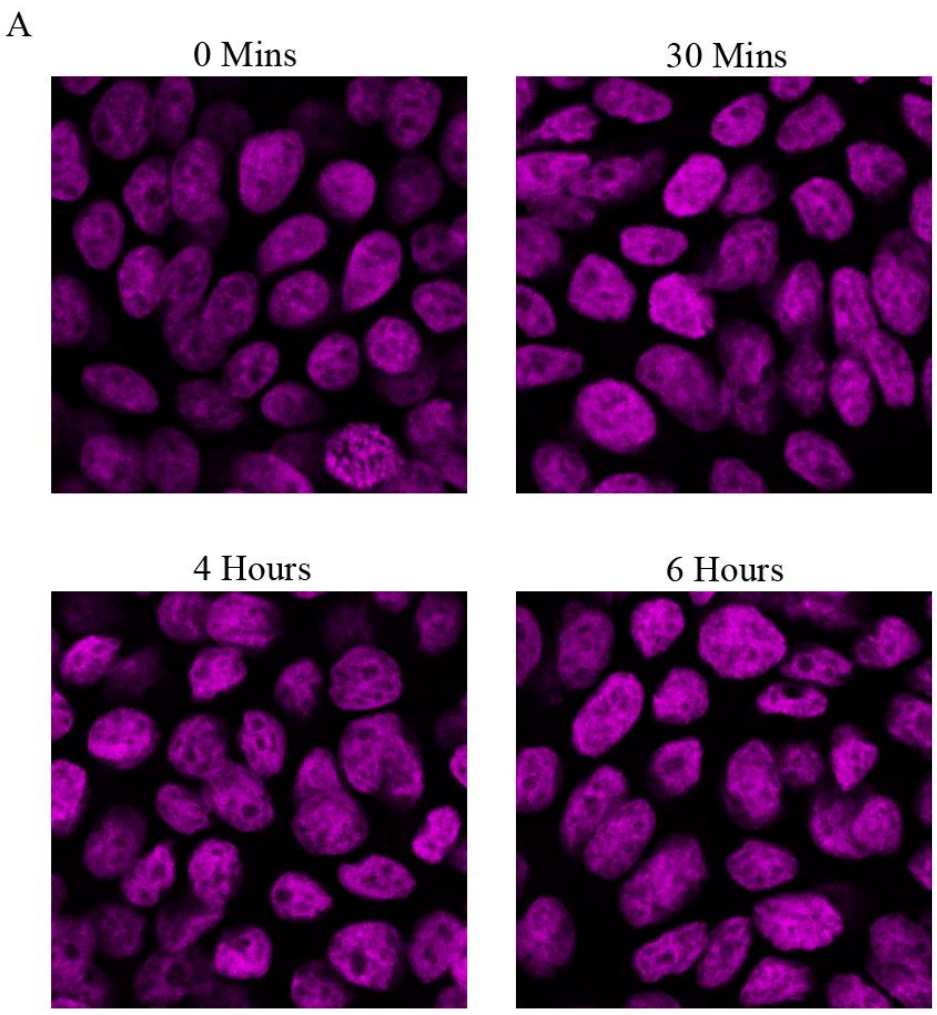

Figure 4.4. Extension of incubation time does not increase TcdA RBD2 binding to HT29 cells at 4°C. (A) Binding of TcdA RBD2 to HT29 cells was carried out as in **Figure 4.3C**, with the addition of 4 and 6 hour timepoints. Increased equilibration time did not result in increased binding or detectable extracellular accumulation of RBD2.

structure of TcdA (~43% beta sheet) and suggests the failure of RBD2 to appreciably bind to cells at 4°C was not due to thermal unfolding of the protein.

4.4.3 RBD2 and CROPs are internalized into EEA1 positive compartments.

Previous studies addressing the kinetics of TcdA entry utilized a classical approach of pre-loading cells at 4°C, followed by shifting to 37°C to allow for coordinated cellular uptake (207). However, the lack of detectable binding by RBD2 at 4°C precludes the possibility of performing a similar experiment. As such, internalization of CROPs and RBD2 at 37°C was confirmed by colocalization with early endosomal antigen 1 (EEA1) (**Figure 4.5A**).

One possible explanation for the lack of appreciable RBD2 binding at 4°C is that it may interact with a small pool of continuously synthesized protein receptors. As such, cells were pretreated with cycloheximide to inhibit protein synthesis and the immunofluorescence binding experiment was repeated. However, cycloheximide treatment had no discernable effect on the uptake of CROPs or RBD2 at 37°C (**Figure 4.5B** and **Figure 4.6**). In order to further investigate this possibility, we treated cells with nocodazole to disrupt microtubule trafficking, which should both prevent endosomal maturation as well as disrupt delivery of newly synthesized receptors to the plasma membrane via the ER-Golgi system. Staining for Golgi matrix protein 130 (GM 130) confirmed disruption of the typical elongated Golgi structure. Similar to treatment with cycloheximide, nocodazole had no effect on the intracellular pattern of CROPs and RBD2 (**Figure 4.5C**). These data argue against a model in which receptors for RBD2 are being continuously synthesized and delivered to the plasma membrane.

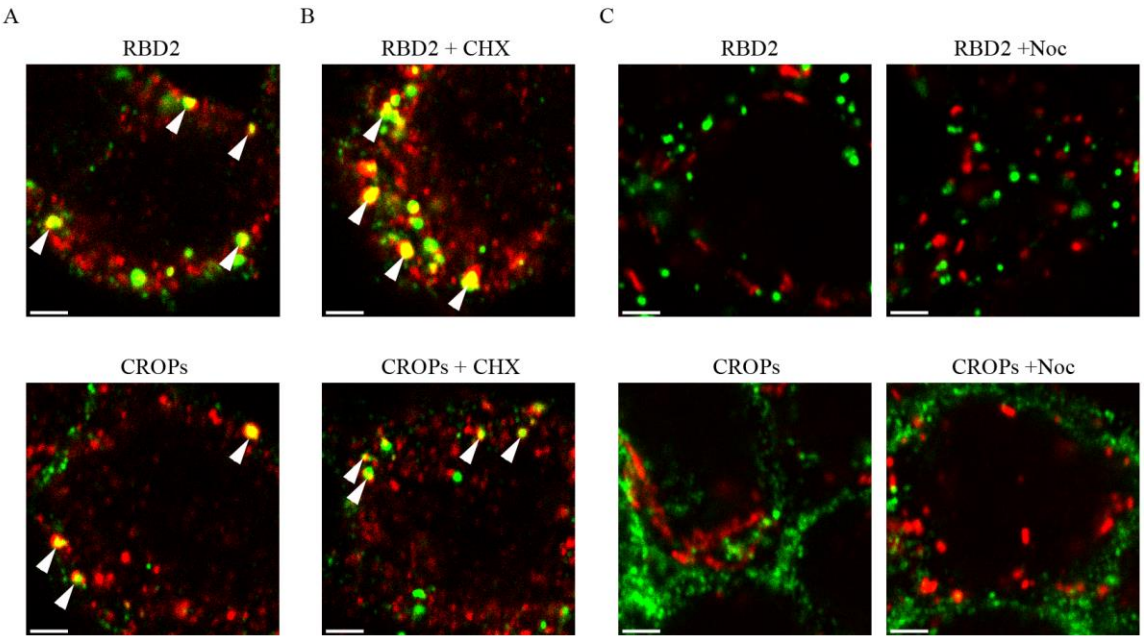

Figure 4.5. TcdA proteins are internalized into early endosomal compartments. **(A)** HT29 cells were treated with 5 µM FLAG-tagged TcdA CROPs or RBD2 at 37°C for 1 hour and visualized by immunofluorescence. TcdA proteins (green) showing colocalization with early endosomal antigen 1 (EEA1, red) are highlighted with white arrows. HT29 cells were pretreated with 50 µg/ml cycloheximide **(B)**, 1 µg/ml nocodazole **(C)** or solvent and then incubated at 37°C for 1 hour in the presence of TcdA proteins. Cells were washed and fixed, and TcdA proteins visualized by immunostaining against the FLAG epitope (green). Colocalization with EEA1 (**B**, red) is highlighted with white arrows. Golgi matrix protein 130 (GM 130) is shown in red (**C**) (100× magnification, scale bar = 2 µm).

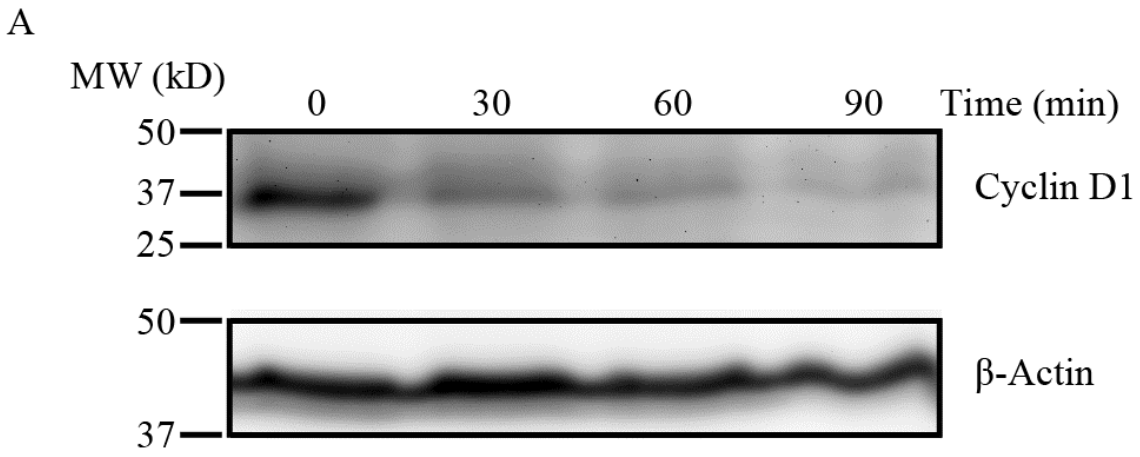

Figure 4.6. Inhibition of protein synthesis leads to rapid degradation of Cyclin D1 in HT29 cells. (A) To verify that cycloheximide treatment inhibited protein synthesis, the degradation of Cyclin D1 was monitored over time. Briefly, HT29 cells were treated with 50 µg/ml cycloheximide for various times up to 90 min. Following treatment, cell lysates were resolved by SDS-PAGE, transferred to PVDF membranes, and successively probed for Cyclin D1 expression (upper panel) and beta-actin (lower panel).

4.4.4 Receptors for TcdA RBD2 may be expressed at lower levels than those of CROPs on the surface of HT29 cells.

An alternate explanation for why RBD2 does not appreciably bind to cells at 4°C may be that its cellular receptor(s) is present on the cell surface in relatively low abundance (and thus below the detection limit of the assays employed). Consistent with this hypothesis, no staining of RBD2 was observed in the absence of detergent permeabilization even when cells were exposed to the protein at 37°C (**Figure 4.7**). In contrast, CROPs staining at the plasma membrane is apparent in either the absence or presence of detergent permeabilization. Interestingly, the amount of intracellular CROPs and RBD2 at 60 minutes (estimated by subtracting non-permeabilized values from their permeabilized counterparts) appears to be somewhat similar. These data may suggest that the amount of intracellular RBD2 is limited by either the rate of internalization (as has been previously supposed), the availability of potential receptors, or some combination of the two. It is important to note that bafilomycin A1 data obtained by Olling and co-workers was used to support the claim that $TcdA^{1-1874}$ enters cells more slowly than TcdA. However, our data seems to suggest that RBD2-mediated entry and cellular accumulation occurs at a similar rate to that of CROPs. Therefore, it is distinctly possible that an alternative explanation, such as delayed endosomal maturation or alternative trafficking, may account for their ability to prevent intoxication by addition of bafilomycin A1 at timepoints up to 30 minutes post-incubation (207).

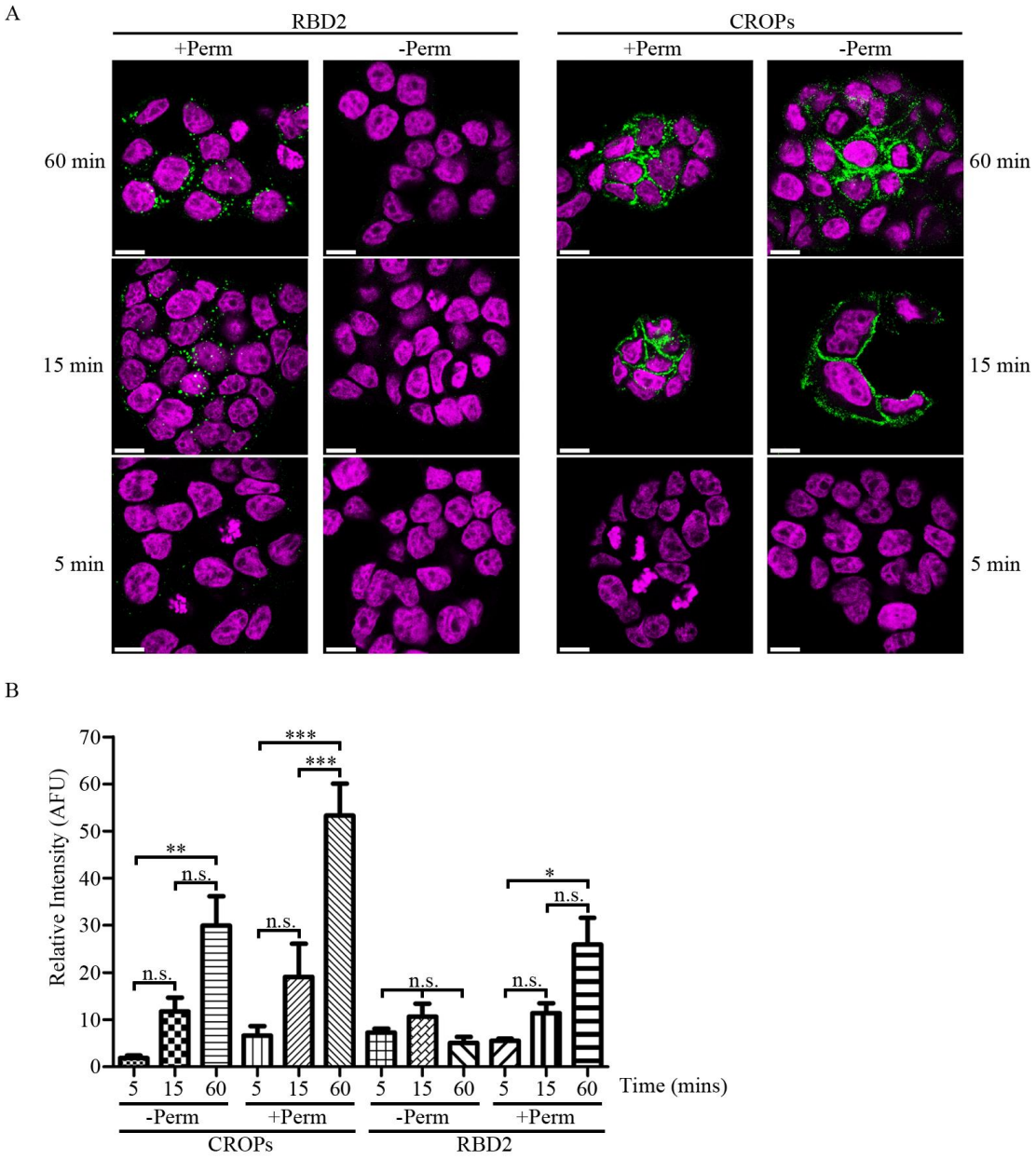

Figure 4.7. TcdA RBD2 is internalized into HT29 cells. **(A)** HT29 cells were treated with 5 µM FLAG-tagged TcdA RBD2 or CROPs for the indicated times. Cells were washed and fixed, and TcdA proteins visualized by immunostaining against the FLAG epitope in the absence or presence of detergent permeabilization. TO-PRO®-3 iodide nuclear stain shown in magenta (40× magnification, scale bar = 10 µm.) **(B)** Total associated protein was quantified by fluorescence and corrected for background. Values expressed as mean ± SEM (2 individual experiments, n≥5 fields per treatment) (***, $p<0.001$; **, $p<0.01$; *, $p<0.05$; n.s., not significant, one-way ANOVA with Tukey post-test).

4.4.5 TcdA CROPs and RBD2 are targeted to the lysosome.

Previous studies have hypothesized that the CROPs domain is endocytosed from the plasma membrane and rapidly targeted to the lysosome where it is degraded (207). In order to investigate this possibility, cells were first treated with bafilomycin A1 to prevent endosomal maturation and therefore trafficking to the lysosome. However, there was no difference in the intracellular staining pattern of either RBD2 or CROPs under these conditions (**Figure 4.8A**).

To more directly address this hypothesis, the colocalization of CROPs and RBD2 with the lysosomal marker LAMP-1 was investigated. Consistent with this hypothesis, colocalization of CROPs with the lysosomal marker LAMP-1 was observed and could be enhanced by pre-treatment of the cells with the lysosomal protease inhibitor leupeptin (**Figure 4.8B**). RBD2 was also observed to colocalize with LAMP-1, albeit to a lesser extent than CROPs. The differences in total fluorescent intensity between the RBD2 and CROPs channels is a result of visualizing both intracellular and extracellular CROPs pools. Thus, direct comparison of LAMP-1 colocalization with RBD2 and CROPs respectively should be interpreted qualitatively at this time.

4.4.6 TcdA CROPs is not sufficient for cellular intoxication.

Previous studies (207,208) in combination with the data presented herein suggest that RBD2 is sufficient to mediate productive binding and internalization of TcdA. However, it was unclear whether the same conclusions could be drawn for the CROPs. Therefore, the activity of a construct containing an internal deletion of RBD2 (henceforth referred to as $TcdA^{\Delta RBD2}$) was investigated. While $TcdA^{\Delta RBD2}$ bound to HT29 cells at

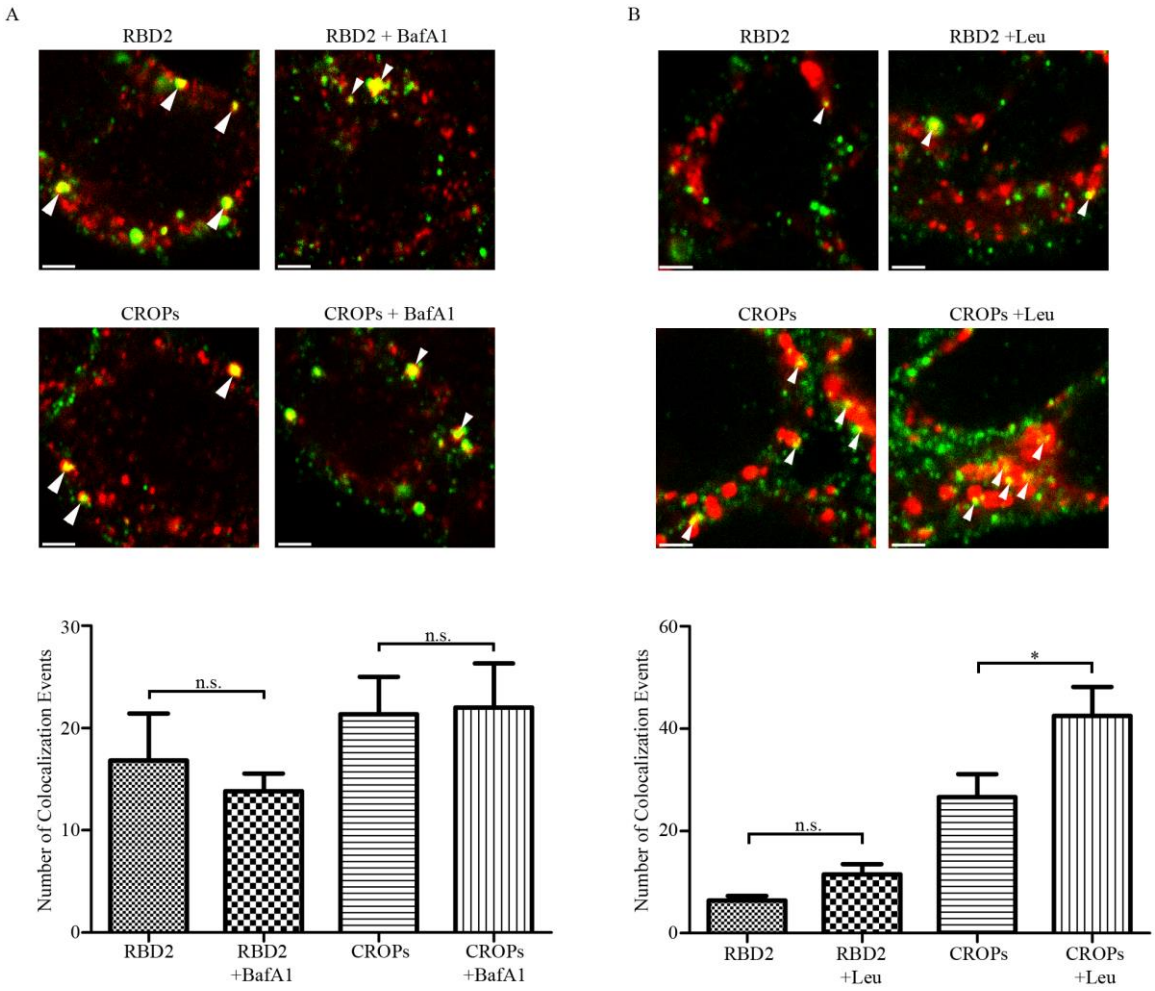

Figure 4.8. TcdA CROPs is rapidly sorted to the lysosome. **(A)** HT29 cells were pretreated with 250nM bafilomycin A1 or solvent for 30 minutes and then incubated at 37°C for 1 hour in the presence of 5 µM FLAG-tagged TcdA proteins. Cells were washed and fixed, and TcdA proteins visualized by immunostaining against the FLAG epitope (green). Colocalization with EEA1 (red) is highlighted with white arrows (top panel, 100× magnification, scale bar = 2 µm.) Colocalization of TcdA proteins with EEA1 was quantified (bottom panel). Values expressed as mean ± SEM (2 individual experiments, n≥6 fields per treatment) (n.s. denotes no significance, Mann-Whitney U test). **(B)** HT29 cells were pretreated with 100 µM leupeptin or solvent for 30 minutes and then incubated at 37°C for 1 hour in the presence of 5 µM FLAG-tagged TcdA RBD2 or CROPs. Cells were washed and fixed, and TcdA proteins visualized by immunostaining against the FLAG epitope (green). Colocalization with LAMP-1 (red) is highlighted with white arrows (top panel, 100× magnification, scale bar equal to 2µm.) Colocalization of TcdA proteins with LAMP-1 was quantified (bottom panel). Values expressed as mean ± SEM (2 individual experiments, n≥5 fields per treatment) (*, $p<0.05$; n.s., no significance, Mann-Whitney U test).

similar levels to CROPs alone (**Figure 4.9A**), it did not promote cell rounding or glucosylation of Rac1 under conditions where TcdA and TcdA$^{1-1874}$ were highly active (**Figure 4.9B-D**). Complementation of the missing domain from TcdA with the corresponding RBD2 from the related TcdB toxin was not able to restore functional activity, suggesting there may be intrinsic differences in the way TcdA and TcdB interact with mammalian cells (**Figure 4.10**).

4.5 Discussion

The clostridial glucosylating toxins produced by *Clostridium difficile* are important modulators of disease severity. Whereas the activities of the TcdA glucosyltransferase (GTD) and cysteine protease (CPD) domains have been well characterized, our understanding of receptor binding and cell entry pathways remains incomplete. In this study we directly addressed the hypothesis that TcdA, similar to TcdB, harbors a second receptor binding domain located between the delivery domain and the combined repetitive oligopeptides (CROPs).

Initially we attempted to localize the second binding domain, hereafter referred to as RBD2, through the construction and analysis of a series of toxin deletions. In agreement with the seminal studies of Gerhard and co-workers (207,208), we confirmed that the deletion mutant TcdA$^{1-1874}$ exhibited only a moderate defect in potency (**Figure 4.2**), supporting the concept that the CROPs domain is not essential for cytotoxicity *in vitro*. Several recent studies strongly support the conclusion that TcdB contains a receptor binding region located between residues 1372 and 1811 (187,210,276,278). Therefore, we generated a further deletion variant, TcdA$^{1-1361}$, which was hypothesized to lack both the CROPs and putative RBD-like region. As anticipated, TcdA$^{1-1361}$ lacked cytotoxicity

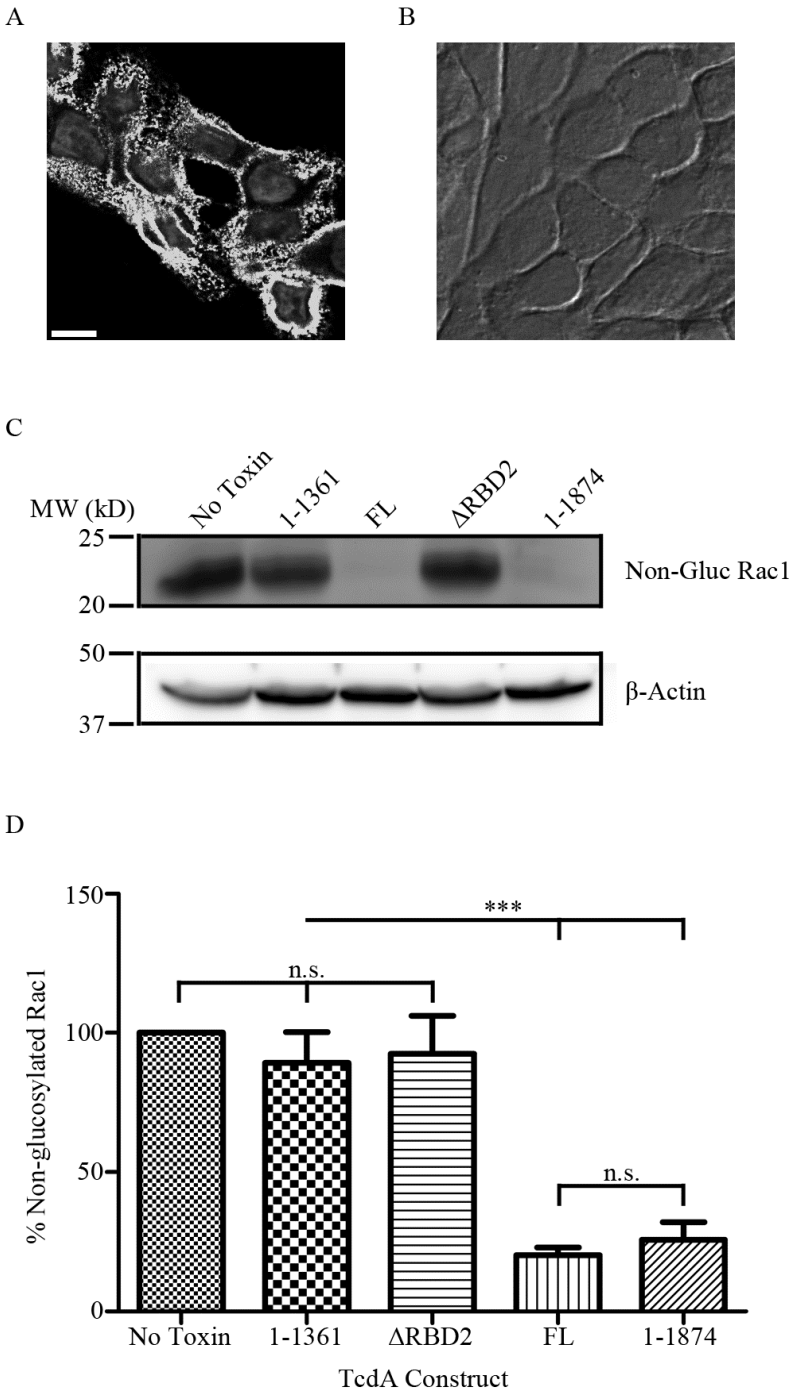

Figure 4.9. Removal of the second receptor binding domain from TcdA abrogates toxicity in HT29 cells. (A) HT29 cells were treated with 5 µM FLAG-tagged $TcdA^{\Delta RBD2}$ at 4°C for 1 hour and visualized by immunofluorescence (40× magnification, scale bar equal to 10 µm.) **(B)** HT29 cells were incubated for 24 hours with 100 nM $TcdA^{\Delta RBD2}$. Cytopathic effect (as evidenced by cell rounding) was observed via DIC imaging. **(C)** HT29 cells were treated for 48 hours with 100 nM TcdA, $TcdA^{1-1361}$, $TcdA^{\Delta RBD2}$, or $TcdA^{1-1874}$. Cell lysates were resolved by SDS-polyacrylamide gel electrophoresis following which non-glucosylated Rac1 and β-actin were detected by Western blot. **(D)** Western blots were quantified by densitometry, and amounts of non-glucosylated Rac1 normalized to β-actin. Values expressed as percentage of non-treated control, mean ± SEM for 3 independent experiments. (***, $p<0.001$; n.s., no significance, one-way ANOVA with Tukey post-test.)

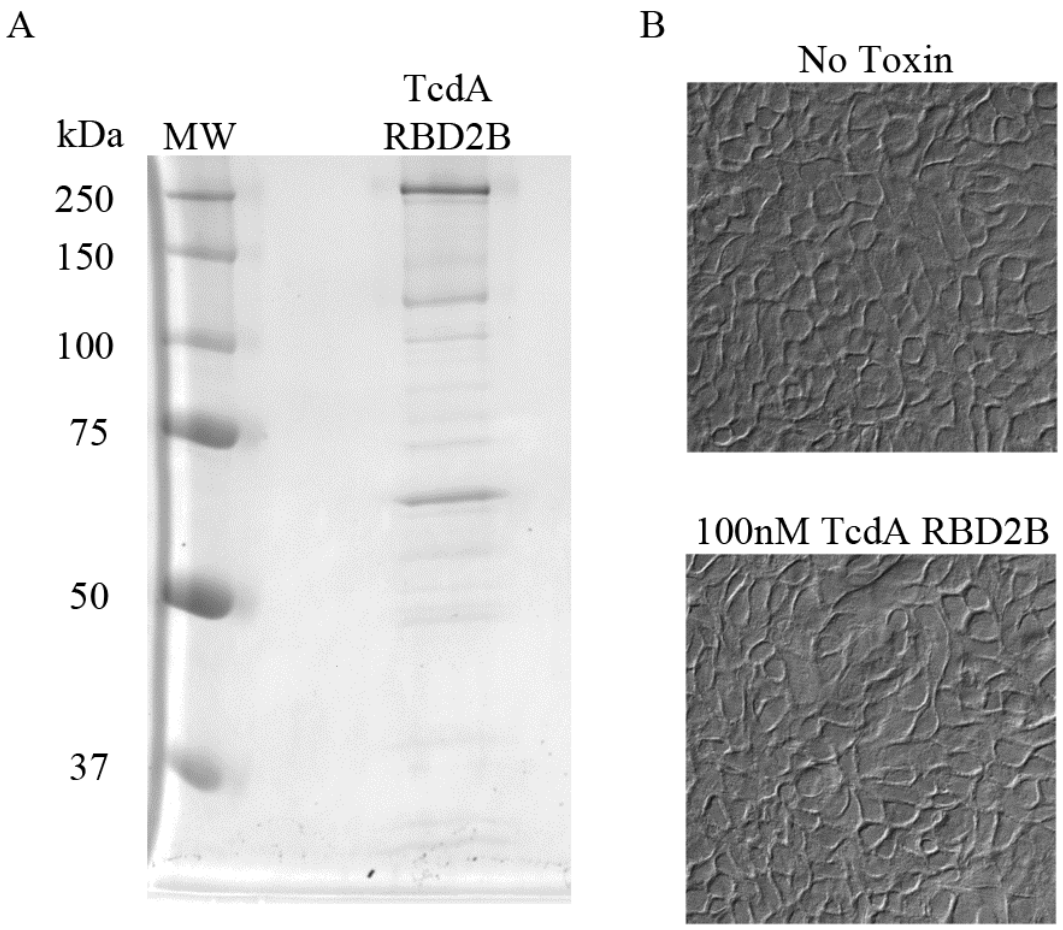

Figure 4.10. TcdA RBD2B does not display toxicity towards HT29 cells. (A) 5 µg of $TcdA^{RBD2B}$, a protein containing the RBD2 domain from TcdB in lieu of that from TcdA, was resolved on a 13.5% (w/v) SDS-polyacrylamide gel and stained with Coomassie Brilliant Blue R-250. **(B)** HT29 cells were incubated for 24 hours with 100 nM $TcdA^{RBD2B}$. Differential interference contrast (DIC) microscopy images were collected and analyzed; no cell rounding was observed.

at concentrations at least 1000-fold greater than TcdA (**Figure 4.2C** and **Figure 4.9**). However, the recently solved crystal structure of a TcdA fragment (residues 1-1832) raised the possibility that this deletion variant may be structurally compromised, particularly with regard to its ability to form pores in lipid bilayers (187,203,280). To test this possibility, we investigated pore formation in large unilamellar vesicles. All TcdA variants induced pH-dependent pore formation with half-maximal release occurring at similar toxin concentrations (**Table 4.1**). This result is consistent with previous reports arguing essential elements of the pore forming domain are located between residues 850-1135 (187,203,280). Thus, the deletion constructs do not appear to be inherently misfolded and inactive.

Next, we asked whether the isolated RBD2 (TcdA residues 1361-1874) and CROPs fragments could inhibit the cytotoxicity of full-length and CROPs-deficient toxins. Unexpectedly, no reduction in the toxicity of TcdA was observed when incubated with a 1000-fold molar excess of CROPs (**Figure 4.2D**), despite a previous report demonstrating competition between the two proteins for binding to HT29 cells at 4°C (207). While the reason for this difference is unclear, it is conceivable that at 37°C the CROPs domain could have become depleted by receptor-mediated internalization, thereby allowing TcdA access to a pool of free receptors. Alternately, given the inability of CROPs to inhibit the activity of $TcdA^{1-1874}$ (**Figure 4.2D**), the toxicity of TcdA could be the result of CROPs-independent internalization similar to the entry mechanism of $TcdA^{1-1874}$. Consistent with a previous report showing that $TcdA^{1-1874}$ caused only a slight reduction in binding of TcdA to HT29 cells (207), RBD2 did not interfere with the activity of TcdA. Conversely, RBD2 was able to reduce the cytopathic effect of $TcdA^{1-}$

Table 4.1. Concentration of TcdA proteins inducing half maximal release from K^+-loaded liposomes.

Protein	Concentration (nM)
TcdA	30±4
$TcdA^{1-1361}$	60±7
$TcdA^{\Delta RBD2}$	60±9
$TcdA^{1-1874}$	8.7±1[#]

3 individual experiments, n=2; #: Protein concentration adjusted for estimated purity of 5%, as per **Figure 4.1**.

^{1874} at all ratios tested (**Figure 4.2D**), presumably through competition for cell surface receptors. These data are consistent with a model in which TcdA, similar to TcdB and TpeL, contains a second binding site localized between the delivery domains and the CROPs.

Binding and entry of CROPs and RBD2 was further analyzed by flow cytometry and fluorescence microscopy. As anticipated from previous studies (207,208), the CROPs domain bound to the surface of HT29 cells in a saturable manner and was subsequently internalized into EEA1-positive structures (**Figure 4.3**, **Figure 4.5**, and **Figure 4.8**). While RBD2 was also observed to accumulate in EEA1-positive structures at 37°C, negligible surface binding was detected at either low or physiologic temperature. This is in apparent contradiction with binding studies performed by Gerhard and co-workers, where TcdA$^{1-1874}$ is shown to interact with HT29 cells at 4°C (207). Nevertheless, the reported binding of TcdA$^{1-1874}$ to HT29 cells appeared minimal, and could be enhanced by over 50-fold by preloading cells with the isolated CROPs domain—suggesting the increased signal intensity resulted from direct interaction between TcdA$^{1-1874}$ and cell surface associated CROPs. It is also conceivable that regions of TcdA located N-terminal to 1361 may also contribute to binding of TcdA$^{1-1874}$, though we have been unable to verify this possibility. Thus, our failure to detect surface binding of RBD2 likely reflects differences in the sensitivity of the different approaches employed in the studies. The inhibition of protein synthesis or disruption of the microtubule network did not affect endocytosis of RBD2, suggesting a requirement for continuous synthesis of new receptors does not account for the failure to observe surface binding of RBD2. Rather, our data seem to imply one of two possibilities; either (1) RBD2 interacts with a highly

abundant, low affinity receptor, or (2) it binds with moderate to high affinity to a low abundance receptor. In either case, visualization of RBD2 by fluorescence microscopy is likely explained by the clustering of multiple toxin-receptor complexes within endosomal compartments. Based on their results, Gerhard and co-workers previously suggested that option 1 could account for their data (207). While we cannot completely rule this out, enthusiasm is dampened by our observations that extended incubation of cells with RBD2 (up to 6 hours, **Figure 4.4**) does not result in increased surface binding and that RBD2 can efficiently block the activity of $TcdA^{1-1874}$. Rather, the latter observation, when combined with the findings that $TcdA^{1-1874}$ exhibits only a moderate defect in potency and that RBD2 accumulates within intracellular compartments, all support the concept that RBD2 binds a low abundance, high affinity receptor.

While our data are consistent with the existence of a second binding domain within TcdA, several questions remain. In particular, what is the function of the CROPs domain in the uptake of TcdA? Analysis of the ~30 Å resolution electron microscopy structure of TcdA in conjunction with the 3.25 Å crystal structure of TcdA fragment 1-1832 suggests the CROPs domain partially occludes the elongated scaffold of β-sheets (~1150-1800) overlapping RBD2 (193,203), and is further supported by biochemical data showing that the intermediate $TcdA^{1102-1847}$ fragment can directly bind to the CROPs region (281). Thus, one function of CROPs-receptor(s) interaction may be to correctly orient the extended delivery domain with respect to the membrane. On the other hand, the CROPs domain could function merely to increase the affinity of RBD2 for its cognate receptor(s). Enthusiasm for this model is limited by the observation that CROPs alone is able to bind and enter mammalian cells (**Figure 4.3**, **Figure 4.5**, and **Figure 4.8**) and

preliminary data showing that TcdA fragment 1361-CT does not enter cells more efficiently than RBD2 alone. Rather, the available data suggest that CROPs and RBD2 function as independent binding moieties, expanding the range of cell types susceptible to the toxin (207). Thus, the increased toxicity of TcdA in HT29 cells relative to $TcdA^{1-1874}$ is the result of additional CROPs-mediated internalization events and is supported by data suggesting the CROPs domain is largely responsible for binding of TcdA to the plasma membrane of HT29 cells. Further supporting this claim is the observation that monoclonal antibodies (mAbs) targeting the CROPs domain are effective at neutralizing TcdA *in vivo* (282). Moreover, CHO-C6 cells, which are seemingly deficient in CROPs binding, show almost identical susceptibility towards full length and truncated TcdA regarding cytopathic effect (207). While our data are consistent with this possibility, it is suggested that CROPs alone is not able to mediate productive intoxication of HT29 cells despite retaining binding and pore-forming functions (**Figure 4.9** and **Table 4.1**). However, it should be noted that excision of residues 1361-1874 removes part of an elongated scaffold of β-sheets which may contribute to the translocation process (203). In an attempt to mitigate these concerns, RBD2 from TcdA was replaced with the corresponding region from TcdB, though this did not result in a functional protein (**Figure 4.10**). This is not surprising in light of recent work indicating that the three most N-terminal short repeats in TcdB CROPs are required for binding of CSPG4 by TcdB RBD2 (283). In conclusion, we have identified a novel region within TcdA which functions as a second, CROPs-independent binding site. Our data are consistent with the recently proposed dual receptor model for the large clostridial glycosylating toxins.

4.6 Supplemental Methods

4.6.1 Cyclin D1 Western blot.

HT29 cells treated with 50 µg/ml of cycloheximide for 30, 60, and 90 minute intervals were lysed with radioimmune precipitation assay (RIPA) buffer at 4°C for 30 min. Total cell lysates were combined with SDS-PAGE sample buffer, resolved on 13.5% (w/v) SDS-polyacrylamide gels, transferred to Immobilon PVDF membranes, and subjected to Western blotting using antibodies against cyclin D1 (1:1000, Santa Cruz Biotechnology) and goat anti-rabbit-HRP (1:80000, Thermo Fisher Scientific). The membranes were washed, incubated with SuperSignal Dura (Thermo Fisher Scientific), and visualized using a CCD imaging system.

4.6.2 Liposome preparation.

Liposomes were freshly prepared by the freeze-thaw and extrusion method as described previously (268). Asolectin (30 mg total lipid) was dissolved in 1 ml chloroform, dried under a gentle stream of nitrogen, and placed under vacuum overnight to remove residual solvent. The dried lipid cake was hydrated in potassium buffer (10 mM HEPES-KOH, 150 mM KCl, 1 mM EDTA, pH 7.4) to a final concentration of 30 mg/ml by brief sonication at 42°C. The rehydrated lipid was then subjected to three cycles of rapid freeze-thaw, followed by extrusion through a 200-nm pore membrane (Nucleopore) using a miniextruder apparatus (Avanti Polar Lipids). Immediately prior to use, liposomes were exchanged into neutral potassium-free buffer (10 mM HEPES-NaOH, 150 mM NaCl, 1 mM EDTA, pH 7.4) by passage over a pre-equilibrated column of G-25 Sephadex.

4.6.3 Potassium ion release assay.

Liposomes (~5 μM) were diluted into 5 ml of low or neutral pH buffer with constant stirring and were allowed to equilibrate. TcdA proteins at a range of concentrations were then added to the solution and potassium release monitored using an ion-selective electrode (Orion, ThermoFisher Scientific) until the change in voltage reached a steady state (~180 seconds for all proteins tested). After 5 minutes of incubation, 50 μl of a 0.1% v/v Triton X-100 solution was added to estimate the total potassium concentration within the system. Specific K^+ release was determined by subtraction of basal release values obtained from liposomes incubated in buffer alone. Additional control assays were performed to ensure the observed release was due to pH-dependent insertion of TcdA proteins (**Figure 4.11**).

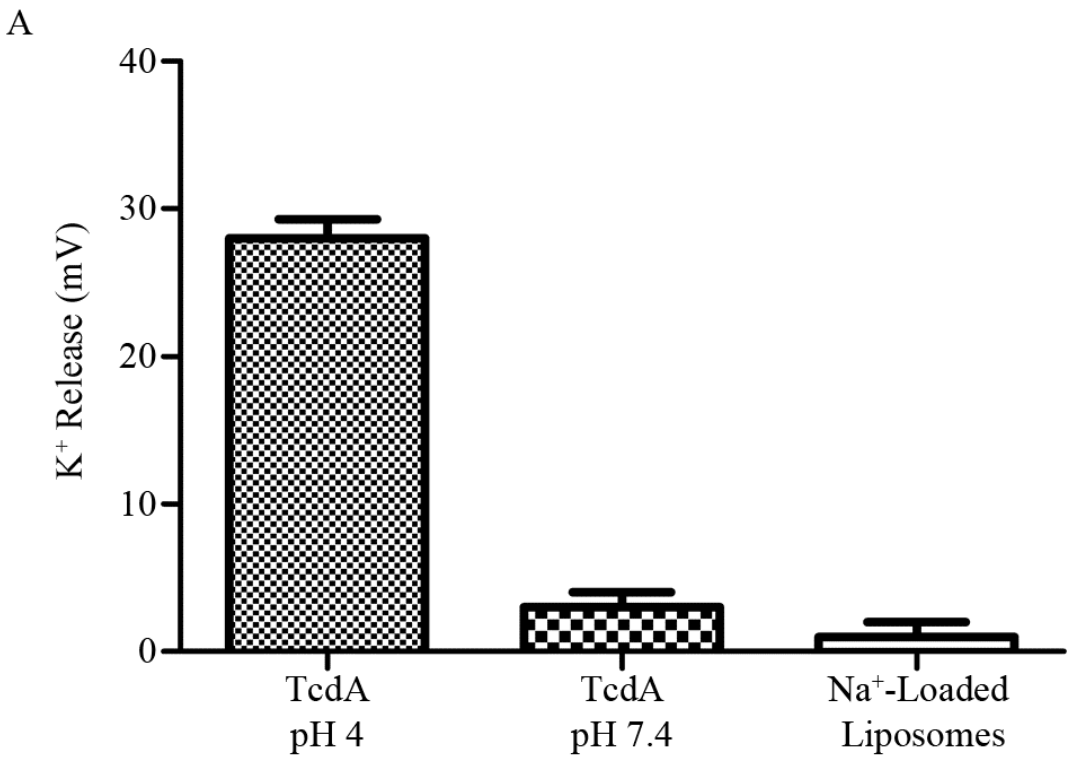

Figure 4.11. The pore-forming activity of recombinant TcdA is pH-dependent. (A) K^+-loaded Asolectin liposomes were incubated with 30 nM TcdA for five minutes at pH 4 or pH 7.4 and total release was recorded using a K^+-sensitive electrode. Values were normalized to liposomes incubated in buffer alone. Specificity of K^+ release by TcdA was further verified by performing this assay using Na^+-loaded liposomes. Values expressed as mean ± SEM (n=2).

CHAPTER 5: GENERAL DISCUSSION

The bacterial genus *Clostridium* contains several species of particular relevance to human disease. A hallmark of these species is the production of potent toxins, which contribute greatly to disease progression and severity. As such, characterization of these toxins is crucial for management of disease. The tetanus, botulinum, and *C. difficile* toxins have, and continue to be, the focus of important research. Despite our best efforts, there is still much to be discovered concerning the mechanisms by which these toxins function. This body of work contributes to our knowledge of clostridial toxins in a number of areas, focusing on the mechanisms of ganglioside binding by the CNTs, the potential role of cytosolic factors in translocation of TeNT, and the identification of a novel second receptor binding domain in TcdA. It is our hope that these studies will represent meaningful contributions to clostridial toxin research, providing insight that can be utilized to combat these diseases as well as be exploited to develop toxin variants that can be used as therapeutics for a number of other diseases.

The first step in intoxication by the CNTs involves HCR-mediated binding to the presynaptic membrane of α-motor neurons through two-receptor interactions. One of these two receptors is always a glycosphingolipid with ≥1 sialic acid sugar, also known as a ganglioside. Our first goal was to understand the basis by which CNTs discriminate between the carbohydrate moieties of individual gangliosides. BoNT and TeNT subtype variants were generated and assayed for their ability to bind various gangliosides. The data summarized in **Table 2.1** suggests that the specificity of ganglioside binding is determined in large part through the interaction of the Sia5 sugar with the hydrophobic A

subsite of the ganglioside binding pocket. Indeed, we generated BoNT variants that bound ganglioside with higher affinity than their wild-type counterparts, and were able to alter the binding specificity of TeNT by introducing targeted mutations, leading to a toxin variant that bound ganglioside in a Sia5-dependent manner. In addition to expanding our understanding of ganglioside binding by the CNTs, these findings have broader implications for the use of CNTs as clinical therapeutics.

A number of BoNT preparations are currently approved to treat a variety of neuromuscular disorders. They are also used for cosmetic purposes, and are sometimes used off-label to treat various other ailments. While effective, their applications and efficacy are limited in part by their immunogenicity and neuronal tropism. We observed that individual amino acid changes at key residues can lead to increased affinity for ganglioside. Furthermore, we directly showed that this increased affinity for ganglioside correlated with increased competition for cellular receptors. As such, it is highly probable that these mutations generate more active toxins, requiring lower therapeutic doses and therefore allow for longer clinical use without concern of neutralization. We were also able to alter the binding specificity of TeNT, such that it bound ganglioside in a similar manner to the BoNTs. This alone is an important finding, as it suggests that activity of TeNT may be localized to the periphery, opening up the possibility of its use as a therapeutic along the same lines as BoNT. This is predicated on the hypothesis that binding to gangliosides lacking Sia5—specifically GM1a—is important for retrograde axonal transport. Although previous work in our lab indicated that this variant retained the binding pattern of wild-type TeNT in CNS neuron cultures (as visualized by immunofluorescence), this hasn't been tested in cultured motor neurons or animals, and

therefore cannot be conclusively ruled out. It is also conceivable that the scope of this research could be expanded, allowing us to create variants that target specific cell types, including non-neuronal cells. Given the two-receptor nature of the CNTs, such work would likely need to include changes in protein receptor specificity as well. In conjunction with modified LCs that target additional substrates, the clinical therapeutic potential of these toxins shows great promise.

Perhaps the least understood mechanism in CNT intoxication is how the catalytically active LC is translocated across the endosomal membrane and released into the cell cytosol. We identified a novel region within HCT/T that appears capable of traversing the endosomal membrane and exposing a lysine-rich motif to the host cell cytosol. This lysine-rich motif (M2) may be important for the recruitment of a cytosolic translocation factor (CTF) complex that is critical for efficient intoxication. While insertion and pore formation by HCT/T are likely independent of this CTF, additional necessary functions (disulfide reduction, LC re-folding) are almost certainly dependent on its constituent parts. We directly showed interactions between HCT/T and two cytosolic factors: HSP90 and COPG. Previous work utilizing diphtheria toxin (DT) suggests that the interaction between lysine residues and COPG is the driving force behind the recruitment of the CTF. It is important to note, however, that a similar motif-containing region (M1) is present elsewhere in HCT/T. As such, characterization of this second region will be important to fully elucidate this mechanism. Based on our findings thus far, we hypothesize that both lysine-rich regions are capable of recruiting the CTF, but that the presence of both regions has a deleterious effect on TeNT intoxication. This is supported by the observation that certain CNTs appear to possess two lysine-rich

regions, while others possess only one. Furthermore, the results of our VAMP2 cleavage assay suggest that the presence of M1 alone leads to more efficient recruitment of the CTF, as compared to M2 alone, but that at least one of these two regions is required for efficient intoxication. The generation and investigation of HCT/T constructs lacking one or more lysine-rich regions will be important to more directly address this hypothesis.

Additional proteins recovered via immunoprecipitation should be subjected to analysis, preferably by mass spectrometry, to determine if there are more components to the CTF than have currently been identified. It is likely that at least one additional COPI component (possibly COPB) is a member of the CTF. Finally, further characterization of binding, pore formation, and LC activity are needed for each of the TeNT constructs to determine the specificity of the introduced mutations. Given that the CTF appears to contribute to intoxication by a number of AB toxins (DT, anthrax toxin, CNTs), this work may help to identify a convenient cellular target(s) for inhibition of these toxins. Based on our current findings, inhibition of HSP90 may be one promising area of investigation.

The mechanisms by which the LCTs bind and enter cells have yet to be fully resolved. We directly addressed the hypothesis that TcdA, similar to TcdB, harbors a second receptor binding domain located between the delivery domain and the combined repetitive oligopeptides (CROPs). We demonstrated that RBD2 is capable of binding and entering cells, although it does not appear to accumulate on the plasma membrane. In conjunction with inhibitor studies aimed at characterizing the intracellular populations of RBD2 and CROPs, we concluded that RBD2 most likely binds a low abundance, high affinity receptor and that it may undergo alternative intracellular trafficking that is important for productive intoxication.

The observation that both RBD2 and CROPs are capable of binding and entering cells raises the question of what exactly their roles are in the context of TcdA intoxication. Why exactly does TcdA need two receptor-binding domains? To answer this question, it is helpful to consider the role of TcdA in the context of *C. difficile* infection. TcdA is generally considered to be responsible for the disruption of the intestinal epithelium, whereas TcdB is most commonly attributed with the intoxication of underlying tissues. As such, the environment into which TcdA is released is almost certainly full of fluid, and therefore its local concentration near the epithelium is likely to be relatively low. If receptors for TcdA RBD2 are indeed low abundance, and RBD2-mediated binding is necessary for productive intoxication, then this constitutes a formidable barrier to TcdA intoxication. While the TcdA CROPs domain is dispensable for toxicity *in vitro*, this context argues that CROPs-mediated binding to abundant cellular receptors is almost certainly required for toxicity *in vivo*. Further supporting this claim is evidence that monoclonal antibodies raised against TcdA CROPs can effectively neutralize TcdA. Therefore, while CROPs and RBD2 are both binding domains, they likely confer complementary functions, both of which are important for TcdA toxicity *in vivo*.

Testing this, however, would be far from straightforward. Ideally, one would generate a mutant strain of *C. difficile* that produced only TcdA 1-1874, and assess the pathogenicity of such a strain in an animal model. Additional approaches, such as direct injection of toxin into the intestinal lumen, or a fluidic colonic explant model, could be informative as well. The main caveat to all of these approaches is that we do not know what the receptor for TcdA RBD2 is, and therefore could not be certain that the results were not simply due to the absence of the receptor.

In contrast to TcdA, efficient intoxication by TcdB may not require its CROPs domain at all. The TcdB CROPs domain is truncated compared to that from TcdA, and there is some evidence that its main function may actually be to modulate binding of the TcdB RBD2 domain. Given that putative receptor(s) for TcdB RBD2 have been identified by immunoprecipitation, they are also likely to be more abundant than those of TcdA RBD2. Finally, binding of isolated TcdB CROPs to cells has never been directly observed. This argues that binding of TcdB may be mediated primarily by its RBD2 domain. If this is true, then perhaps the RBD2 domains of TcdB and TcdA share similar intracellular properties. Until putative receptors for TcdA RBD2 can be identified, investigation of the interactions between TcdB RBD2 and its receptors may represent the most informative line of questioning concerning the exact intracellular pathways utilized by TcdA RBD2. In either case, future work should focus on the identification of putative receptors for TcdA RBD2, as the inference that these two toxins are similar in this respect may not be correct. Additionally, while we ruled out temperature-mediated structural changes in TcdA RBD2 as the reason we were unable to observe binding to HT29 cells at 4°C, knowing the identity of the receptor for TcdA RBD2 would allow us to perform a similar set of experiments with regards to its thermal stability.

This body of work has focused on elucidating a number of fundamental mechanisms governing clostridial toxin binding and translocation. More specifically, mechanisms of ganglioside binding by the CNTs, the potential role of cytosolic factors in translocation of TeNT, and the identification of a novel second receptor binding domain in TcdA.

CHAPTER 6: LITERATURE CITED

1. Lemichez, E., and Barbieri, J. T. (2013) General aspects and recent advances on bacterial protein toxins. *Cold Spring Harb Perspect Med* **3**, a013573
2. Popoff, M. R., and Bouvet, P. (2009) Clostridial toxins. *Future Microbiol* **4**, 1021-1064
3. Popoff, M. R., and Bouvet, P. (2013) Genetic characteristics of toxigenic *Clostridia* and toxin gene evolution. *Toxicon* **75**, 63-89
4. Popoff, M. R. (2014) Clostridial pore-forming toxins: powerful virulence factors. *Anaerobe* **30**, 220-238
5. Verherstraeten, S., Goossens, E., Valgaeren, B., Pardon, B., Timbermont, L., Haesebrouck, F., Ducatelle, R., Deprez, P., Wade, K. R., Tweten, R., and Van Immerseel, F. (2015) Perfringolysin O: The Underrated *Clostridium perfringens* Toxin? *Toxins (Basel)* **7**, 1702-1721
6. Voth, D. E., and Ballard, J. D. (2005) *Clostridium difficile* toxins: mechanism of action and role in disease. *Clin Microbiol Rev* **18**, 247-263
7. Aktories, K. (2011) Bacterial protein toxins that modify host regulatory GTPases. *Nat Rev Microbiol* **9**, 487-498
8. Kelly, C. P., and LaMont, J. T. (2008) *Clostridium difficile*--more difficult than ever. *N Engl J Med* **359**, 1932-1940
9. Loo, V. G., Poirier, L., Miller, M. A., Oughton, M., Libman, M. D., Michaud, S., Bourgault, A. M., Nguyen, T., Frenette, C., Kelly, M., Vibien, A., Brassard, P., Fenn, S., Dewar, K., Hudson, T. J., Horn, R., Rene, P., Monczak, Y., and Dascal, A. (2005) A predominantly clonal multi-institutional outbreak of *Clostridium difficile*-associated diarrhea with high morbidity and mortality. *N Engl J Med* **353**, 2442-2449
10. McDonald, L. C., Killgore, G. E., Thompson, A., Owens, R. C., Jr., Kazakova, S. V., Sambol, S. P., Johnson, S., and Gerding, D. N. (2005) An epidemic, toxin gene-variant strain of *Clostridium difficile*. *N Engl J Med* **353**, 2433-2441
11. Busch, C., and Aktories, K. (2000) Microbial toxins and the glycosylation of rho family GTPases. *Curr Opin Struct Biol* **10**, 528-535
12. Montal, M. (2010) Botulinum neurotoxin: a marvel of protein design. *Annu Rev Biochem* **79**, 591-617
13. Schiavo, G., Matteoli, M., and Montecucco, C. (2000) Neurotoxins affecting neuroexocytosis. *Physiol Rev* **80**, 717-766
14. Hatheway, C. L. (1990) Toxigenic *clostridia*. *Clin Microbiol Rev* **3**, 66-98
15. McCroskey, L. M., Hatheway, C. L., Fenicia, L., Pasolini, B., and Aureli, P. (1986) Characterization of an organism that produces type E botulinal toxin but which resembles *Clostridium butyricum* from the feces of an infant with type E botulism. *J Clin Microbiol* **23**, 201-202
16. McCroskey, L. M., Hatheway, C. L., Woodruff, B. A., Greenberg, J. A., and Jurgenson, P. (1991) Type F botulism due to neurotoxigenic *Clostridium baratii* from an unknown source in an adult. *J Clin Microbiol* **29**, 2618-2620
17. Altwegg, M., and Hatheway, C. L. (1988) Multilocus enzyme electrophoresis of *Clostridium argentinense* (*Clostridium botulinum* toxin type G) and phenotypically similar asaccharolytic *clostridia*. *J Clin Microbiol* **26**, 2447-2449

18. Bruggemann, H., Brzuszkiewicz, E., Chapeton-Montes, D., Plourde, L., Speck, D., and Popoff, M. R. (2015) Genomics of *Clostridium tetani*. *Res Microbiol* **166**, 326-331
19. Barash, J. R., and Arnon, S. S. (2014) A novel strain of *Clostridium botulinum* that produces type B and type H botulinum toxins. *J Infect Dis* **209**, 183-191
20. Hill, K. K., and Smith, T. J. (2013) Genetic diversity within *Clostridium botulinum* serotypes, botulinum neurotoxin gene clusters and toxin subtypes. *Curr Top Microbiol Immunol* **364**, 1-20
21. Smith, T. J., Lou, J., Geren, I. N., Forsyth, C. M., Tsai, R., Laporte, S. L., Tepp, W. H., Bradshaw, M., Johnson, E. A., Smith, L. A., and Marks, J. D. (2005) Sequence variation within botulinum neurotoxin serotypes impacts antibody binding and neutralization. *Infect Immun* **73**, 5450-5457
22. Poulet, S., Hauser, D., Quanz, M., Niemann, H., and Popoff, M. R. (1992) Sequences of the botulinal neurotoxin E derived from *Clostridium botulinum* type E (strain Beluga) and *Clostridium butyricum* (strains ATCC 43181 and ATCC 43755). *Biochem Biophys Res Commun* **183**, 107-113
23. Peck, M. W. (2009) Biology and genomic analysis of *Clostridium botulinum*. *Adv Microb Physiol* **55**, 183-265, 320
24. Arnon, S. S., Schechter, R., Inglesby, T. V., Henderson, D. A., Bartlett, J. G., Ascher, M. S., Eitzen, E., Fine, A. D., Hauer, J., Layton, M., Lillibridge, S., Osterholm, M. T., O'Toole, T., Parker, G., Perl, T. M., Russell, P. K., Swerdlow, D. L., Tonat, K., and Working Group on Civilian, B. (2001) Botulinum toxin as a biological weapon: medical and public health management. *JAMA* **285**, 1059-1070
25. Gill, D. M. (1982) Bacterial toxins: a table of lethal amounts. *Microbiol Rev* **46**, 86-94
26. Maksymowych, A. B., Reinhard, M., Malizio, C. J., Goodnough, M. C., Johnson, E. A., and Simpson, L. L. (1999) Pure botulinum neurotoxin is absorbed from the stomach and small intestine and produces peripheral neuromuscular blockade. *Infect Immun* **67**, 4708-4712
27. Pappas, G., Kiriaze, I. J., and Falagas, M. E. (2008) Insights into infectious disease in the era of Hippocrates. *Int J Infect Dis* **12**, 347-350
28. Montecucco, C., and Schiavo, G. (1995) Structure and function of tetanus and botulinum neurotoxins. *Q Rev Biophys* **28**, 423-472
29. Montecucco, C., Schiavo, G., and Rossetto, O. (1996) The mechanism of action of tetanus and botulinum neurotoxins. *Arch Toxicol Suppl* **18**, 342-354
30. Erbguth, F. J. (2004) Historical notes on botulism, *Clostridium botulinum*, botulinum toxin, and the idea of the therapeutic use of the toxin. *Mov Disord* **19 Suppl 8**, S2-6
31. CDC. (2015) Epidemiology and Prevention of Vaccine-Preventable Diseases, 13th Edition.
32. Chalya, P. L., Mabula, J. B., Dass, R. M., Mbelenge, N., Mshana, S. E., and Gilyoma, J. M. (2011) Ten-year experiences with Tetanus at a Tertiary hospital in Northwestern Tanzania: A retrospective review of 102 cases. *World J Emerg Surg* **6**, 20

33. Collins, S., White, J., Ramsay, M., and Amirthalingam, G. (2015) The importance of tetanus risk assessment during wound management. *IDCases* **2**, 3-5
34. Lisboa, T., Ho, Y. L., Henriques Filho, G. T., Brauner, J. S., Valiatti, J. L., Verdeal, J. C., and Machado, F. R. (2011) Guidelines for the management of accidental tetanus in adult patients. *Rev Bras Ter Intensiva* **23**, 394-409
35. Stiehm, E. R. (1979) Standard and special human immune serum globulins as therapeutic agents. *Pediatrics* **63**, 301-319
36. Hottle, G. A., Nigg, C., and Lichty, J. A. (1947) Studies on botulinum toxoid, types A and B; methods for determining antigenicity in animals. *J Immunol* **55**, 255-262
37. Nigg, C., Hottle, G. A., and et al. (1947) Studies on botulinum toxoid, types A and P; production of alum precipitated toxoids. *J Immunol* **55**, 245-254
38. Reames, H. R., Kadull, P. J., and et al. (1947) Studies on botulinum toxoids, types A and B; immunization of man. *J Immunol* **55**, 309-324
39. Smith, L. A., and Rusnak, J. M. (2007) Botulinum neurotoxin vaccines: past, present, and future. *Crit Rev Immunol* **27**, 303-318
40. Webb, R. P., and Smith, L. A. (2013) What next for botulism vaccine development? *Expert Rev Vaccines* **12**, 481-492
41. Webb, R. P., Smith, T. J., Wright, P., Brown, J., and Smith, L. A. (2009) Production of catalytically inactive BoNT/A1 holoprotein and comparison with BoNT/A1 subunit vaccines against toxin subtypes A1, A2, and A3. *Vaccine* **27**, 4490-4497
42. Przedpelski, A., Tepp, W. H., Kroken, A. R., Fu, Z., Kim, J. J., Johnson, E. A., and Barbieri, J. T. (2013) Enhancing the protective immune response against botulism. *Infect Immun* **81**, 2638-2644
43. Liu, B., Shi, D., Chang, S., Gong, X., Yu, Y., Sun, Z., and Wu, J. (2015) Characterization and immunological activity of different forms of recombinant secreted Hc of botulinum neurotoxin serotype B products expressed in yeast. *Sci Rep* **5**, 7678
44. Chang, G. Y., and Ganguly, G. (2003) Early antitoxin treatment in wound botulism results in better outcome. *Eur Neurol* **49**, 151-153
45. Sobel, J. (2005) Botulism. *Clin Infect Dis* **41**, 1167-1173
46. Lacy, D. B., and Stevens, R. C. (1999) Sequence homology and structural analysis of the clostridial neurotoxins. *J Mol Biol* **291**, 1091-1104
47. Lacy, D. B., Tepp, W., Cohen, A. C., DasGupta, B. R., and Stevens, R. C. (1998) Crystal structure of botulinum neurotoxin type A and implications for toxicity. *Nat Struct Biol* **5**, 898-902
48. Binz, T., and Rummel, A. (2009) Cell entry strategy of clostridial neurotoxins. *J Neurochem* **109**, 1584-1595
49. Pirazzini, M., Rossetto, O., Bolognese, P., Shone, C. C., and Montecucco, C. (2011) Double anchorage to the membrane and intact inter-chain disulfide bond are required for the low pH induced entry of tetanus and botulinum neurotoxins into neurons. *Cell Microbiol* **13**, 1731-1743
50. Vaidyanathan, V. V., Yoshino, K., Jahnz, M., Dorries, C., Bade, S., Nauenburg, S., Niemann, H., and Binz, T. (1999) Proteolysis of SNAP-25 isoforms by botulinum neurotoxin types A, C, and E: domains and amino acid residues

controlling the formation of enzyme-substrate complexes and cleavage. *J Neurochem* **72**, 327-337
51. Foran, P., Shone, C. C., and Dolly, J. O. (1994) Differences in the protease activities of tetanus and botulinum B toxins revealed by the cleavage of vesicle-associated membrane protein and various sized fragments. *Biochemistry* **33**, 15365-15374
52. Rummel, A. (2013) Double receptor anchorage of botulinum neurotoxins accounts for their exquisite neurospecificity. *Curr Top Microbiol Immunol* **364**, 61-90
53. Kumaran, D., Eswaramoorthy, S., Furey, W., Navaza, J., Sax, M., and Swaminathan, S. (2009) Domain organization in *Clostridium botulinum* neurotoxin type E is unique: its implication in faster translocation. *J Mol Biol* **386**, 233-245
54. Swaminathan, S., and Eswaramoorthy, S. (2000) Structural analysis of the catalytic and binding sites of *Clostridium botulinum* neurotoxin B. *Nat Struct Biol* **7**, 693-699
55. Masuyer, G., Conrad, J., and Stenmark, P. (2017) The structure of the tetanus toxin reveals pH-mediated domain dynamics. *EMBO Rep* **18**, 1306-1317
56. Van Heyningen, W. E. (1961) The relation between the fixation and inactivation of tetanus toxin by ganglioside. *Br J Exp Pathol* **42**, 397-398
57. Van Heyningen, W. E., and Miller, P. A. (1961) The fixation of tetanus toxin by ganglioside. *J Gen Microbiol* **24**, 107-119
58. Rummel, A., Mahrhold, S., Bigalke, H., and Binz, T. (2004) The HCC-domain of botulinum neurotoxins A and B exhibits a singular ganglioside binding site displaying serotype specific carbohydrate interaction. *Mol Microbiol* **51**, 631-643
59. Karlsson, K. A. (1998) On the character and functions of sphingolipids. *Acta Biochim Pol* **45**, 429-438
60. Strotmeier, J., Lee, K., Volker, A. K., Mahrhold, S., Zong, Y., Zeiser, J., Zhou, J., Pich, A., Bigalke, H., Binz, T., Rummel, A., and Jin, R. (2010) Botulinum neurotoxin serotype D attacks neurons via two carbohydrate-binding sites in a ganglioside-dependent manner. *Biochem J* **431**, 207-216
61. Kroken, A. R., Karalewitz, A. P., Fu, Z., Baldwin, M. R., Kim, J. J., and Barbieri, J. T. (2011) Unique ganglioside binding by botulinum neurotoxins C and D-SA. *FEBS J* **278**, 4486-4496
62. Rummel, A., Hafner, K., Mahrhold, S., Darashchonak, N., Holt, M., Jahn, R., Beermann, S., Karnath, T., Bigalke, H., and Binz, T. (2009) Botulinum neurotoxins C, E and F bind gangliosides via a conserved binding site prior to stimulation-dependent uptake with botulinum neurotoxin F utilising the three isoforms of SV2 as second receptor. *J Neurochem* **110**, 1942-1954
63. Fotinou, C., Emsley, P., Black, I., Ando, H., Ishida, H., Kiso, M., Sinha, K. A., Fairweather, N. F., and Isaacs, N. W. (2001) The crystal structure of tetanus toxin Hc fragment complexed with a synthetic GT1b analogue suggests cross-linking between ganglioside receptors and the toxin. *J Biol Chem* **276**, 32274-32281
64. Benson, M. A., Fu, Z., Kim, J. J., and Baldwin, M. R. (2011) Unique ganglioside recognition strategies for clostridial neurotoxins. *J Biol Chem* **286**, 34015-34022

65. Rummel, A., Bade, S., Alves, J., Bigalke, H., and Binz, T. (2003) Two carbohydrate binding sites in the H(CC)-domain of tetanus neurotoxin are required for toxicity. *J Mol Biol* **326**, 835-847
66. Chen, C., Baldwin, M. R., and Barbieri, J. T. (2008) Molecular basis for tetanus toxin coreceptor interactions. *Biochemistry* **47**, 7179-7186
67. Chen, C., Fu, Z., Kim, J. J., Barbieri, J. T., and Baldwin, M. R. (2009) Gangliosides as high affinity receptors for tetanus neurotoxin. *J Biol Chem* **284**, 26569-26577
68. Karalewitz, A. P., Fu, Z., Baldwin, M. R., Kim, J. J., and Barbieri, J. T. (2012) Botulinum neurotoxin serotype C associates with dual ganglioside receptors to facilitate cell entry. *J Biol Chem* **287**, 40806-40816
69. Peng, L., Berntsson, R. P., Tepp, W. H., Pitkin, R. M., Johnson, E. A., Stenmark, P., and Dong, M. (2012) Botulinum neurotoxin D-C uses synaptotagmin I and II as receptors, and human synaptotagmin II is not an effective receptor for type B, D-C and G toxins. *J Cell Sci* **125**, 3233-3242
70. Fu, Z., Chen, C., Barbieri, J. T., Kim, J. J., and Baldwin, M. R. (2009) Glycosylated SV2 and gangliosides as dual receptors for botulinum neurotoxin serotype F. *Biochemistry* **48**, 5631-5641
71. Dong, M., Liu, H., Tepp, W. H., Johnson, E. A., Janz, R., and Chapman, E. R. (2008) Glycosylated SV2A and SV2B mediate the entry of botulinum neurotoxin E into neurons. *Mol Biol Cell* **19**, 5226-5237
72. Dong, M., Yeh, F., Tepp, W. H., Dean, C., Johnson, E. A., Janz, R., and Chapman, E. R. (2006) SV2 is the protein receptor for botulinum neurotoxin A. *Science* **312**, 592-596
73. Bercsenyi, K., Schmieg, N., Bryson, J. B., Wallace, M., Caccin, P., Golding, M., Zanotti, G., Greensmith, L., Nischt, R., and Schiavo, G. (2014) Tetanus toxin entry. Nidogens are therapeutic targets for the prevention of tetanus. *Science* **346**, 1118-1123
74. Rummel, A., Eichner, T., Weil, T., Karnath, T., Gutcaits, A., Mahrhold, S., Sandhoff, K., Proia, R. L., Acharya, K. R., Bigalke, H., and Binz, T. (2007) Identification of the protein receptor binding site of botulinum neurotoxins B and G proves the double-receptor concept. *Proc Natl Acad Sci U S A* **104**, 359-364
75. Schmitt, J., Karalewitz, A., Benefield, D. A., Mushrush, D. J., Pruitt, R. N., Spiller, B. W., Barbieri, J. T., and Lacy, D. B. (2010) Structural analysis of botulinum neurotoxin type G receptor binding. *Biochemistry* **49**, 5200-5205
76. Chai, Q., Arndt, J. W., Dong, M., Tepp, W. H., Johnson, E. A., Chapman, E. R., and Stevens, R. C. (2006) Structural basis of cell surface receptor recognition by botulinum neurotoxin B. *Nature* **444**, 1096-1100
77. Dong, M., Richards, D. A., Goodnough, M. C., Tepp, W. H., Johnson, E. A., and Chapman, E. R. (2003) Synaptotagmins I and II mediate entry of botulinum neurotoxin B into cells. *J Cell Biol* **162**, 1293-1303
78. Benecke, R., Takano, K., Schmidt, J., and Henatsch, H. D. (1977) Tetanus toxin induced actions on spinal Renshaw cells and Ia-inhibitory interneurones during development of local tetanus in the cat. *Exp Brain Res* **27**, 271-286

79. Deinhardt, K., Salinas, S., Verastegui, C., Watson, R., Worth, D., Hanrahan, S., Bucci, C., and Schiavo, G. (2006) Rab5 and Rab7 control endocytic sorting along the axonal retrograde transport pathway. *Neuron* **52**, 293-305
80. Koriazova, L. K., and Montal, M. (2003) Translocation of botulinum neurotoxin light chain protease through the heavy chain channel. *Nat Struct Biol* **10**, 13-18
81. Fischer, A., Sambashivan, S., Brunger, A. T., and Montal, M. (2012) Beltless translocation domain of botulinum neurotoxin A embodies a minimum ion-conductive channel. *J Biol Chem* **287**, 1657-1661
82. Burns, J. R., and Baldwin, M. R. (2014) Tetanus neurotoxin utilizes two sequential membrane interactions for channel formation. *J Biol Chem* **289**, 22450-22458
83. Fischer, A., and Montal, M. (2007) Crucial role of the disulfide bridge between botulinum neurotoxin light and heavy chains in protease translocation across membranes. *J Biol Chem* **282**, 29604-29611
84. Fischer, A., Mushrush, D. J., Lacy, D. B., and Montal, M. (2008) Botulinum neurotoxin devoid of receptor binding domain translocates active protease. *PLoS Pathog* **4**, e1000245
85. Brunger, A. T., Breidenbach, M. A., Jin, R., Fischer, A., Santos, J. S., and Montal, M. (2007) Botulinum neurotoxin heavy chain belt as an intramolecular chaperone for the light chain. *PLoS Pathog* **3**, 1191-1194
86. Mushrush, D. J., Koteiche, H. A., Sammons, M. A., Link, A. J., McHaourab, H. S., and Lacy, D. B. (2011) Studies of the mechanistic details of the pH-dependent association of botulinum neurotoxin with membranes. *J Biol Chem* **286**, 27011-27018
87. Parikh, S., and Singh, B. R. (2007) Comparative membrane channel size and activity of botulinum neurotoxins A and E. *Protein J* **26**, 19-28
88. Cai, S., Kukreja, R., Shoesmith, S., Chang, T. W., and Singh, B. R. (2006) Botulinum neurotoxin light chain refolds at endosomal pH for its translocation. *Protein J* **25**, 455-462
89. Fu, F. N., Busath, D. D., and Singh, B. R. (2002) Spectroscopic analysis of low pH and lipid-induced structural changes in type A botulinum neurotoxin relevant to membrane channel formation and translocation. *Biophys Chem* **99**, 17-29
90. Montecucco, C., and Schiavo, G. (1994) Mechanism of action of tetanus and botulinum neurotoxins. *Mol Microbiol* **13**, 1-8
91. Schiavo, G., Benfenati, F., Poulain, B., Rossetto, O., Polverino de Laureto, P., DasGupta, B. R., and Montecucco, C. (1992) Tetanus and botulinum-B neurotoxins block neurotransmitter release by proteolytic cleavage of synaptobrevin. *Nature* **359**, 832-835
92. Arndt, J. W., Yu, W., Bi, F., and Stevens, R. C. (2005) Crystal structure of botulinum neurotoxin type G light chain: serotype divergence in substrate recognition. *Biochemistry* **44**, 9574-9580
93. Schiavo, G., Shone, C. C., Rossetto, O., Alexander, F. C., and Montecucco, C. (1993) Botulinum neurotoxin serotype F is a zinc endopeptidase specific for VAMP/synaptobrevin. *J Biol Chem* **268**, 11516-11519
94. Guo, J., and Chen, S. (2013) Unique substrate recognition mechanism of the botulinum neurotoxin D light chain. *J Biol Chem* **288**, 27881-27887

95. Schiavo, G., Rossetto, O., Catsicas, S., Polverino de Laureto, P., DasGupta, B. R., Benfenati, F., and Montecucco, C. (1993) Identification of the nerve terminal targets of botulinum neurotoxin serotypes A, D, and E. *J Biol Chem* **268**, 23784-23787
96. Yamasaki, S., Binz, T., Hayashi, T., Szabo, E., Yamasaki, N., Eklund, M., Jahn, R., and Niemann, H. (1994) Botulinum neurotoxin type G proteolyses the Ala81-Ala82 bond of rat synaptobrevin 2. *Biochem Biophys Res Commun* **200**, 829-835
97. Yamasaki, S., Hu, Y., Binz, T., Kalkuhl, A., Kurazono, H., Tamura, T., Jahn, R., Kandel, E., and Niemann, H. (1994) Synaptobrevin/vesicle-associated membrane protein (VAMP) of *Aplysia californica*: structure and proteolysis by tetanus toxin and botulinal neurotoxins type D and F. *Proc Natl Acad Sci U S A* **91**, 4688-4692
98. Foran, P., Lawrence, G. W., Shone, C. C., Foster, K. A., and Dolly, J. O. (1996) Botulinum neurotoxin C1 cleaves both syntaxin and SNAP-25 in intact and permeabilized chromaffin cells: correlation with its blockade of catecholamine release. *Biochemistry* **35**, 2630-2636
99. Schiavo, G., Santucci, A., Dasgupta, B. R., Mehta, P. P., Jontes, J., Benfenati, F., Wilson, M. C., and Montecucco, C. (1993) Botulinum neurotoxins serotypes A and E cleave SNAP-25 at distinct COOH-terminal peptide bonds. *FEBS Lett* **335**, 99-103
100. Binz, T., Blasi, J., Yamasaki, S., Baumeister, A., Link, E., Sudhof, T. C., Jahn, R., and Niemann, H. (1994) Proteolysis of SNAP-25 by types E and A botulinal neurotoxins. *J Biol Chem* **269**, 1617-1620
101. Schiavo, G., Shone, C. C., Bennett, M. K., Scheller, R. H., and Montecucco, C. (1995) Botulinum neurotoxin type C cleaves a single Lys-Ala bond within the carboxyl-terminal region of syntaxins. *J Biol Chem* **270**, 10566-10570
102. Pirazzini, M., Azarnia Tehran, D., Zanetti, G., Lista, F., Binz, T., Shone, C. C., Rossetto, O., and Montecucco, C. (2015) The thioredoxin reductase--Thioredoxin redox system cleaves the interchain disulphide bond of botulinum neurotoxins on the cytosolic surface of synaptic vesicles. *Toxicon* **107**, 32-36
103. Breidenbach, M. A., and Brunger, A. T. (2004) Substrate recognition strategy for botulinum neurotoxin serotype A. *Nature* **432**, 925-929
104. Chen, S., Hall, C., and Barbieri, J. T. (2008) Substrate recognition of VAMP-2 by botulinum neurotoxin B and tetanus neurotoxin. *J Biol Chem* **283**, 21153-21159
105. Fu, Z., Chen, S., Baldwin, M. R., Boldt, G. E., Crawford, A., Janda, K. D., Barbieri, J. T., and Kim, J. J. (2006) Light chain of botulinum neurotoxin serotype A: structural resolution of a catalytic intermediate. *Biochemistry* **45**, 8903-8911
106. Chen, S., and Barbieri, J. T. (2006) Unique substrate recognition by botulinum neurotoxins serotypes A and E. *J Biol Chem* **281**, 10906-10911
107. Eleopra, R., Tugnoli, V., Rossetto, O., De Grandis, D., and Montecucco, C. (1998) Different time courses of recovery after poisoning with botulinum neurotoxin serotypes A and E in humans. *Neurosci Lett* **256**, 135-138
108. Keller, J. E., Neale, E. A., Oyler, G., and Adler, M. (1999) Persistence of botulinum neurotoxin action in cultured spinal cord cells. *FEBS Lett* **456**, 137-142
109. Chen, S., and Barbieri, J. T. (2009) Engineering botulinum neurotoxin to extend therapeutic intervention. *Proc Natl Acad Sci U S A* **106**, 9180-9184

110. Davletov, B., Bajohrs, M., and Binz, T. (2005) Beyond BOTOX: advantages and limitations of individual botulinum neurotoxins. *Trends Neurosci* **28**, 446-452
111. Lawson, P. A., Citron, D. M., Tyrrell, K. L., and Finegold, S. M. (2016) Reclassification of *Clostridium difficile* as *Clostridioides difficile* (Hall and O'Toole 1935) Prevot 1938. *Anaerobe* **40**, 95-99
112. Just, I., Wilm, M., Selzer, J., Rex, G., von Eichel-Streiber, C., Mann, M., and Aktories, K. (1995) The enterotoxin from *Clostridium difficile* (ToxA) monoglucosylates the Rho proteins. *J Biol Chem* **270**, 13932-13936
113. Just, I., Selzer, J., Wilm, M., von Eichel-Streiber, C., Mann, M., and Aktories, K. (1995) Glucosylation of Rho proteins by *Clostridium difficile* toxin B. *Nature* **375**, 500-503
114. Just, I., and Gerhard, R. (2004) Large clostridial cytotoxins. *Rev Physiol Biochem Pharmacol* **152**, 23-47
115. von Eichel-Streiber, C., Boquet, P., Sauerborn, M., and Thelestam, M. (1996) Large clostridial cytotoxins--a family of glycosyltransferases modifying small GTP-binding proteins. *Trends Microbiol* **4**, 375-382
116. Schirmer, J., and Aktories, K. (2004) Large clostridial cytotoxins: cellular biology of Rho/Ras-glucosylating toxins. *Biochim Biophys Acta* **1673**, 66-74
117. Hall, I. C., and O'Toole, E. (1935) Intestinal flora in newborn infants with a description of a new pathogenic anaerobe, *Bacillus difficilis*. *Am J Dis Child* **49**, 390-402
118. Kachrimanidou, M., and Malisiovas, N. (2011) *Clostridium difficile* infection: a comprehensive review. *Crit Rev Microbiol* **37**, 178-187
119. Fekety, R., and Shah, A. B. (1993) Diagnosis and treatment of *Clostridium difficile* colitis. *JAMA* **269**, 71-75
120. Falsen, E., Kaijser, B., Nehls, L., Nygren, B., and Svedhem, A. (1980) *Clostridium difficile* in relation to enteric bacterial pathogens. *J Clin Microbiol* **12**, 297-300
121. Delmee, M., Verellen, G., Avesani, V., and Francois, G. (1988) Clostridium difficile in neonates: serogrouping and epidemiology. *Eur J Pediatr* **147**, 36-40
122. Davies, A. H., Roberts, A. K., Shone, C. C., and Acharya, K. R. (2011) Super toxins from a super bug: structure and function of *Clostridium difficile* toxins. *Biochem J* **436**, 517-526
123. Bryant, K., and McDonald, L. C. (2009) *Clostridium difficile* infections in children. *Pediatr Infect Dis J* **28**, 145-146
124. Kelly, C. P., and LaMont, J. T. (1998) *Clostridium difficile* infection. *Annu Rev Med* **49**, 375-390
125. Kelly, C. P., Pothoulakis, C., and LaMont, J. T. (1994) *Clostridium difficile* colitis. *N Engl J Med* **330**, 257-262
126. Bartlett, J. G., Moon, N., Chang, T. W., Taylor, N., and Onderdonk, A. B. (1978) Role of *Clostridium difficile* in antibiotic-associated pseudomembranous colitis. *Gastroenterology* **75**, 778-782
127. Knoop, F. C., Owens, M., and Crocker, I. C. (1993) *Clostridium difficile*: clinical disease and diagnosis. *Clin Microbiol Rev* **6**, 251-265
128. Hummel, R. P., Altemeier, W. A., and Hill, E. O. (1964) Iatrogenic Staphylococcal Enterocolitis. *Ann Surg* **160**, 551-560

129. Khan, M. Y., and Hall, W. H. (1966) Staphylococcal enterocolitis--treatment with oral vancomycin. *Ann Intern Med* **65**, 1-8
130. Lessa, F. C., Mu, Y., Bamberg, W. M., Beldavs, Z. G., Dumyati, G. K., Dunn, J. R., Farley, M. M., Holzbauer, S. M., Meek, J. I., Phipps, E. C., Wilson, L. E., Winston, L. G., Cohen, J. A., Limbago, B. M., Fridkin, S. K., Gerding, D. N., and McDonald, L. C. (2015) Burden of *Clostridium difficile* infection in the United States. *N Engl J Med* **372**, 825-834
131. Kyne, L., Hamel, M. B., Polavaram, R., and Kelly, C. P. (2002) Health care costs and mortality associated with nosocomial diarrhea due to *Clostridium difficile*. *Clin Infect Dis* **34**, 346-353
132. Wilkins, T. D., and Lyerly, D. M. (2003) *Clostridium difficile* testing: after 20 years, still challenging. *J Clin Microbiol* **41**, 531-534
133. Gerding, D. N., Muto, C. A., and Owens, R. C., Jr. (2008) Measures to control and prevent *Clostridium difficile* infection. *Clin Infect Dis* **46 Suppl 1**, S43-49
134. Shim, J. K., Johnson, S., Samore, M. H., Bliss, D. Z., and Gerding, D. N. (1998) Primary symptomless colonisation by *Clostridium difficile* and decreased risk of subsequent diarrhoea. *Lancet* **351**, 633-636
135. Sohn, S., Climo, M., Diekema, D., Fraser, V., Herwaldt, L., Marino, S., Noskin, G., Perl, T., Song, X., Tokars, J., Warren, D., Wong, E., Yokoe, D. S., Zembower, T., Sepkowitz, K. A., and Prevention Epicenter, H. (2005) Varying rates of *Clostridium difficile*-associated diarrhea at prevention epicenter hospitals. *Infect Control Hosp Epidemiol* **26**, 676-679
136. Farrell, R. J., and LaMont, J. T. (2000) Pathogenesis and clinical manifestations of *Clostridium difficile* diarrhea and colitis. *Curr Top Microbiol Immunol* **250**, 109-125
137. Johal, S. S., Hammond, J., Solomon, K., James, P. D., and Mahida, Y. R. (2004) *Clostridium difficile* associated diarrhoea in hospitalised patients: onset in the community and hospital and role of flexible sigmoidoscopy. *Gut* **53**, 673-677
138. Rubin, M. S., Bodenstein, L. E., and Kent, K. C. (1995) Severe *Clostridium difficile* colitis. *Dis Colon Rectum* **38**, 350-354
139. Bartlett, J. G. (2002) Clinical practice. Antibiotic-associated diarrhea. *N Engl J Med* **346**, 334-339
140. Kim, K. H., Fekety, R., Batts, D. H., Brown, D., Cudmore, M., Silva, J., Jr., and Waters, D. (1981) Isolation of *Clostridium difficile* from the environment and contacts of patients with antibiotic-associated colitis. *J Infect Dis* **143**, 42-50
141. Gerding, D. N., Johnson, S., Peterson, L. R., Mulligan, M. E., and Silva, J., Jr. (1995) *Clostridium difficile*-associated diarrhea and colitis. *Infect Control Hosp Epidemiol* **16**, 459-477
142. Bartlett, J. G. (2006) Narrative review: the new epidemic of *Clostridium difficile*-associated enteric disease. *Ann Intern Med* **145**, 758-764
143. Bartlett, J. G. (1981) Antimicrobial agents implicated in *Clostridium difficile* toxin-associated diarrhea of colitis. *Johns Hopkins Med J* **149**, 6-9
144. McFarland, L. V., Surawicz, C. M., and Stamm, W. E. (1990) Risk factors for *Clostridium difficile* carriage and *C. difficile*-associated diarrhea in a cohort of hospitalized patients. *J Infect Dis* **162**, 678-684

145. McFarland, L. V., Bauwens, J. E., Melcher, S. A., Surawicz, C. M., Greenberg, R. N., and Elmer, G. W. (1995) Ciprofloxacin-associated *Clostridium difficile* disease. *Lancet* **346**, 977-978
146. Bauwens, J. E., McFarland, L. V., and Melcher, S. A. (1997) Recurrent *Clostridium difficile* disease following ciprofloxacin use. *Ann Pharmacother* **31**, 1090
147. Poutanen, S. M., and Simor, A. E. (2004) *Clostridium difficile*-associated diarrhea in adults. *CMAJ* **171**, 51-58
148. Elliott, B., Chang, B. J., Golledge, C. L., and Riley, T. V. (2007) *Clostridium difficile*-associated diarrhoea. *Intern Med J* **37**, 561-568
149. Rouphael, N. G., O'Donnell, J. A., Bhatnagar, J., Lewis, F., Polgreen, P. M., Beekmann, S., Guarner, J., Killgore, G. E., Coffman, B., Campbell, J., Zaki, S. R., and McDonald, L. C. (2008) *Clostridium difficile*-associated diarrhea: an emerging threat to pregnant women. *Am J Obstet Gynecol* **198**, 635 e631-636
150. Bartlett, J. G. (2010) *Clostridium difficile*: progress and challenges. *Ann N Y Acad Sci* **1213**, 62-69
151. Dial, S., Delaney, J. A., Barkun, A. N., and Suissa, S. (2005) Use of gastric acid-suppressive agents and the risk of community-acquired *Clostridium difficile*-associated disease. *JAMA* **294**, 2989-2995
152. Rodemann, J. F., Dubberke, E. R., Reske, K. A., Seo, D. H., and Stone, C. D. (2007) Incidence of *Clostridium difficile* infection in inflammatory bowel disease. *Clin Gastroenterol Hepatol* **5**, 339-344
153. Keven, K., Basu, A., Re, L., Tan, H., Marcos, A., Fung, J. J., Starzl, T. E., Simmons, R. L., and Shapiro, R. (2004) *Clostridium difficile* colitis in patients after kidney and pancreas-kidney transplantation. *Transpl Infect Dis* **6**, 10-14
154. Mullane, K. (2014) Fidaxomicin in *Clostridium difficile* infection: latest evidence and clinical guidance. *Ther Adv Chronic Dis* **5**, 69-84
155. Lamontagne, F., Labbe, A. C., Haeck, O., Lesur, O., Lalancette, M., Patino, C., Leblanc, M., Laverdiere, M., and Pepin, J. (2007) Impact of emergency colectomy on survival of patients with fulminant *Clostridium difficile* colitis during an epidemic caused by a hypervirulent strain. *Ann Surg* **245**, 267-272
156. Cohen, S. H., Gerding, D. N., Johnson, S., Kelly, C. P., Loo, V. G., McDonald, L. C., Pepin, J., Wilcox, M. H., Society for Healthcare Epidemiology of, A., and Infectious Diseases Society of, A. (2010) Clinical practice guidelines for *Clostridium difficile* infection in adults: 2010 update by the society for healthcare epidemiology of America (SHEA) and the infectious diseases society of America (IDSA). *Infect Control Hosp Epidemiol* **31**, 431-455
157. Pepin, J., Routhier, S., Gagnon, S., and Brazeau, I. (2006) Management and outcomes of a first recurrence of *Clostridium difficile*-associated disease in Quebec, Canada. *Clin Infect Dis* **42**, 758-764
158. Aas, J., Gessert, C. E., and Bakken, J. S. (2003) Recurrent *Clostridium difficile* colitis: case series involving 18 patients treated with donor stool administered via a nasogastric tube. *Clin Infect Dis* **36**, 580-585
159. Dove, C. H., Wang, S. Z., Price, S. B., Phelps, C. J., Lyerly, D. M., Wilkins, T. D., and Johnson, J. L. (1990) Molecular characterization of the *Clostridium difficile* toxin A gene. *Infect Immun* **58**, 480-488

160. Barroso, L. A., Wang, S. Z., Phelps, C. J., Johnson, J. L., and Wilkins, T. D. (1990) Nucleotide sequence of *Clostridium difficile* toxin B gene. *Nucleic Acids Res* **18**, 4004
161. Dupuy, B., Raffestin, S., Matamouros, S., Mani, N., Popoff, M. R., and Sonenshein, A. L. (2006) Regulation of toxin and bacteriocin gene expression in *Clostridium* by interchangeable RNA polymerase sigma factors. *Mol Microbiol* **60**, 1044-1057
162. Dupuy, B., Govind, R., Antunes, A., and Matamouros, S. (2008) *Clostridium difficile* toxin synthesis is negatively regulated by TcdC. *J Med Microbiol* **57**, 685-689
163. Tan, K. S., Wee, B. Y., and Song, K. P. (2001) Evidence for holin function of *tcdE* gene in the pathogenicity of *Clostridium difficile*. *J Med Microbiol* **50**, 613-619
164. Lyerly, D. M., Saum, K. E., MacDonald, D. K., and Wilkins, T. D. (1985) Effects of *Clostridium difficile* toxins given intragastrically to animals. *Infect Immun* **47**, 349-352
165. Lyerly, D. M., Barroso, L. A., Wilkins, T. D., Depitre, C., and Corthier, G. (1992) Characterization of a toxin A-negative, toxin B-positive strain of *Clostridium difficile*. *Infect Immun* **60**, 4633-4639
166. Lyras, D., O'Connor, J. R., Howarth, P. M., Sambol, S. P., Carter, G. P., Phumoonna, T., Poon, R., Adams, V., Vedantam, G., Johnson, S., Gerding, D. N., and Rood, J. I. (2009) Toxin B is essential for virulence of *Clostridium difficile*. *Nature* **458**, 1176-1179
167. Cohen, S. H., Tang, Y. J., Hansen, B., and Silva, J., Jr. (1998) Isolation of a toxin B-deficient mutant strain of *Clostridium difficile* in a case of recurrent *C. difficile*-associated diarrhea. *Clin Infect Dis* **26**, 410-412
168. Drudy, D., Fanning, S., and Kyne, L. (2007) Toxin A-negative, toxin B-positive *Clostridium difficile*. *Int J Infect Dis* **11**, 5-10
169. Hecht, G., Pothoulakis, C., LaMont, J. T., and Madara, J. L. (1988) *Clostridium difficile* toxin A perturbs cytoskeletal structure and tight junction permeability of cultured human intestinal epithelial monolayers. *J Clin Invest* **82**, 1516-1524
170. Lyerly, D. M., Krivan, H. C., and Wilkins, T. D. (1988) *Clostridium difficile*: its disease and toxins. *Clin Microbiol Rev* **1**, 1-18
171. Sullivan, N. M., Pellett, S., and Wilkins, T. D. (1982) Purification and characterization of toxins A and B of *Clostridium difficile*. *Infect Immun* **35**, 1032-1040
172. Kuehne, S. A., Cartman, S. T., and Minton, N. P. (2011) Both, toxin A and toxin B, are important in *Clostridium difficile* infection. *Gut Microbes* **2**, 252-255
173. Geric, B., Carman, R. J., Rupnik, M., Genheimer, C. W., Sambol, S. P., Lyerly, D. M., Gerding, D. N., and Johnson, S. (2006) Binary toxin-producing, large clostridial toxin-negative *Clostridium difficile* strains are enterotoxic but do not cause disease in hamsters. *J Infect Dis* **193**, 1143-1150
174. Warny, M., Pepin, J., Fang, A., Killgore, G., Thompson, A., Brazier, J., Frost, E., and McDonald, L. C. (2005) Toxin production by an emerging strain of *Clostridium difficile* associated with outbreaks of severe disease in North America and Europe. *Lancet* **366**, 1079-1084

175. Pepin, J., Valiquette, L., and Cossette, B. (2005) Mortality attributable to nosocomial *Clostridium difficile*-associated disease during an epidemic caused by a hypervirulent strain in Quebec. *CMAJ* **173**, 1037-1042
176. Merrigan, M., Venugopal, A., Mallozzi, M., Roxas, B., Viswanathan, V. K., Johnson, S., Gerding, D. N., and Vedantam, G. (2010) Human hypervirulent *Clostridium difficile* strains exhibit increased sporulation as well as robust toxin production. *J Bacteriol* **192**, 4904-4911
177. Killgore, G., Thompson, A., Johnson, S., Brazier, J., Kuijper, E., Pepin, J., Frost, E. H., Savelkoul, P., Nicholson, B., van den Berg, R. J., Kato, H., Sambol, S. P., Zukowski, W., Woods, C., Limbago, B., Gerding, D. N., and McDonald, L. C. (2008) Comparison of seven techniques for typing international epidemic strains of *Clostridium difficile*: restriction endonuclease analysis, pulsed-field gel electrophoresis, PCR-ribotyping, multilocus sequence typing, multilocus variable-number tandem-repeat analysis, amplified fragment length polymorphism, and surface layer protein A gene sequence typing. *J Clin Microbiol* **46**, 431-437
178. Stabler, R. A., He, M., Dawson, L., Martin, M., Valiente, E., Corton, C., Lawley, T. D., Sebaihia, M., Quail, M. A., Rose, G., Gerding, D. N., Gibert, M., Popoff, M. R., Parkhill, J., Dougan, G., and Wren, B. W. (2009) Comparative genome and phenotypic analysis of *Clostridium difficile* 027 strains provides insight into the evolution of a hypervirulent bacterium. *Genome Biol* **10**, R102
179. Hofmann, F., Busch, C., Prepens, U., Just, I., and Aktories, K. (1997) Localization of the glucosyltransferase activity of *Clostridium difficile* toxin B to the N-terminal part of the holotoxin. *J Biol Chem* **272**, 11074-11078
180. Genth, H., Aktories, K., and Just, I. (1999) Monoglucosylation of RhoA at threonine 37 blocks cytosol-membrane cycling. *J Biol Chem* **274**, 29050-29056
181. Busch, C., Hofmann, F., Selzer, J., Munro, S., Jeckel, D., and Aktories, K. (1998) A common motif of eukaryotic glycosyltransferases is essential for the enzyme activity of large clostridial cytotoxins. *J Biol Chem* **273**, 19566-19572
182. Jank, T., Giesemann, T., and Aktories, K. (2007) *Clostridium difficile* glucosyltransferase toxin B-essential amino acids for substrate binding. *J Biol Chem* **282**, 35222-35231
183. Reinert, D. J., Jank, T., Aktories, K., and Schulz, G. E. (2005) Structural basis for the function of *Clostridium difficile* toxin B. *J Mol Biol* **351**, 973-981
184. Reineke, J., Tenzer, S., Rupnik, M., Koschinski, A., Hasselmayer, O., Schrattenholz, A., Schild, H., and von Eichel-Streiber, C. (2007) Autocatalytic cleavage of *Clostridium difficile* toxin B. *Nature* **446**, 415-419
185. Egerer, M., Giesemann, T., Jank, T., Satchell, K. J., and Aktories, K. (2007) Auto-catalytic cleavage of *Clostridium difficile* toxins A and B depends on cysteine protease activity. *J Biol Chem* **282**, 25314-25321
186. Pruitt, R. N., Chagot, B., Cover, M., Chazin, W. J., Spiller, B., and Lacy, D. B. (2009) Structure-function analysis of inositol hexakisphosphate-induced autoprocessing in *Clostridium difficile* toxin A. *J Biol Chem* **284**, 21934-21940
187. Genisyuerek, S., Papatheodorou, P., Guttenberg, G., Schubert, R., Benz, R., and Aktories, K. (2011) Structural determinants for membrane insertion, pore formation and translocation of *Clostridium difficile* toxin B. *Mol Microbiol* **79**, 1643-1654

188. Egerer, M., Giesemann, T., Herrmann, C., and Aktories, K. (2009) Autocatalytic processing of *Clostridium difficile* toxin B. Binding of inositol hexakisphosphate. *J Biol Chem* **284**, 3389-3395
189. Barth, H., Pfeifer, G., Hofmann, F., Maier, E., Benz, R., and Aktories, K. (2001) Low pH-induced formation of ion channels by *Clostridium difficile* toxin B in target cells. *J Biol Chem* **276**, 10670-10676
190. Qa'Dan, M., Spyres, L. M., and Ballard, J. D. (2000) pH-induced conformational changes in *Clostridium difficile* toxin B. *Infect Immun* **68**, 2470-2474
191. Giesemann, T., Jank, T., Gerhard, R., Maier, E., Just, I., Benz, R., and Aktories, K. (2006) Cholesterol-dependent pore formation of *Clostridium difficile* toxin A. *J Biol Chem* **281**, 10808-10815
192. Pfeifer, G., Schirmer, J., Leemhuis, J., Busch, C., Meyer, D. K., Aktories, K., and Barth, H. (2003) Cellular uptake of *Clostridium difficile* toxin B. Translocation of the N-terminal catalytic domain into the cytosol of eukaryotic cells. *J Biol Chem* **278**, 44535-44541
193. Pruitt, R. N., Chambers, M. G., Ng, K. K., Ohi, M. D., and Lacy, D. B. (2010) Structural organization of the functional domains of *Clostridium difficile* toxins A and B. *Proc Natl Acad Sci U S A* **107**, 13467-13472
194. Jank, T., and Aktories, K. (2008) Structure and mode of action of clostridial glucosylating toxins: the ABCD model. *Trends Microbiol* **16**, 222-229
195. von Eichel-Streiber, C., and Sauerborn, M. (1990) *Clostridium difficile* toxin A carries a C-terminal repetitive structure homologous to the carbohydrate binding region of streptococcal glycosyltransferases. *Gene* **96**, 107-113
196. Ho, J. G., Greco, A., Rupnik, M., and Ng, K. K. (2005) Crystal structure of receptor-binding C-terminal repeats from *Clostridium difficile* toxin A. *Proc Natl Acad Sci U S A* **102**, 18373-18378
197. Greco, A., Ho, J. G., Lin, S. J., Palcic, M. M., Rupnik, M., and Ng, K. K. (2006) Carbohydrate recognition by *Clostridium difficile* toxin A. *Nat Struct Mol Biol* **13**, 460-461
198. Albesa-Jove, D., Bertrand, T., Carpenter, E. P., Swain, G. V., Lim, J., Zhang, J., Haire, L. F., Vasisht, N., Braun, V., Lange, A., von Eichel-Streiber, C., Svergun, D. I., Fairweather, N. F., and Brown, K. A. (2010) Four distinct structural domains in *Clostridium difficile* toxin B visualized using SAXS. *J Mol Biol* **396**, 1260-1270
199. Krivan, H. C., Clark, G. F., Smith, D. F., and Wilkins, T. D. (1986) Cell surface binding site for *Clostridium difficile* enterotoxin: evidence for a glycoconjugate containing the sequence Gal alpha 1-3Gal beta 1-4GlcNAc. *Infect Immun* **53**, 573-581
200. Na, X., Kim, H., Moyer, M. P., Pothoulakis, C., and LaMont, J. T. (2008) gp96 is a human colonocyte plasma membrane binding protein for *Clostridium difficile* toxin A. *Infect Immun* **76**, 2862-2871
201. Pothoulakis, C., Gilbert, R. J., Cladaras, C., Castagliuolo, I., Semenza, G., Hitti, Y., Montcrief, J. S., Linevsky, J., Kelly, C. P., Nikulasson, S., Desai, H. P., Wilkins, T. D., and LaMont, J. T. (1996) Rabbit sucrase-isomaltase contains a functional intestinal receptor for *Clostridium difficile* toxin A. *J Clin Invest* **98**, 641-649

202. von Eichel-Streiber, C., Laufenberg-Feldmann, R., Sartingen, S., Schulze, J., and Sauerborn, M. (1992) Comparative sequence analysis of the *Clostridium difficile* toxins A and B. *Mol Gen Genet* **233**, 260-268
203. Chumbler, N. M., Rutherford, S. A., Zhang, Z., Farrow, M. A., Lisher, J. P., Farquhar, E., Giedroc, D. P., Spiller, B. W., Melnyk, R. A., and Lacy, D. B. (2016) Crystal structure of *Clostridium difficile* toxin A. *Nat Microbiol* **1**, 15002
204. Pruitt, R. N., and Lacy, D. B. (2012) Toward a structural understanding of *Clostridium difficile* toxins A and B. *Front Cell Infect Microbiol* **2**, 28
205. Huang, J. H., Shen, Z. Q., Lien, S. P., Hsiao, K. N., Leng, C. H., Chen, C. C., Siu, L. K., and Chong, P. C. (2015) Biochemical and Immunological Characterization of Truncated Fragments of the Receptor-Binding Domains of *C. difficile* Toxin A. *PLoS One* **10**, e0135045
206. Frisch, C., Gerhard, R., Aktories, K., Hofmann, F., and Just, I. (2003) The complete receptor-binding domain of *Clostridium difficile* toxin A is required for endocytosis. *Biochem Biophys Res Commun* **300**, 706-711
207. Olling, A., Goy, S., Hoffmann, F., Tatge, H., Just, I., and Gerhard, R. (2011) The repetitive oligopeptide sequences modulate cytopathic potency but are not crucial for cellular uptake of *Clostridium difficile* toxin A. *PLoS One* **6**, e17623
208. Gerhard, R., Frenzel, E., Goy, S., and Olling, A. (2013) Cellular uptake of *Clostridium difficile* TcdA and truncated TcdA lacking the receptor binding domain. *J Med Microbiol* **62**, 1414-1422
209. LaFrance, M. E., Farrow, M. A., Chandrasekaran, R., Sheng, J., Rubin, D. H., and Lacy, D. B. (2015) Identification of an epithelial cell receptor responsible for *Clostridium difficile* TcdB-induced cytotoxicity. *Proc Natl Acad Sci U S A* **112**, 7073-7078
210. Tao, L., Zhang, J., Meraner, P., Tovaglieri, A., Wu, X., Gerhard, R., Zhang, X., Stallcup, W. B., Miao, J., He, X., Hurdle, J. G., Breault, D. T., Brass, A. L., and Dong, M. (2016) Frizzled proteins are colonic epithelial receptors for *C. difficile* toxin B. *Nature* **538**, 350-355
211. Yuan, P., Zhang, H., Cai, C., Zhu, S., Zhou, Y., Yang, X., He, R., Li, C., Guo, S., Li, S., Huang, T., Perez-Cordon, G., Feng, H., and Wei, W. (2015) Chondroitin sulfate proteoglycan 4 functions as the cellular receptor for *Clostridium difficile* toxin B. *Cell Res* **25**, 157-168
212. Papatheodorou, P., Zamboglou, C., Genisyuerek, S., Guttenberg, G., and Aktories, K. (2010) Clostridial glucosylating toxins enter cells via clathrin-mediated endocytosis. *PLoS One* **5**, e10673
213. Johnson, E. A. (1999) Clostridial toxins as therapeutic agents: benefits of nature's most toxic proteins. *Annu Rev Microbiol* **53**, 551-575
214. Williamson, C. H., Sahl, J. W., Smith, T. J., Xie, G., Foley, B. T., Smith, L. A., Fernandez, R. A., Lindstrom, M., Korkeala, H., Keim, P., Foster, J., and Hill, K. (2016) Comparative genomic analyses reveal broad diversity in botulinum-toxin-producing *Clostridia*. *BMC Genomics* **17**, 180
215. Kull, S., Schulz, K. M., Weisemann, J., Kirchner, S., Schreiber, T., Bollenbach, A., Dabrowski, P. W., Nitsche, A., Kalb, S. R., Dorner, M. B., Barr, J. R., Rummel, A., and Dorner, B. G. (2015) Isolation and functional characterization of the novel *Clostridium botulinum* neurotoxin A8 subtype. *PLoS One* **10**, e0116381

216. Montecucco, C., and Rasotto, M. B. (2015) On botulinum neurotoxin variability. *MBio* **6**
217. Hill, K. K., Xie, G., Foley, B. T., and Smith, T. J. (2015) Genetic diversity within the botulinum neurotoxin-producing bacteria and their neurotoxins. *Toxicon* **107**, 2-8
218. Smith, T. J., Hill, K. K., and Raphael, B. H. (2015) Historical and current perspectives on *Clostridium botulinum* diversity. *Res Microbiol* **166**, 290-302
219. Binz, T. (2013) Clostridial neurotoxin light chains: devices for SNARE cleavage mediated blockade of neurotransmission. *Curr Top Microbiol Immunol* **364**, 139-157
220. Pier, C. L., Chen, C., Tepp, W. H., Lin, G., Janda, K. D., Barbieri, J. T., Pellett, S., and Johnson, E. A. (2011) Botulinum neurotoxin subtype A2 enters neuronal cells faster than subtype A1. *FEBS Lett* **585**, 199-206
221. Wang, D., Krilich, J., Pellett, S., Baudys, J., Tepp, W. H., Barr, J. R., Johnson, E. A., and Kalb, S. R. (2013) Comparison of the catalytic properties of the botulinum neurotoxin subtypes A1 and A5. *Biochim Biophys Acta* **1834**, 2722-2728
222. Whitemarsh, R. C., Tepp, W. H., Bradshaw, M., Lin, G., Pier, C. L., Scherf, J. M., Johnson, E. A., and Pellett, S. (2013) Characterization of botulinum neurotoxin A subtypes 1 through 5 by investigation of activities in mice, in neuronal cell cultures, and in vitro. *Infect Immun* **81**, 3894-3902
223. Pellett, S., Tepp, W. H., Whitemarsh, R. C., Bradshaw, M., and Johnson, E. A. (2015) In vivo onset and duration of action varies for botulinum neurotoxin A subtypes 1-5. *Toxicon* **107**, 37-42
224. Torii, Y., Goto, Y., Nakahira, S., Kozaki, S., Kaji, R., and Ginnaga, A. (2015) Comparison of Systemic Toxicity between Botulinum Toxin Subtypes A1 and A2 in Mice and Rats. *Basic Clin Pharmacol Toxicol* **116**, 524-528
225. Koizumi, H., Goto, S., Okita, S., Morigaki, R., Akaike, N., Torii, Y., Harakawa, T., Ginnaga, A., and Kaji, R. (2014) Spinal Central Effects of Peripherally Applied Botulinum Neurotoxin A in Comparison between Its Subtypes A1 and A2. *Front Neurol* **5**, 98
226. Mukai, Y., Shimatani, Y., Sako, W., Asanuma, K., Nodera, H., Sakamoto, T., Izumi, Y., Kohda, T., Kozaki, S., and Kaji, R. (2014) Comparison between botulinum neurotoxin type A2 and type A1 by electrophysiological study in healthy individuals. *Toxicon* **81**, 32-36
227. Akaike, N., Shin, M. C., Wakita, M., Torii, Y., Harakawa, T., Ginnaga, A., Kato, K., Kaji, R., and Kozaki, S. (2013) Transsynaptic inhibition of spinal transmission by A2 botulinum toxin. *J Physiol* **591**, 1031-1043
228. Ma, L., Nagai, J., Sekino, Y., Goto, Y., Nakahira, S., and Ueda, H. (2012) Single application of A2 NTX, a botulinum toxin A2 subunit, prevents chronic pain over long periods in both diabetic and spinal cord injury-induced neuropathic pain models. *J Pharmacol Sci* **119**, 282-286
229. Torii, Y., Akaike, N., Harakawa, T., Kato, K., Sugimoto, N., Goto, Y., Nakahira, S., Kohda, T., Kozaki, S., Kaji, R., and Ginnaga, A. (2011) Type A1 but not type A2 botulinum toxin decreases the grip strength of the contralateral foreleg through axonal transport from the toxin-treated foreleg of rats. *J Pharmacol Sci* **117**, 275-285

230. Torii, Y., Kiyota, N., Sugimoto, N., Mori, Y., Goto, Y., Harakawa, T., Nakahira, S., Kaji, R., Kozaki, S., and Ginnaga, A. (2011) Comparison of effects of botulinum toxin subtype A1 and A2 using twitch tension assay and rat grip strength test. *Toxicon* **57**, 93-99
231. Stenmark, P., Dupuy, J., Imamura, A., Kiso, M., and Stevens, R. C. (2008) Crystal structure of botulinum neurotoxin type A in complex with the cell surface co-receptor GT1b-insight into the toxin-neuron interaction. *PLoS Pathog* **4**, e1000129
232. Berntsson, R. P., Peng, L., Dong, M., and Stenmark, P. (2013) Structure of dual receptor binding to botulinum neurotoxin B. *Nat Commun* **4**, 2058
233. Baldwin, M. R., Tepp, W. H., Pier, C. L., Bradshaw, M., Ho, M., Wilson, B. A., Fritz, R. B., Johnson, E. A., and Barbieri, J. T. (2005) Characterization of the antibody response to the receptor binding domain of botulinum neurotoxin serotypes A and E. *Infect Immun* **73**, 6998-7005
234. Thornton, J. A. (2016) Splicing by Overlap Extension PCR to Obtain Hybrid DNA Products. *Methods Mol Biol* **1373**, 43-49
235. Kroken, A. R., Blum, F. C., Zuverink, M., and Barbieri, J. T. (2017) Entry of Botulinum Neurotoxin Subtypes A1 and A2 into Neurons. *Infect Immun* **85**
236. Roy, A., Kucukural, A., and Zhang, Y. (2010) I-TASSER: a unified platform for automated protein structure and function prediction. *Nat Protoc* **5**, 725-738
237. Rummel, A. (October 23, 2012) Transport Protein Which Is Used To Introduce Chemical Compounds Into Nerve Cells. U.S. Patent in *USPTO* (USPTO ed., IPSEN BIOINNOVATION Ltd United States of America
238. Baldwin, M. R., and Barbieri, J. T. (2007) Association of botulinum neurotoxin serotypes a and B with synaptic vesicle protein complexes. *Biochemistry* **46**, 3200-3210
239. Kitamura, M., Iwamori, M., and Nagai, Y. (1980) Interaction between Clostridium botulinum neurotoxin and gangliosides. *Biochim Biophys Acta* **628**, 328-335
240. Ochanda, J. O., Syuto, B., Ohishi, I., Naiki, M., and Kubo, S. (1986) Binding of Clostridium botulinum neurotoxin to gangliosides. *J Biochem* **100**, 27-33
241. Dong, M., Tepp, W. H., Liu, H., Johnson, E. A., and Chapman, E. R. (2007) Mechanism of botulinum neurotoxin B and G entry into hippocampal neurons. *J Cell Biol* **179**, 1511-1522
242. Yeh, F. L., Dong, M., Yao, J., Tepp, W. H., Lin, G., Johnson, E. A., and Chapman, E. R. (2010) SV2 mediates entry of tetanus neurotoxin into central neurons. *PLoS Pathog* **6**, e1001207
243. Peng, L., Tepp, W. H., Johnson, E. A., and Dong, M. (2011) Botulinum neurotoxin D uses synaptic vesicle protein SV2 and gangliosides as receptors. *PLoS Pathog* **7**, e1002008
244. Rummel, A., Karnath, T., Henke, T., Bigalke, H., and Binz, T. (2004) Synaptotagmins I and II act as nerve cell receptors for botulinum neurotoxin G. *J Biol Chem* **279**, 30865-30870
245. Strotmeier, J., Willjes, G., Binz, T., and Rummel, A. (2012) Human synaptotagmin-II is not a high affinity receptor for botulinum neurotoxin B and G: increased therapeutic dosage and immunogenicity. *FEBS Lett* **586**, 310-313

246. Tighe, A. P., and Schiavo, G. (2013) Botulinum neurotoxins: mechanism of action. *Toxicon* **67**, 87-93
247. Rossetto, O., Pirazzini, M., and Montecucco, C. (2014) Botulinum neurotoxins: genetic, structural and mechanistic insights. *Nat Rev Microbiol* **12**, 535-549
248. Montecucco, C. (1986) How do tetanus and botulinum toxins bind to neuronal membranes? *Trends Biochem Sci* **11**, 314-317
249. Hamark, C., Berntsson, R. P., Masuyer, G., Henriksson, L. M., Gustafsson, R., Stenmark, P., and Widmalm, G. (2017) Glycans Confer Specificity to the Recognition of Ganglioside Receptors by Botulinum Neurotoxin A. *J Am Chem Soc* **139**, 218-230
250. Takamizawa, K., Iwamori, M., Kozaki, S., Sakaguchi, G., Tanaka, R., Takayama, H., and Nagai, Y. (1986) TLC immunostaining characterization of *Clostridium botulinum* type A neurotoxin binding to gangliosides and free fatty acids. *FEBS Lett* **201**, 229-232
251. Yowler, B. C., Kensinger, R. D., and Schengrund, C. L. (2002) Botulinum neurotoxin A activity is dependent upon the presence of specific gangliosides in neuroblastoma cells expressing synaptotagmin I. *J Biol Chem* **277**, 32815-32819
252. Rapoport, T. A. (2007) Protein translocation across the eukaryotic endoplasmic reticulum and bacterial plasma membranes. *Nature* **450**, 663-669
253. Wernick, N. L., Chinnapen, D. J., Cho, J. A., and Lencer, W. I. (2010) Cholera toxin: an intracellular journey into the cytosol by way of the endoplasmic reticulum. *Toxins (Basel)* **2**, 310-325
254. Oh, K. J., Senzel, L., Collier, R. J., and Finkelstein, A. (1999) Translocation of the catalytic domain of diphtheria toxin across planar phospholipid bilayers by its own T domain. *Proc Natl Acad Sci U S A* **96**, 8467-8470
255. Zhang, S., Udho, E., Wu, Z., Collier, R. J., and Finkelstein, A. (2004) Protein translocation through anthrax toxin channels formed in planar lipid bilayers. *Biophys J* **87**, 3842-3849
256. Hoch, D. H., Romero-Mira, M., Ehrlich, B. E., Finkelstein, A., DasGupta, B. R., and Simpson, L. L. (1985) Channels formed by botulinum, tetanus, and diphtheria toxins in planar lipid bilayers: relevance to translocation of proteins across membranes. *Proc Natl Acad Sci U S A* **82**, 1692-1696
257. Blaustein, R. O., Koehler, T. M., Collier, R. J., and Finkelstein, A. (1989) Anthrax toxin: channel-forming activity of protective antigen in planar phospholipid bilayers. *Proc Natl Acad Sci U S A* **86**, 2209-2213
258. Jiang, J., Pentelute, B. L., Collier, R. J., and Zhou, Z. H. (2015) Atomic structure of anthrax protective antigen pore elucidates toxin translocation. *Nature* **521**, 545-549
259. Wu, Z., Jakes, K. S., Samelson-Jones, B. S., Lai, B., Zhao, G., London, E., and Finkelstein, A. (2006) Protein translocation by bacterial toxin channels: a comparison of diphtheria toxin and colicin Ia. *Biophys J* **91**, 3249-3256
260. Pirazzini, M., Azarnia Tehran, D., Leka, O., Zanetti, G., Rossetto, O., and Montecucco, C. (2016) On the translocation of botulinum and tetanus neurotoxins across the membrane of acidic intracellular compartments. *Biochim Biophys Acta* **1858**, 467-474

261. Azarnia Tehran, D., Pirazzini, M., Leka, O., Mattarei, A., Lista, F., Binz, T., Rossetto, O., and Montecucco, C. (2017) Hsp90 is involved in the entry of clostridial neurotoxins into the cytosol of nerve terminals. *Cell Microbiol* **19**
262. Pirazzini, M., Bordin, F., Rossetto, O., Shone, C. C., Binz, T., and Montecucco, C. (2013) The thioredoxin reductase-thioredoxin system is involved in the entry of tetanus and botulinum neurotoxins in the cytosol of nerve terminals. *FEBS Lett* **587**, 150-155
263. Ratts, R., Zeng, H., Berg, E. A., Blue, C., McComb, M. E., Costello, C. E., vanderSpek, J. C., and Murphy, J. R. (2003) The cytosolic entry of diphtheria toxin catalytic domain requires a host cell cytosolic translocation factor complex. *J Cell Biol* **160**, 1139-1150
264. Trujillo, C., Taylor-Parker, J., Harrison, R., and Murphy, J. R. (2010) Essential lysine residues within transmembrane helix 1 of diphtheria toxin facilitate COPI binding and catalytic domain entry. *Mol Microbiol* **76**, 1010-1019
265. Ratts, R., Trujillo, C., Bharti, A., vanderSpek, J., Harrison, R., and Murphy, J. R. (2005) A conserved motif in transmembrane helix 1 of diphtheria toxin mediates catalytic domain delivery to the cytosol. *Proc Natl Acad Sci U S A* **102**, 15635-15640
266. Burger, S., Tatge, H., Hofmann, F., Genth, H., Just, I., and Gerhard, R. (2003) Expression of recombinant *Clostridium difficile* toxin A using the *Bacillus megaterium* system. *Biochem Biophys Res Commun* **307**, 584-588
267. Yang, G., Zhou, B., Wang, J., He, X., Sun, X., Nie, W., Tzipori, S., and Feng, H. (2008) Expression of recombinant *Clostridium difficile* toxin A and B in *Bacillus megaterium*. *BMC Microbiol* **8**, 192
268. Sun, J., Vernier, G., Wigelsworth, D. J., and Collier, R. J. (2007) Insertion of anthrax protective antigen into liposomal membranes: effects of a receptor. *J Biol Chem* **282**, 1059-1065
269. Montal, M. S., Blewitt, R., Tomich, J. M., and Montal, M. (1992) Identification of an ion channel-forming motif in the primary structure of tetanus and botulinum neurotoxins. *FEBS Lett* **313**, 12-18
270. White, S. H., and Wimley, W. C. (1999) Membrane protein folding and stability: physical principles. *Annu Rev Biophys Biomol Struct* **28**, 319-365
271. Snider, C., Jayasinghe, S., Hristova, K., and White, S. H. (2009) MPEx: a tool for exploring membrane proteins. *Protein Sci* **18**, 2624-2628
272. Chattopadhyay, A. (1990) Chemistry and biology of N-(7-nitrobenz-2-oxa-1,3-diazol-4-yl)-labeled lipids: fluorescent probes of biological and model membranes. *Chem Phys Lipids* **53**, 1-15
273. Loura, L. M., Fedorov, A., and Prieto, M. (2001) Fluid-fluid membrane microheterogeneity: a fluorescence resonance energy transfer study. *Biophys J* **80**, 776-788
274. Amimoto, K., Noro, T., Oishi, E., and Shimizu, M. (2007) A novel toxin homologous to large clostridial cytotoxins found in culture supernatant of *Clostridium perfringens* type C. *Microbiology* **153**, 1198-1206
275. Guttenberg, G., Hornei, S., Jank, T., Schwan, C., Lu, W., Einsle, O., Papatheodorou, P., and Aktories, K. (2012) Molecular characteristics of

Clostridium perfringens TpeL toxin and consequences of mono-O-GlcNAcylation of Ras in living cells. *J Biol Chem* **287**, 24929-24940
276. Schorch, B., Song, S., van Diemen, F. R., Bock, H. H., May, P., Herz, J., Brummelkamp, T. R., Papatheodorou, P., and Aktories, K. (2014) LRP1 is a receptor for *Clostridium perfringens* TpeL toxin indicating a two-receptor model of clostridial glycosylating toxins. *Proc Natl Acad Sci U S A* **111**, 6431-6436
277. Kuehne, S. A., Cartman, S. T., Heap, J. T., Kelly, M. L., Cockayne, A., and Minton, N. P. (2010) The role of toxin A and toxin B in *Clostridium difficile* infection. *Nature* **467**, 711-713
278. Manse, J. S., and Baldwin, M. R. (2015) Binding and entry of *Clostridium difficile* toxin B is mediated by multiple domains. *FEBS Lett* **589**, 3945-3951
279. Sreerama, N., and Woody, R. W. (2004) On the analysis of membrane protein circular dichroism spectra. *Protein Sci* **13**, 100-112
280. Zhang, Z., Park, M., Tam, J., Auger, A., Beilhartz, G. L., Lacy, D. B., and Melnyk, R. A. (2014) Translocation domain mutations affecting cellular toxicity identify the *Clostridium difficile* toxin B pore. *Proc Natl Acad Sci U S A* **111**, 3721-3726
281. Olling, A., Huls, C., Goy, S., Muller, M., Krooss, S., Rudolf, I., Tatge, H., and Gerhard, R. (2014) The combined repetitive oligopeptides of *Clostridium difficile* toxin A counteract premature cleavage of the glucosyl-transferase domain by stabilizing protein conformation. *Toxins (Basel)* **6**, 2162-2176
282. Kroh, H. K., Chandrasekaran, R., Rosenthal, K., Woods, R., Jin, X., Ohi, M. D., Nyborg, A. C., Rainey, G. J., Warrener, P., Spiller, B. W., and Lacy, D. B. (2017) Use of a neutralizing antibody helps identify structural features critical for binding of *Clostridium difficile* toxin TcdA to the host cell surface. *J Biol Chem* **292**, 14401-14412
283. Gupta, P., Zhang, Z., Sugiman-Marangos, S. N., Tam, J., Raman, S., Julien, J. P., Kroh, H. K., Lacy, D. B., Murgolo, N., Bekkari, K., Therien, A. G., Hernandez, L. D., and Melnyk, R. A. (2017) Functional defects in *Clostridium difficile* TcdB toxin uptake identify CSPG4 receptor-binding determinants. *J Biol Chem* **292**, 17290-17301

VITA

Gregory Stephen Lambert was born in 1989 in St. Louis, Missouri to Stephen and Mary Lambert. He has two siblings: Lindsay Marie (sister), and Brian Christopher (brother). In 2007, Gregory graduated from Parkway North High School in Creve Coeur, Missouri. While attending Parkway North, Gregory was a member of the National Honor Society, as well as the soccer and track teams. As a part of the track team, he was an influential figure in the school's newly-resurrected pole vault program.

While attending Truman State University in Kirksville, Missouri, Gregory was a member of the βββ (biology honors) and ΔX (social) fraternities, where he held a number of positions. He also conducted undergraduate research under the mentorship of Dr. Cynthia Cooper. Gregory spent the summer of 2010 as a National Science Foundation fellow at the University of Minnesota-Twin Cities, conducting research under Dr. Sandra Armstrong as a part of their LSSURP program. In 2011, Gregory graduated *summa cum laude* with a Bachelor's of Science degree in Biology from Truman State University.

Gregory was accepted to the Molecular Microbiology-Veterinary Pathobiology (MMI-VPB) graduate program at the University of Missouri-Columbia School of Medicine in 2011. Shortly thereafter, he joined the laboratory of Dr. Michael Baldwin, with whom he conducted the research contained within this document. After receiving his doctorate, Gregory intends to utilize the skills he has obtained to pursue a career in the biotechnology industry.